SEQUENCE STRATIGRAPHY AND CHEMOSTRATIGRAPHY ACROSS THE PERMO-TRIASSIC EXTINCTION EVENT, UPPER KHUFF CARBONATES, GHAWAR FIELD, SAUDI ARABIA

Raed Khalil Al-Dukhayyil

Dissertation submitted to the faculty of the
Virginia Polytechnic Institute and State University
in partial fulfillment of the requirements for the degree of

DOCTOR OF PHILOSOPHY

in

GEOSCIENCES

J. Fred Read, Chair
Kenneth A. Eriksson
Shuhai Xiao
Aus Al-Tawil

May 02, 2012

Blacksburg, Virginia

Keywords: Permo-Triassic boundary, Khuff Fm., Carbonates, Sequence stratigraphy, C/O isotopes, Uranium depletion, Ghawar Field

SEQUENCE STRATIGRAPHY AND CHEMOSTRATIGRAPHY ACROSS THE PERMO-TRIASSIC EXTINCTION EVENT, UPPER KHUFF CARBONATES, GHAWAR FIELD, SAUDI ARABIA

Raed Khalil Al-Dukhayyil

ABSTRACT

Logging of cores of the Upper Permian and Lower Triassic Khuff Formation, Ghawar, Saudi Arabia, has allowed a high resolution sequence stratigraphic framework to be generated. The lithofacies of this huge, arid epeiric ramp succession include: subaqueous - and supratidal anhydrite, tidal flat laminites, lagoonal mudstone, ooid-peloid grainstone, and subtidal off-shoal open marine mudstone.

Third order sequences include the Late Permian upper Khuff C, the Early Triassic Khuff B and the Khuff A sequences, which corrrelate with global cycles. Seven high frequency sequences (HFSs) make up the Changhsingian upper Khuff C. These HFSs are ~400 k.y. duration and probably driven by long term eccentricity. The Early Triassic Khuff B and A sequences are made up of 4 HFSs each, which appear to be ~100 to 200 k.y. duration and not easily tied to eccentricity forcing. The HFSs are in turn composed of parasequences, which appear to be 10 to 20 k.y. average durations, suggesting precessional and half precessional forcing. However, many thin locally developed cycles may be autocycles or subprecessional cycles.

Sequence stratigraphic cross sections and facies maps document progradation directions on the platform, reflecting the subtle interplay between the Ghawar structure and regional paleoslopes. Anhydrites are rare in the Permian Upper Khuff C except near the base of the studied interval. Anhydrites are well developed in the Triassic Khuff B and Khuff A where

some form transgressive deposits while others are highstand deposits of high frequency sequences.

The Permian-Triassic boundary (PTB) on the Arabian Platform marks a significant relative sea-level drop, that exposed from the outcrop belt to somewhere east of Ghawar. This contrasts with transgressive PTB settings elsewhere. Across the PTB the mass extinction is marked by a major decrease in biotic groups. The extinction was followed by development of subtidal thrombolites and increased microbial calcification due to decreased bioskeletonization.

The dominant reservoirs in the Permian Upper Khuff C occur in oolite in the uppermost high frequency sequence. In the Triassic Khuff B and A the reservoir facies are commonly non-dolomitized oolitic facies associated with open lagoon carbonates distant from evaporitic tidal flats. Within dolomitized units, best reservoirs are associated with oomoldic porosity, but oolite units proximal to evaporitic tidal flats have porosity plugged by anhydrite.

Carbon and oxgyen isotope profiles up to 150 m long were obtained from cored wells of the Khuff Formation, Ghawar Field, Saudi Arabia, across the Permian-Triassic boundary. Major global excursions are at the Changhsingian-Wuchiapingian boundary and the Permian-Triassic boundary, but several smaller excursions also appear to correlate with excursions elsewhere. The presence of the negative C-isotope excursions globally in both $\delta^{13}C_{carbonate}$ and $\delta^{13}C_{organic}$ as well as in deeper water sections lacking emergence surfaces, strongly supports the idea of these excursions being global phenomena related global C cycling.

Over 75% of the negative carbon isotope excursions in Ghawar occur beneath emergence surfaces, including the two major excursions at the Wuchiapingian and Changhsingian stage boundaries. The $\delta^{13}C$ profiles beneath the boundaries resemble those

associated with early diagenesis associated with isotopically light soil gas. The $\delta^{18}O$ profiles beneath the surfaces are variable, perhaps reflecting variable effects of evaporation on the meteoric input, mixing or overprinting by burial diagenesis. This suggests that the C-isotope excursions on the Arabian Platform, although global in origin, appear to have been modified by early diagenesis.

U depletion across the boundary is compatible with the postulated origins of the PTB event with bottom waters becoming stagnant and reducing, as a result of warming induced by volcanogenic CO_2 released by Siberian trap volcanism, methane release from thermal metamorphism of coals and destabilization of clathrates in the deep sea due to ocean warming. The global extent of the C-isotope and U excursions provides a high resolution correlation tool for Late Permian and Early Triassic successions.

DEDICATION

This doctoral dissertation is dedicated to my beloved deceased parents: Khalil and Qomashah Al-Ibrahim Al-Dukhayyil, for instilling many core values: love of family, the value of higher education, importance of hard work and having dreams and aspirations.

ACKNOWLEDGMENTS

I would like to express my gratitude and appreciation to my advisor Prof. J. Fred Read for his steady and invaluable support, guidance and patience, and for always making his students a priority. I would like to thank my committee members Prof. Ken Eriksson and Prof. Shuhai Xiao for their valuable help and constructive comments. Very special thanks go to Dr. Aus Al-Tawil, my mentor of Saudi Aramco Specialist Development Program and external committee member, for endless outstanding support, motivation, patience and constructive discussions and suggestions.

Very sincere thanks go to Suadi Aramco, Exploration Organization, Reservoir Characterization Department, Gas Fields Characterization Division and Exploration Planning and Support Division in Dhahran, and Aramco Services Company in Houston for granting permission to present Aramco data, and for outstanding encouragement and support.

I am grateful to R. Kamal, R. Koepnick, W. Hughes and R. Lindsay for constructive critiques and valuable interaction and discussion on Khuff throughout the study. I also thank R. Davis, N. Al-Talhah, J. Al-Hajhog, G. Al-Eid and N. Al-Qahtani for providing some Khuff data and references.

I would like to thank L. Al-Mana, A. Al-Masri, A. Al-Zahrani, H. Al-Uraij, A. Al-Shulaibi and the operations team at the world-class Core Lab facilities in Saudi Aramco for providing the best facility and services while characterizing the Khuff cores. I also thank A. Al-Qarni, N. Al-Malki and all members of Core Handling Team for facilitating the acquisition and analysis of the Khuff cores, and providing great support and assistance.

Finaly, I would like to express my high appreciation and thanks to my brothers and colleagues in “Al-Carbonate Lab”; K. AlTemimi and F. Al-Khaldi for their valuable interactions, assistance and great time in the lab. I also would like to extend my sincere thanks to my best friends who really deserve every respect for their emotional support during the length of this study; N. Al-Talhah, S. Al-Humoud, M. Al-Mashhadi, H. Dhaify, E. Abduljabbar, S. Al-Khunaifer, S. Al-Sheridi, I. Al-Goba, A. Al-Belwi, M. Al-Hassnah, A. Al-Sheridi and N. Al-Mashrafy. They were always there for me when I needed their help; therefore, I wish them the best of luck and a great success life.

Last but not least, I wish to express my deepest gratitude and highest appreciation to my wife J. Al-Juail and lovely children; Yazeed, Talal, Remas and Toleen for their continuing outstanding support, encouragement and blessings throughout the program. Their invaluable patience and waiting, in Saudi Arabia, for the first and last year of the program is very highly acknowledged. I also deeply appreciate my brother Bader and brother-in-law Anwar for taking care of my family in Saudi Arabia during my absence. I wish to thank my brothers and sisters for their moral support, encouragements and prayers throughout the years.

TABLE OF CONTENTS

LIST OF TABLES

LIST OF FIGURES

CHAPTER 1

GENERAL INTRODUCTION

The first paper of this dissertation (Chapter 2) describes the sequence development of the Permian-Triassic Khuff carbonates and evaporites in Ghawar, Saudi Arabia, using a set of cores logged as part of the project. The Khuff Formation was deposited on immense shallow water, carbonate ramp under an arid climate setting, and given its size modern analogs are lacking. In addition, the cores span the major extinction event of the Phanerozoic. The Ghawar structure is the world's largest oil field with most of the oil and gas hosted by carbonate rocks, with evaporite seals (Al-Jallal, 1989; Wender et al, 1998). The main aims of this project were to document the facies stacking within the cores, develop a more refined depositional model, perform a sequence stratigraphic analysis and generate facies maps for selected intervals. From this, a high resolution sea level curve was generated for comparison with global curves. The study documents a major relative sea level fall at the Permian Triassic Boundary (PTB) in contrast to many areas in which the contact appears to be conformable. Prior to the study the effects of the Ghawar structure on deposition on the shallow platform, and the directions of progradation of the facies were poorly known. The study provides a better understanding of the controls on porosity preservation associated with anhydrite plugging in the oolitic reservoir facies, associated with distance or proximity to evaporitic salinas and tidal flats.

The second part of the dissertation documents the C and O isotope profiles obtained from the carbonate sediments in the cores, across the Permian Triassic boundary (PTB). Previous workers have shown elsewhere that the PTB is characterized by major C isotope

excursions, which appear to relate to massive injection of light C into the atmosphere and oceans. This caused warming and ultimately the mass extinction in which ~95% of the marine species became extinct (Erwin, 2006). This study provides detailed C and O isotope profiles tied to high resolution, detailed lithologic logs, in contrast to many studies, for which the lithologic data is highly simplified. This approach has allowed the local versus global influences on the isotope excursions to be examined. In addition, the depletion of the U concentration of the carbonates across the PTB defined by gamma ray logs, also is documented for Ghawar and its origin evaluated. The study has shown that besides the two major, commonly documented C isotope excursions, several other excursions also appear to be correlative globally, suggesting that they could provide a high resolution correlation tool.

CHAPTER 2

SEQUENCE DEVELOPMENT ACROSS THE PERMO-TRIASSIC EXTINCTION EVENT, UPPER KHUFF CARBONATES, GHAWAR FIELD, SAUDI ARABIA

ABSTRACT

Logging of cores of the Upper Permian and Lower Triassic Khuff Formation, Ghawar, Saudi Arabia, has allowed a high resolution sequence stratigraphic framework to be generated. The lithofacies of this huge, arid epeiric ramp succession include: subaqueous-and supratidal anhydrite, tidal flat laminites, lagoonal mudstone, ooid-peloid grainstone, and subtidal off-shoal open marine mudstone.

Third order sequences include the Late Permian, upper Khuff C, the Early Triassic Khuff B and the Khuff A sequences, which correlate with global cycles. Seven high frequency sequences (HFSs) make up the Changhsingian upper Khuff C. These HFSs are ~400 k.y. duration and probably driven by long term eccentricity. The Early Triassic Khuff B and A are made up of 4 HFSs each, appear to be ~100 to 200 k.y. duration and not easily tied to eccentricity forcing. The HFSs are in turn composed of parasequences, which appear to be 10 to 20 k.y. average durations, suggesting precessional and half precessional forcing. However, many thin locally developed cycles may be autocycles or subprecessional cycles.

Sequence stratigraphic cross sections and facies maps document progradation directions on the platform, reflecting the subtle interplay between the Ghawar structure and regional paleoslopes. Anhydrites are rare in the Permian Upper Khuff C except near the base of the studied interval. Anhydrites are well developed in the Triassic Khuff B and Khuff A where

some form transgressive deposits while others are highstand deposits of high frequency sequences.

The Permo-Triassic boundary (PTB) on the Arabian Platform marks a significant relative sea-level drop, that exposed from the outcrop belt to somewhere east of Ghawar. This contrasts with transgressive PTB settings elsewhere. Across the PTB the mass extinction is marked by a major decrease in biotic groups. The extinction was followed by development of subtidal thrombolites, and increased microbial calcification due to decreased bioskeletonization.

The dominant reservoirs in the Permian Upper Khuff C occur in oolite in the uppermost high frequency sequence. , In the Triassic Khuff B and A the reservoir facies are commonly non-dolomitized oolitic facies associated with open lagoon facies distant from evaporitic tidal flats. Within dolomitized units, best reservoirs are associated with oomoldic porosity, but oolite proximal to evaporitic tidal flats have porosity plugged by anhydrite.

INTRODUCTION

This study documents the high resolution sequence stratigraphy of the Late Permian-Early Triassic Khuff carbonates and evaporites in Ghawar Field, which is the world's largest oil field (Fig. 2.1 a, b). The Khuff Formation contains major gas reserves in the Middle East, and the interval is a major gas producer in both onshore and offshore Saudi Arabia. It formed within the interior of a major epeiric platform on the north eastern passive margin of Gondwana. The Khuff Platform was an immense carbonate-evaporite platform (2,500 by 1,500 km) that extended throughout the Middle East and into the present Zagros fold-thrust belt to the north east. The platform was several times the size of the modern Bahamas

Platform, and much larger than any modern analogs. Thus the study provides insight into processes in the interior of such a large epeiric platform.

The Permian-Triassic also was a time of global greenhouse, relatively ice free conditions and so the Khuff succession consists of a bewildering array of meter and sub-meter-scale parasequences. The Permian-Triassic also was a time of aragonite-high Mg seas which controlled the mineralogy and dolomitization potential of the deposited carbonates (Scotese et al., 1999; Stanley and Hardie, 1998).

The cored rocks of the Khuff Formation provide a relatively continuous record across the Permian-Triassic boundary (PTB), which is the most severe mass extinction in the earth's history. As such, the cores should record the sea-level-, oceanographic, climatic and tectonic history of the region leading up to, during and following this major event. The studied succession at Ghawar is unusual in that paleosols mark short periods of emergence during PTB time, in contrast to many areas where this is a time of transgression (Erwin, 2006; Inslaco et al., 2006). The high resolution sequence framework generated allows the evaluation of the subtle interplay of tectonics and shallow water carbonate deposition across the Ghawar structure, which for much of its Late Paleozoic to Cenozoic history resisted subsidence compared to the surrounding region. The study also documents the two carbon isotope excursions in the late Permian interval (Baud et al., 1989; Erwin, 2006), the upper coinciding with the Permian-Triassic extinction. The excursions have been ascribed to volcanic outgassing coeval with development of several large igneous provinces, methane releaseand a possible impact event (Krull and Retallack, 2000; Jin et al., 2000; Erwin, 2006). Spectral gamma ray and total gamma ray logs of the cored wells (Inslaco et al., 2006) were

used to track redox conditions of the global ocean and sequestering of Uranium across the PTB.

GEOLOGICAL SETTING OF THE KHUFF FORMATION, GHAWAR

Paleogeography, Regional Setting and Structure

Separation of the Arabian Plate and the Iran-Turkey Plate began in early Late Devonian time and was completed by the early Late Permian, and allowed the Palaeo-Tethys Sea to advance from the south onto the Arabian Plate (Fig. 2.2). This allowed shallow seas to cover present-day Syria, Iran, southern Turkey, Arabia and Iraq. During the Permo-Carboniferous ice age, the Arabian Plate was between 30ºS and 55ºS, moving northward with Gondwana (Sharief, 1983; Ziegler et al., 1997; Konert et al., 2001). By Late Permian onset of greenhouse conditions (Frakes et al., 1992; Fielding et al., 2008), the Arabian Plate lay at 10ºS to 35ºS and by the end of Khuff deposition in the Early Triassic, northernmost Arabia had reached 5ºS (Fig. 2.2; Konert et al., 2001; Sharland et al., 2001).

A major unconformity underlies the Khuff Formation, and is a Middle Permian break-up unconformity (Fig. 2.3), termed the "Pre-Khuff Unconformity". Its age is approximately 268 Ma (Ogg et al. 2008 time chart), and it marks inception of the Neo-Tethys Ocean along the present-day Zagros-Oman suture, as well as the major Permian transgression. This resulted in expansion of the Neo-Tethys Ocean (Al-Aswad, 1997; Sharland et al., 2001; Konert et al., 2001). Shallow seas spread over most of the Arabian platform during this major transgressive event, which marks a change from mainly siliciclastic- to carbonate-evaporite deposition as the Arabian Plate moved northward to warmer and drier, lower latitudes. This caused shallow marine carbonates and evaporites to be deposited over much of the Arabian Plate (Fig. 2.4;

Al-Jallal, 1989 and 1995; Ziegler, 2001). Sea-floor spreading within the Neo-Tethys ocean basin continued through the Early Triassic (Al-Aswad, 1997).

The Permian-Triassic Khuff Formation was deposited on a huge, east-facing, arid ramp (Al-Dukhayyil et al., 2006; Insalaco et al., 2006) that formed an eastward thickening wedge, up to 450 m in the Ghawar study area, and up to 1500 m in Iran in the fold thrust belt (Fig. 2.5) (Al-Jallal, 1995). Between the Arabian Shield and Ghawar the Khuff units thicken slowly, but across Ghawar there is a major increase in thickness, after which the Khuff then thickens gradually into eastern Arabia (Fig. 2.6 a, b). Updip, the Khuff succession crops out along a 1200 km long, north-south trending belt in the west near the Arabian Shield (Fig. 2.1). Outer-shelf and shelf edge facies are exposed in Oman and Iran (Angiolini et al., 2003; Heydari et al., 2000; Insalaco et al., 2006; Koehrer et al., 2010).

Subtle syndepositional growth of structures, extensive carbonate sand and evaporite deposition, along with subsequent diagenetic events resulted in the development of high quality reservoirs in the Khuff carbonates. Wide, broad and gentle structures that mostly include folds and domes, formed during the Precambrian-Early Paleozoic along the eastern part of the Arabian Plate within the Zagros Foreland (Al-Husseini, 2000). These structures are major domal features with 4-way closure and set the stage for some of the world's best oil and gas reservoirs (Al-Jallal, 1989 and 1995; Konert et al., 2001). The proven regional Silurian hydrocarbon source rock and the extensive regional seal of thick Triassic red-beds, evaporites, and carbonates complete an optimum hydrocarbon system (Konert et al., 2001; Wender et al., 1998).

The Ghawar structure which makes up the study area, forms the southern part of the 500 km long En Nala anticline (Fig. 2.1; Al-Husseini, 2000). The Ghawar is located on the

interior of the Khuff platform, some 650 km from the platform margin in Iran. The Ghawar structure developed over N-S trending basement-involved uplifts (Konert et al., 2001; Wender et al., 1998). It is a 240 km long by 30 km wide and is an elongate dome with 4-way closure. Subtle highs occur in the north and the south of the structure. The structure likely was active in the Permian and Triassic, perhaps as a subtle positive area on the regional platform. The structure has continued to increase in structural relief throughout the Mesozoic and Cenozoic (Wender et al., Al-Husseini, 2000).

Stratigraphy and Age

In the subsurface of Ghawar Field, eastern Saudi Arabia, the Khuff Formation lies at depths of 3000 m (10,000 ft), and overlies Permo-Carboniferous Unayzah siliciclastics (Fig. 2.3). It is 450 m thick with the gas-bearing reservoir intervals within the upper 270 meters (900 feet). It is overlain by Triassic Sudair Shale.

***Biostratigraphy*:** The subsurface Khuff Formation (Fig. 2.3) is divided into the Khuff D, including the Basal Khuff Clastics (BKC) or "Khuff E" of Al-Jallal (1995), lower Khuff C, upper Khuff C of Permian age and Khuff B and Khuff A of Triassic age (Al-Dukhayyil et al., 2006; Hughes, 2005 and 2009). The best porosity in developed in the Khuff A, B, and C units. Manivit et al. (1986) assigned the exposed Khuff Formation a late Permian to early Triassic age in western Saudi Arabia. More recently, Vaslet et al (2006) refined the ages of all Khuff members in outcrop (Fig. 2.3) based on small benthic foraminifers, algae, and ostracods. The age of the Khuff Formation across the Arabian Plate ranges from Middle Permian, Wordian stage to Early Triassic Induan stage (Sharland et al 2001; Hughes, 2005; Alsharhan, 2006; Insalaco et al., 2006). In the Saudi Arabian subsurface (Fig. 2.3), Khuff D Carbonates (including the Basal Khuff Clastics), are possibly late Wordian (?) to Capitanian.

The Lower Khuff C Carbonate Member is Wuchiapingian to Changhsingian (?) and the upper Khuff C is Changhsingian (Alsharhan, 2006; Hughes, 2009). The Khuff B and A Carbonates are early Triassic (Induan) (Al-Jallal, 1995; Hughes, 2009).

The present study proposes that the Wuchiapingian-Changhsingian boundary is placed in the upper part of a 5.5 m thick interval of six mudcracked, tidal flat-dominated parasequences each capped by emergence breccias, which mark a major sequence boundary (Fig. 2.7). This brecciated zone has the thickest stacked breccias within the upper Khuff Formation in Ghawar, indicating a major relative sea-level fall. Paleontologically, this boundary separates the underlying almost barren section from the overlying foraminiferal-rich interval. This biodiverse Changhsingian Khuff unit is dominated by miliolid and fusulinid foraminifera, green and red calcareous algae, bivalves and gastropods. Lagenids foraminifera and ostracods are less common, whereas bryozoans, crinoids, and brachiopods are restricted to the uppermost Changhsingian units, 3-4 m below the Permo-Triassic boundary.

***Carbon Isotope Chemostratigraphy*:** Ages of units also were broadly constrained by carbon-isotope chemostratigraphy (Fig. 2.8; Chapter 3). The Ghawar C-isotope profile correlates reasonably well with the C isotope profile of Koehrer et al. (2010) for the Saiq Fm (Permian Khuff equivalent) in Oman, and that of Baud et al. (1989) for the Changhsing Formation at Meishan section, China (Fig. 2.8). The C-isotope profile shows a short lived major negative C excursion across the sequence boundary zone spanning the Wuchiapingian-Changhsingian boundary that correlates well with China. The $\delta^{13}C$ values just below the boundary are about $+5‰_{PDB}$, which decrease sharply near the boundary to as low as $0‰_{PDB}$ then quickly recovering to $+4‰_{PDB}$ above the boundary. A grossly similar signal is evident in the Oman

section, although the $\delta^{13}C$ values above the boundary do not return to the high values before the boundary.

There are several negative followed by positive excursions within the Changhsingian which appear to correlate with the other sections. These smaller events appear to be associated with sequence boundaries within the Ghawar section.

The PTB at Meishan shows the classic $\delta^{13}C$ excursion across the boundary, starting with a major negative excursion of about 5‰ $_{PDB,}$ after which it stays relatively low (Fig. 2.8). Ghawar exhibits a similar signal, although the details vary from well to well, in terms of the position of the most negative part of the curve relative to the PTB (Fig. 2.8). It has a distinctive C-isotope signal that shows a gradual decrease across the PTB.

METHODS

Thirty cores were logged at the at the Saudi Aramco Core Laboratory in Dhahran, Saudi Arabia, with an aggregate total of 2,135 meters of core spanning the upper Khuff C, B, and A members. Fourteen cores and wireline logs were selected for generating high resolution sequence stratigraphic cross sections on the basis of having the most complete continuous cored intervals (typically 75-155 m long) from the Early Triassic to Latest Permian. The remaining 16 cores logged, along with sixteen cores described by Aramco geologists (Aus Al-Tawil, Ghazi Al-Eid, Roger Barnaby and Nasser Al-Ghamdi) were used to develop the facies distribution maps.

Descriptive core logs include percent mineralogy (porosity, calcite, dolomite, anhydrite), sedimentary structures, lithologic contacts or surfaces (paleosols, erosion surfaces, hardgrounds, firmgrounds), carbonate texture (Extended Dunham Classification (Dunham,

1962; Embry and Klovan 1971), grain size, sorting, relative abundance of non skeletal grains and fossils and any diagenetic features..

Core runs were depth shifted against the wireline logs (caliper, gamma, sonic, density, neutron porosity) using the following: a. gamma logs done on the cores along with drillers depths, were used to tie the cores to the log gamma b. the observed percent porosity in the cores also were used to tie to porosity logs and c. pure anhydrite intervals in core were tied to bulk density logs.

The carbonate/evaporite facies (from core, wireline logs and thin sections of core plugs) were used to characterize the facies types, which were color coded on the lithologic columns. Parasequences were defined based on flooding surfaces. Using Walther's Law, a depositional facies model was developed to arrange the facies for near shore to offshore along a ramp profile. Fischer (accommodation) plots from the cycle data logged in the cores, using the Excel program of Husinec et al (2008) were used to test whether these would define accommodation changes throughout the sections, for comparison with the global sea-level cycle charts (Haq and Al-Qahtani 2005; Haq and Schutter 2008; Markello et al 2008).

Two dimensional cross sections were constructed from the core data to map regional extent of parasequences, parasequence-sets, and various scales of depositional sequences defined on bounding surfaces (sequence boundaries and maximum flooding surfaces). Using the cross sections, 3rd order and component 4th and 5th order sequences were mapped throughout the study area. For each sequence, facies maps were constructed for the maximum flooding interval, the dominant highstand facies and the late highstand facies directly beneath the overlying sequence boundary. These helped to better understand 2-D lateral variation in facies, directions of progradation, and any subtle interplay of tectonics and sedimentation.

Thin sections of core plugs were examined under the petrographic microscope to document biodiversity changes across the PTB. Fossils were identified at the generic or (where this was difficult) group level, and the data plotted alongside the stratigraphic columns. Whole rock C/O isotope sampling was done by drilling butts of cores on a meter-scale spacing to define any major C/O excursions (significant excursion at PTB), define any isotopic shifts beneath paleosols and better understand the origin of the dolomites in the succession.

UPPER KHUFF FACIES AND DEPOSITIONAL ENVIRONMENTS

The facies in the Upper Khuff carbonate-evaporite succession are summarized in Table 2.1, their relative distribution shown on the depositional model (Fig. 2.9), and slab photos of the facies are shown in Figure 2.10. Figure 2.11 shows rock examples of paleosols, and the vertical distribution of facies within idealized parasequences are shown in Figure 2.12. The vertical stacking in one well is shown in Fig. 2.13 a, b. The regional vertical and lateral facies distribution is shown on the cross-sections (Figs. 2.14 and 2.15).

Paleosol Breccias with Root Traces

These units (Table 2.1; Fig. 2.10 a, 2.11) are generally 0.15 m to 2.0 m thick and commonly overlie units with desiccation cracks and microbial lamination. They are grey-to-tan, and consist of fitted-fabric breccias with root traces and karstic collapse features infilled with angular sand to gravel sized intraclasts of unfossiliferous anhydritic dolomudstone and wackestone in a lime mudstone matrix. Paleosols characterize the PTB, as well as many of the sequence boundaries (at least locally), and also occur on tops of some parasequences locally.

These facies were formed during subaerial exposure characterized by alternating periods of desiccation, dissolution, and brecciation induced by alternating heating, cooling and root disruption (Al-Jallal, 1989; Esteban and Klappa, 1983; Insalaco et al 2006). The relative absence of caliche indicates lack of seasonal wet/dry conditions (James, 1979) implying a dry climate perhaps with meteoric waters from rare flash floods causing dissolution of the exposed carbonates.

White Nodular-to-Massive Anhydrite (Supratidal Sabkha)

Nodular to massive anhydrites (Table 2.1; Fig. 2.10 b) occur in beds from 5 cm to 1.5 meters thick. The anhydrite units typically are displacive, and occur within 0.3 m below the exposure surface. They consist of white-to-grayish white anhydrite that is massive, nodular or bedded with locally developed fine lamination. The nodules are scattered within mudcracked or laminated dolomite or in packed clusters (chicken-wire anhydrite) with gray-to-black seams of dolomudstone or organic residue commonly between nodules. Rip-up clasts and/or peloid grains float in the anhydrite.

These massive to nodular anhydrites were deposited in supratidal sabkhas, by displacive growth of anhydrite and possibly some replacement of carbonate (Al-Jallal, 1989; Kendall, 1979a; Warren and Kendall, 1985). Salinities of groundwaters were in the anhydrite field implying low activity of water (related to extreme evaporation of groundwaters due to arid climate) (Hardie 1967).

Laminated Anhydrite (Subaqueous Salina/Saltern)

This laminated anhydrite facies (Table 2.1; Fig. 2.10 c) is from 0.1 to 4.0 m thick and generally rests either with sharp or gradational contact on peritidal dolomite. It grades up into

or is overlain with sharp contact by peritidal dolomite. These anhydrites are black or dark grey to white, laminated, non-displacive and locally are interlayered with massive or nodular anhydrite Black carbon-rich laminae in the anhydrites are degraded microbial layers, while disseminated carbon causes the dark coloration of the anhydrite.

These facies were deposited in extensive subaqueous restricted ponds or salinas with waters in the sulphate precipitation field, indicated by well preserved lamination, and lack of mudcracks or dolomitic laminites. Rare burrow mottling was produced by salinity tolerant organisms, possibly shrimp. Relative scarcity of vertical growth fabrics suggests that substrate-attached crystal growth was rare (Al-Jallal, 1989; Kendall, 1979b; Warren, 2006). The black anhydrites probably formed in slightly deeper, more stagnant waters with abundant microbial organics than laterally equivalent white anhydrites.

Crinkly Laminated Dolomudstone (Intertidal Flat)

The crinkly laminated dolomites (Table 2.1; Fig. 2.10 d) commonly cap parasequences, and generally are overlain by subaerial exposure surfaces. They form ~5 cm to 2 m thick beds of dolomudstone and rare skeletal pellet wackestone that are light-to-medium grey and brown, with crinkly microbial lamination (locally micrograded), fenestrae, burrow-mottles, and mud cracks.

Mudcracked crinkly laminated facies formed in intertidal flats. Laminites could have developed burrow-mottling in lower intertidal (to shallowest subtidal?) settings. Fenestrae in laminated dolomites probably also formed in lower intertidal to very shallow subtidal settings due to tiny worm dwelling burrows, desiccation and gas evolution (James, 1977; Demicco and Hardie, 1994).

Ripple Laminated Dolosiltites (Shallow Lagoonal Sand-Flats)

These ripple laminated dolomites (Table 2.1; Fig. 2.10 e) occur in beds from 5 cm to 1 m thick. They are tan to brown, ripple-laminated and are composed of dolosiltite (precursor fine pellet grainstone-packstone) with small anhydrite nodules, common horizontal burrows (less than 5 mm diameter) and are unfossiliferous.

These ripple-laminated dolomites were deposited on gentle wave- and tidal current reworked, shallow subtidal to lower intertidal sandflats bordering intertidal flats (Wilson and Jordan, 1983; cf. Evans 1975). High substrate mobility probably inhibited growth of mats, and sparse infaunal organisms formed horizontal burrows.

Vertical Tubular Dolomudstone-to-Wackestone (Shallow Hypersaline Restricted Lagoon)

This distinctive facies (Table 2.1; Fig. 2.10 f) is confined to the Latest Permian interval (cf. Insalaco et al 2006), and forms beds from 0.5 to 3.5 m thick. They are tan to dark grey, massive units with vertical tubes (up to 25 cm long, and up to 1 cm diameter); lithologies are dolomudstone to very fine peloid wackestone, with scattered anhydrite nodules. The tubes commonly are filled with nodular white anhydrite or clear burial anhydrite.

These facies formed in restricted low energy lagoons in which infaunal organism formed vertical dwelling burrows (cf. Insalaco et al., 2006). Although some could be root traces (Insalaco et al., 2006), the lack of bifurcation argues against this, unless they are analogous to pneumatophores of modern mangroves (but formed by a non-angiosperm plant).

Massive-to-Laminated Muddy Carbonates and Thrombolites (Moderately Restricted Lagoon)

These facies (Table 2.1; Fig. 2.10 g) form beds from 20 cm to 3 m thick, that are grey-to-dark grey, massive, thin- to medium-bedded. They have millimeter-to-centimeter, planar-to-wavy, millimeter to centimeter lamination, vertical and horizontal burrows, hardgrounds and rare microbial lamination. They are composed of lime mudstone to fine peloid skeletal wackestone. In the Early Triassic units, but not the Permian, clotted gastropod-bearing thrombolitic packstone/wackestone and/or digitate stromatolites are associated with these mudstone/wackestones.

These muddy facies were deposited in low-energy subtidal lagoons on or behind grainstone barrier shoals (Al-Jallal, 1989; Wilson and Jordon, 1983). Laminated mudstones possibly were deposited in very shallow restricted settings, in which bioturbation was inhibited perhaps by high salinity. Massive mudstone were formed in slightly deeper, more distal settings in which layering was destroyed by bioturbation (Al-Jallal, 1989). The thrombolitic and digitate stromatolite units of the Early Triassic were formed in settings with impoverished biotas that resulted from the end-Permian extinction. Thrombolites likely formed on heads covered by calcified coccoid mats (Kennard and James, 1986) whereas digitate stromatolites formed beneath filamentous colloform mats in the shallow subtidal zone (cf. Logan et al., 1974; Jahnert and Collins, 2012).

Skeletal Peloid Packstone/Grainstone (Sand Sheets)

This facies (Table 2.1; Fig. 2.10 h) forms a relatively coarse grained sheet-like unit 1 to 2 m thick in the Early Triassic upper Khuff A Sequence, occurring in both back shoal and intershoal positions, as well as on the shoal crest. It is a brown, massive skeletal peloid

dolopackstone/grainstone, and less common peloid skeletal packstone/wackestone composed of poor-to-moderately sorted fine-to-coarse peloids, and abundant granule- to pebble- size whole and fragmented bivalves and gastropods. Greenish gray clay-to-silt sized carbonate and anhydrite fills skeletal molds and/or less commonly interparticle pores.

The regional sheet-like distribution of this Early Triassic unit, extending across the region in both on shoal and inter-shoal positions, suggests that it marks a regional shallowing event of relatively high energy. It differs from the back-shoal grainstones of the Permo-Triassic in that it is much more widespread and not confined to backshoal locations (Al-Dukhayyil, 2007).

Wackestone-to-Packstone (Back Shoal)

These facies (Table 2.1; Fig. 2.10 i) form 0.3 to 1.5 m thick units that are brown, horizontally burrowed to intensely bioturbated to structureless (Fig. 2.10 i). They are lime- to dolomitic lime- wackestone-to-packstone, composed of moderately sorted, very fine-to-medium and less common coarse sand-size peloids and/or ooids, bivalve and gastropod debris, ostracods and minor pebble-size carbonate mud intraclasts.

The location of this facies behind and above grainstone shoals suggests that it formed in protected, low energy back-shoal and inactive shoal crest settings. This resulted in poorly winnowed facies, burrow-mixed grainy and muddy layers, and bioturbation and destruction of any mechanical sedimentary structures that formed during intermittent higher energy events (Wilson and Jordan, 1983; Handford, 1988).

Oolitic Grainstone (Shoal)

These form 0.2 to 12 m thick carbonate sand units from tens to hundreds of meters wide. They are light to medium brown and cross-bedded with planar, millimeter-to-centimeter cross-strata (Figs. 2.10 j and k). They range from undolomitized to completely dolomitized grainstone composed of well-sorted, fine-to-medium and less common coarse sand-size ooids with concentric structures, along with peloids. In the Permian units, there are also foraminifera, green algae, and rare brachiopod, bryozoans and crinoid debris. More restricted assemblages of bivalves, ostracods and gastropods characterize the Triassic. Oomoldic porosity is common.

These cross bedded oolitic grainstones were formed on high energy shoal crests with highly mobile substrates reworked by fair-weather waves and tidal currents, indicated by cross-bedding and limited burrowing (Harris, 1983; Harris et al., 1993; Wilson and Jordan, 1983; Rankey et al., 2006). These ooids formed in aragonite seas with high Mg/Ca ratios (Stanley and Hardie, 1999), indicated by concentric structures within ooids and common oomoldic porosity. They indicate high levels of supersaturation with respect to aragonite in the marine platform interior, likely related to elevated salinities due to arid climate and high evaporation, and low abundance of calcareous biotas.

Intraclast Ooid Packstone/Grainstone (Storm Influenced Fore-Shoal)

This facies (Table 2.1; Fig. 2.10 l) is up to 2 m thick, and is interbedded with mudstone-to-wackestone. It consists of medium to dark brown, thin to medium layered, undolomitized to dolomitized packstone-to-grainstone, composed of fine to medium sand size ooids and peloids and granule- to pebble-size intraclasts which locally form flat pebble conglomerate layers.

These intraclast-ooid sands formed on the storm-influenced flanks of shoals. This is indicated by their close association with subtidal muddy facies, and the updip thickening of the lime sand units into oolitic shoal complexes (Seilacher and Aigner, 1991).

Lime Mudstone (Off-Shoal Open Marine)

These lime mudstones form up to 8 m thick units in the Early Triassic (Table 2.1; Fig. 2.10 m, n and o). They are dark gray-to-dark brown units that occur down-dip of oolitic shoals. These lime mudstones are associated with decimeter-scale cycles of microbial laminites and thrombolites with rare horizontal burrows. Thrombolites contain up to 25% gastropod shells.

These lime mudstones are considered the most distal facies in the studied succession. Their downdip position is indicated by position underneath and downdip of oolitic shoals (Al-Dukhayyil, 2007). They formed in distal marine, possibly low-oxygen, low-energy settings below storm-wave base that favored accumulation of carbonate mud. In the Permian, this facies contains crinoids and bryozoans in the offshore fields of Saudi Arabia (personal observation) and Iran (cf. Insalaco et al 2006). Thrombolites that are common in this facies in the Triassic formed in a manner similar to those in the restricted lagoon facies.

STACKING OF FACIES IN PARASEQUENCES

Facies within the Permian and Triassic Khuff Formation are arranged in parasequences in which successively more seaward facies are overlain by more landward facies, and whose tops are bounded by flooding surfaces. In defining parasequences, water depth was considered of lesser importance than the relative landward or seaward position on the ramp, given the inferred subtle topography related to shoals, lagoons and salinas. Six basic types of

parasequences (Fig. 2.12) occur, and include 1. open marine, lime mudstone-dominated (open lagoon), 2. ooid grainstone-dominated (shoal), 3. restricted carbonate mudstone-dominated (lagoon), 4. carbonate laminite-dominated (peritidal flats), 5. anhydrite capped parasequences (very restricted lagoon), and 6. subaqueous and supratidal anhydrite parasequences (evaporitic salinas and sabkhas). Exposure features such as paleosols or breccias are common near sequence boundary zones. These parasequences occur repeatedly throughout the upper Khuff in Ghawar.

Open marine, lime mudstone-dominated parasequences (open lagoon): These parasequences are 0.3 to 17 m thick, and typically consist of transgressive, thin beds of peloid/ooid grainstone and interlayered carbonate mudstone passing up into open lagoon, thick lime mudstone (and thrombolites in some Triassic units), shallowing up into thin or relatively thick beds of grainstone. Some cycles have thrombolites capping grainstone units. In a few cycles in the Triassic Khuff B sequence, the upper grainstone unit shallows up into thin restricted lagoonal mudstone.

Ooid grainstone-dominated parasequences (shoal): These parasequences are 0.2 to 5 m thick, and typically consist of ooid grainstone and packstone, commonly with a basal transgressive intraclast lag overlain by lagoonal carbonate mudstone and tidal flat carbonate laminite (may be absent). They are locally thrombolitic in the Triassic Khuff Formation. These parasequences may capped by fitted-fabric or incipient breccias or paleosols. This parasequence type is present throughout the study interval (upper Khuff Formation).

Restricted carbonate mudstone dominated parasequences (lagoon): These parasequences are 0.2 to 4 m thick, and commonly have a thin basal grainstone/packstone, a relatively thick restricted lagoonal carbonate mudstone, overlain by tidal flat microbial laminites-to-

mudcracked mudstone with nodular anhydrite. Incipient/fitted-fabric breccias or paleosols may cap the parasequence. In the Permian, the restricted lagoonal mudstone commonly has vertical burrows or/and root-like structures. This facies is locally thrombolitic in the Triassic.

Anhydrite Capped Parasequences (very restricted lagoon): These parasequences are 2 to 4 m thick, and commonly consist of thick ooid/peloid grainstone, that is rarely overlain by thin restricted peritidal carbonate, and commonly capped by subaqueous anhydrite. This parasequence type is dominant in the Triassic Khuff A sequence.

Laminite-dominated parasequences (peritidal flats): These parasequences are 0.1 to 2 m thick, and consist of thin basal grainstone/packstone (may be absent), a relatively thin restricted carbonate mudstone, capped by well-developed microbial laminites that may have mudcracks and evaporate nodules. Breccias or paleosols cap some parasequences. This parasequence type is present throughout the study interval.

Anhydrite dominated parasequences (salina/sabkha): These parasequences are 0.1 to 4 thick, and may contain a thin basal carbonate, commonly with a thin microbial top, overlain by a thicker unit of layered anhydrite (subaqueous salina) and nodular anhydrite (sabkha). This type of parasequence occurs in the Triassic Khuff sequences.

DEPOSITIONAL SEQUENCE STRATIGRAPHY

Depositional sequences are genetically related rock units bounded by unconformities and their correlative conformities; they reflect a cycle of relative sea-level lowstand, followed by increasing and then decreasing accommodation (Mitchum and Van Wagoner, 1991; Vail, et al., 1977). Depositional sequences in the upper Permian-Triassic Khuff Formation were mapped on the basis of landward and basinward shifts in facies, stacking patterns of

parasequences, and presence of exposure surfaces. *Sequence boundaries* were picked on single or multiple exposure surfaces (fitted-fabric breccias and paleosols), or on top of peritidal carbonates or evaporites units, beneath more open-marine facies. The exposure breccias either formed a single horizon marking sequence boundaries, or commonly in the upper Permian, sequence boundary zones containing multiple breccia layers (cf. Montanez and Osleger 1993; Markello et al 1992). Transgressive- and Highstand Systems Tracts (TST and HST respectively) were defined by mapping the intervening *maximum flooding surface* MFS*).* The maximum flooding surfaces in these highly cyclic, aggraded platform successions were placed at the turnaround between open marine, thick parasequences of the higher accommodation TST and the overlying thinner parasequences dominated by tidal flat carbonate/evaporites marking decreased accommodation of the HST (Sarg, 1988; Koerschner and Read 1989; Montanez and Osleger 1993).

The characteristics of the Latest Permian-Early Triassic Khuff sequences are summarized in Tables 2.2 and 2.3 and the facies stacking in selected wells is shown in Figures 2.12 a and b. The regional facies distribution, sequences and bounding surfaces are shown on the cross-sections in Figures 2.13 and 2.14. In the sequence-stratigraphic cross sections (Figs. 2.14, 2.15), individual facies are lumped into the following facies associations: supratidal sabkha, subaqueous salina, intertidal flat, restricted lagoon, backshoal, shoal, foreshoal and open lagoon (Fig. 2.9), characterized by their associated parasequence types (Fig. 2.12). Facies maps showing the distribution of facies during MFS, HST and immediately beneath the top sequence boundary, are shown in Figure 2.16.

Second Order Supersequence and Composite Sequences, Late Permian to Early Triassic Khuff Formation, Ghawar Field

Late Permian Early Triassic Supersequence: The upper Middle Permian basal Khuff clastics, along with the Late Permian-Early Triassic Khuff carbonates and evaporites (Khuff D, lower C, upper C, B and A units) and the overlying Early Triassic Sudair shale, form a second order supersequence (Fig. 2.3) approximately 21 m.y. in duration, bounded at the base and top by major unconformities (Haq and Al-Qahtani 2005; their Enclosure 2).

***Composite Sequences*:** The Basal Khuff clastics along with the Permian Khuff D, lower Khuff C and upper C carbonate-evaporite units, form a Late Permian composite sequence approximately 15.5 m.y. duration (Fig. 2.3). The Khuff D interval contains the maximum flooding surface P20, the lower Khuff C contains the maximum flooding surface P30 and the upper Khuff C contains the maximum flooding surface P40 of Sharland et al., (2001).

A second composite sequence is formed by the Early Triassic Khuff B, the overlying Khuff A interval, and the Sudair Formation (approximatley 5 m.y. duration). The Khuff B and the A form the TST (80-110 m thick and approximately 1.5 m.y. duration) and contain the maximum flooding surfaces Tr10 and Tr20 respectively of Sharland et al. (2001). The overlying shale-prone Sudair Formation forms the HST of this upper composite sequence (Fig. 2.3).

Late Permian Upper Khuff C High Frequency Sequences

The late Permian part of the Khuff study interval (up to 111 m thick) spans the upper third of the lower Khuff C (capping the Khuff C reservoir), and the entire upper Khuff C interval (up to 66 m thick). This study recognizes seven high frequency sequences (HFS UC-1

to 7) in the upper Khuff C interval, although sequences 1, 2 and lower 3 are penetrated only by a single core, which extends down into the lower Khuff C sequence 5 (LC 5; Fig. 2.14).

Late Permian Sequence Boundaries: Most of the basal boundaries of the upper Khuff C sequences (Table 2.2) are planar to slightly erosional surfaces on anhydrite, laminite or breccia. The breccias may occur as a single bed or a zone (1.5 to 5 m thick) composed of two or more breccia horizons.

On the cross section the basal sequence boundaries of sequences LC-5 and UC-2 occur on a regional subaqueous anhydrite. In northern Ghawar, the basal sequence boundaries of UC-1, 4, 5 and 6 are underlain by several breccia horizons that make up the sequence boundary zone. The other basal sequence boundaries are generally planar to erosional surfaces underlain by fitted-fabric breccia, incipient breccia and paleosols and/or laminites.

Maps showing the facies beneath the overlying sequence boundaries (latest HST maps) are shown in Figure 2.16 a suggest that the directions of progradatoin were to the north in UC-6a and to the south in UC-6b and UC-7. For facies capping sequences UC-5 to UC-7, emergence breccias show localized development at the north and south of Ghawar in UC-5, to local development in southern Ghawar and local islands in UC-6a, to local islands and exposure in north Ghawar in UC-6b. This culminates in regional exposure over Ghawar at the top of UC-7, at the Permian Triassic boundary. Overall, these facies maps suggest that the directions of progradatoin were to the north in UC-6a and to the south in UC-6b and UC-7.

Late Permian Transgressive Systems Tracts (TSTs): The facies stacking within the TSTs is shown on the cross section (Figure 2.14). Based on the few cores cut through most of LC-5 (beneath the study interval), the TST of LC-5 is dominated by restricted lagoonal

dolomudstone parasequences. Packstone/grainstone units are thin and relatively minor, and most parasequences are capped by tidal flat laminated dolomudstone, and less commonly by sub-aqueous salina anhydrite. The TSTs of UC-1 to 5 consist of peritidal mudstone parasequences that pass upward into grainstone parasequences. In UC-6, the TST is dominated by peritidal parasequences, with very minor thin grainstone facies in the northern and southern Ghawar, and thicker grainstone/packstone parasequences in central Ghawar. The TST of UC-7 consists of dolomitic ooid grainstones, which are bryozoan-crinoid-bearing in northern Ghawar. The MFSs of UC-1 to 7 were placed above the grainstone intervals (Figure 2.14).

Facies maps of the maximum flooding facies (Fig. 2.16 a) show that ooid grainstones blanket the bulk of Ghawar in UC-5 and 6a, whereas in UC-6b the ooid grainstones occur in northern Ghawar, with back-shoal packstones over southern Ghawar. In UC-7, there is a return to widespread oolite deposition over Ghawar (Fig. 2.16 a).

Late Permian Highstand Systems Tracts (HSTs): Facies stacking within the HSTs is shown on the cross section (Figure 2.14). The progradation directions are not clear in the cross section (Fig. 2.15) although facies packaging shows more open conditions to the south in UC-5 and UC-7, and to the north in UC-6b. The HST of LC-5 is made up of restricted mudstone parasequences that grade up into laminite- and supratidal anhydrite capped parasequences, some of which are capped by breccia. The HSTs of UC-1 to UC-6 consist of thin-grainstone based, mudstone-dominated parasequences that grade up into laminate-capped parasequences. The tidal flat facies thicken over the subtle southern and central highs. In southern and northern Ghawar, the HST of UC-7 consists of grainstone-based parasequences, that grade in

central Ghawar into mudstone- and laminite-dominated parasequences. Many parasequences near sequence boundaries are capped by thin breccias.

Facies maps show that the progradation directions of the dominant Late Permian highstand facies are south and northeast in UC-6a and UC-7, and more to the northeast in UC-6b (Fig. 16 a). The maps show that the tidal flat- and lagoonal facies are the dominant late highstand facies. Tidal flats are limited to northern and southern Ghawar and minor islands in UC-5, and these become more extensive in western, and south-central Ghawar in UC-6a with minor island development. The tidal flats re-establish in northern and southernmost Ghawar in UC-6b and expand in UC-7 to cover much of Ghawar with local re-entrants of lagoonal facies in eastern Ghawar.

Early Triassic Khuff Sequences and High Frequency Sequences

The carbonate-evaporite portion of the Early Triassic composite sequence (Fig. 3) is approximately 80 to 110 m thick, and ~1.5 m.y. duration (Hughes, 2005; Inslaco et al., 2006; Ogg et al. 2008). It is unconformable on the Permian Khuff unit and is conformably overlain by the Sudair Shale highstand. The TST of the Triassic Khuff composite sequence is composed of the Khuff B, Lower Khuff A and Upper Khuff A small scale sequences (Al-Dukhayyil et al., 2012). These small scale sequences are in turn composed of high frequency sequences, HFSs B-1 to 4 and A-1 to 4 respectively. The facies stacking for a selected well is shown in Figure 2.13 b and the regional facies distribution and sequences are shown on the cross sections (Figure 2.15).

Early Triassic Khuff B High Frequency Sequences:

The Early Triassic Khuff B sequence B-1 to 4, together form an overall upward shallowing succession from lime mudstone and oolitic carbonates up into evaporites. In

southern Ghawar, B-1 can be subdivided into subsequences B-1a and 1b, which are separated by a late highstand oolite but these cannot be separated in the northern oolite dominated sections. Thrombolites are common in B-1 and 2, especially in the lagoonal mudstone facies.

Early Triassic Khuff B Sequence Boundaries: Only the basal Khuff B sequence boundary, which is the Permo-Triassic unconformity, has emergent fitted-fabric breccia and paleosols that are developed all over Ghawar (Fig. 2.15). The other HFS boundaries are conformable to slightly erosional on underlying tidal flat or lagoonal carbonates or anhydrite.

Maps showing the facies immediately beneath the overlying sequence boundaries are shown in Figure 2.16 b. The sequence boundary on sequence B-1a is developed on lagoonal facies over much of Ghawar, with oolite in the south. In sequence B-1b, the upper sequence boundary is on exposure breccias and tidal flats over northern Ghawar, with southern Ghawar being covered with oolite, similar to B-1a. Breccias generally are absent from the top of B-2, with the top sequence boundary on tidal flat facies in the north and lagoonal facies in the south. For sequences B-3 and 4, the overlying sequence boundaries are on anhydrites that become progressively more widespread, with tidal flats in the south at the top of B-3, and subaqueous anhydrites completely covering Ghawar at the top of B-4. Except for sequence 1b, breccias capping sequences are relatively rare, being restricted to local islands in central Ghawar at tops of B-1b, 2 and 3.

Early Triassic Khuff B Transgressive Systems Tracts (TSTs): Stacking of facies making up the TSTs are shown in the cross section (Figure 2.15). In southern Ghawar, the TSTs of B-1 and 2 consist of open marine lime mudstone- and lesser oolite-dominated parasequences, whereas in northern Ghawar, the TSTs tend to be made up of oolite-dominated parasequences, with a thin lime mudstone near the base of B-1. Thrombolites are common, associated with

open marine lime mudstone-parasequences, and less commonly with oolite dominated parasequences. The TST of B-3 in southern Ghawar is dominated by oolite parasequences, but these pass northward into black anhydrite-dominated parasequences. The TST of B-4 consists of thin oolite-thick subaqueous black anhydrite parasequences especially in the north, although the oolite facies locally is absent near the base of the sequence elsewhere.

The *maximum flooding surfaces* were placed at the top of the interval of open marine, lime mudstone parasequences, beneath oolite parasequences. Facies maps of the flooding facies are shown in Figure 2.16 b. Sequence B-1a has open lagoon mudstones over southern Ghawar and oolite over northern Ghawar; these open lagoon mudstones blanket Ghawar in B-1b. Lagoonal mudstones become confined to southern Ghawar in B-2, with oolite covering much of Ghawar. The maximum flooding facies of B-3 and 4 again are oolite-dominated over much of northern and southern Ghawar, with a central zone of backshoal packstone and lagoonal muds.

Early Triassic Khuff B Highstand Systems Tracts (HSTs): The facies stacking within the HSTs of the Triassic sequence B are shown on the cross section (Figure 2.15). The cross section shows that the Khuff B highstand prograded to the south, shown by the interfingering and progressive "younging" and forestepping of the bases of the highstand grainstones with respect to the underlying deeper lagoonal muds. The B-1 highstand consists of southward prograding oolitic parasequences, with restricted-mudstone and lesser laminite-dominated parasequences tending to become more abundant over the subtle southern and central highs. The HST of B-2 is dominated by south-prograding oolite-parasequences and minor laminate-dominated parasequences, grading northward into laminate- and anhydrite-dominated parasequences. Similarly, the HST of B-3 consists of southward prograding laminite-

dominated parasequences in the south that pass northward into supratidal- and then subaqueous anhydrite-dominated parasequences. The HST of B-4 is dominated by subaqueous anhydrite parasequences, with anhydritic, laminate-capped parasequences becoming more abundant in southern Ghawar.

Facies maps of the dominant HST facies (Fig. 2.16 b) also show southward progradation in the Khuff B. In B-1a, open lagoonal muds are restricted to southernmost Ghawar, and are prograded by oolite bounding a restricted mudstone facies. Southward progradation is not obvious in the B-1b highstand facies, which has restricted carbonate mudstone facies expanding over central Ghawar, with oolite to the north-west and south. Southward progradation agains is evident in B-2, with oolite facies in southern Ghawar being prograded by tidal flats over most of northern Ghawar. Similarly, southerly progradation is evident in B-3 and 4, with anhydrites prograding southward from northern Ghawar into central Ghawar over tidal flats to the south.

Early Triassic Khuff A High Frequency Sequences

The Lower Khuff A small scale sequence is made up of two HFSs TrA-1 and TrA-2, and the Upper Khuff A and an undetermined portion of the Sudair Formation is made up of HFSs A-3 and A-4 (Figure 2.15). A-4 was only cored in a few wells.

Early Triassic Khuff A Sequence Boundaries: The basal sequence boundaries of the Early Triassic Khuff A (Table 2.2) were placed either on anhydrite, carbonate laminite or fitted-fabric breccia. Only the basal sequence boundary of HFS A-1 rests on regional subaqueous black anhydrite. The basal sequence boundary of A-2 commonly rests on anhydrite and locally on carbonate laminite or fitted-fabric breccia. The A-3 sequence boundary is a planar

to irregular erosional surface on anhydrite, carbonate laminite and locally fitted-fabric breccia. The basal sequence boundary of A-4 is a planar to erosional surface on back-shoal packstone and lagoonal mudstone cycles in southern Ghawar and peritidal laminites capped by incipient breccia and paleosols up dip to the north.

Facies maps showing the distribution of facies beneath sequence boundaries of the Triassic Khuff A are shown in Figure 2.16 c and suggest that progradation directions were to the north in A-1 and to the south in A-2 and A-3. Facies capping sequences A-1 and A-2, consist of subaqueous anhydrite over much of Ghawar. Tidal flat facies cap sequence A-1 in northern Ghawar, whereas tidal flat facies are confined to southern Ghawar at the top of A-2. Tidal flat facies capping A-3 are widespread over northern and central Ghawar while lagoonal and back-shoal packstone facies covered southern Ghawar. Emergence breccias were developed over local highs in north central Ghawar at the top of A1, northernmost, central, and southern Ghawar at the top of A-2, and in central and north central of Ghawar at the top of A-3.

Early Triassic Khuff A Transgressive Systems Tracts (TSTs): Facies stacking within the TSTs are shown on the cross section (Figure 2.15). In southern and northern Ghawar the TST of A-1 is dominated by ooid grainstone parasequences. Upward in the TST, the ooid grainstone parasequences become restricted to southern and central Ghawar, with the northern area being dominated by subaqueous anhydrite parasequences. Most carbonate parasequences are capped by carbonate laminite whereas subaqueous anhydrite caps many of the anhydrite dominated parasequences. The TST of A-2 consists of lagoonal mudstone parasequences with relatively thin grainstone/packstone in southern Ghawar, grainstone-dominated parasequences in north-central Ghawar and subaqueous anhydrite dominated cycles in

northern Ghawar. At the parasequence scale, these northern Ghawar subaqueous anhydrites in A-2 appear to be late highstand to lowstand units that fill in accommodation above thin carbonates (Fig. 2.15). The TST of A-3 is dominated by thick-grainstone parasequences in southern and north central Ghawar while in northern Ghawar, it consists of grainstone-poor anhydrite-dominated parasequences overlain by peritidal parasequences capped by thin-grainstone based parasequences; in the south, the TST of A-3 consists of lagoonal mudstone parasequences with only thin grainstone, passing up grainstone-parasequences. The TST of A-4 consists of lagoonal mudstone-parasequences with minor thin grainstones; limestone and lesser dolomite is dominant in the south passing northward into dolomite. Distinctive digitate stromatolites and thrombolites are common near the base of the TST of A-4 regionally, but extend upward throughout the TST (and HST) in the south.

Facies maps of the maximum flooding facies the Khuff A (Fig. 2.16 c) show that ooid grainstones blanket the bulk of Ghawar in A-1 and A-3. In contrast, in A-2 the ooid grainstones occur in northern and southern Ghawar, with back-shoal packstones and lagoonal muds over central Ghawar while localized tidal flat facies occur in northernmost Ghawar.

Early Triassic Khuff A Highstand Systems Tracts (HSTs): The facies stacking of HSTs in the Triassic Khuff A are shown on the cross section (Figure 2.15). Although progradation direction of HFS A-1 is not clear on the cross section (Fig. 2.15) southward progradation of A-2 and A-3 is shown by more open facies to the south. The cross section strongly suggests that the HSTs of A-1 and A-2 consist of anhydrite capped parasequences in southern and central Ghawar, that grade up-dip into laminate-dominated parasequences, with minor oolite parasequences in subtle lows. In northernmost Ghawar, the HST of A-1 consists of restricted mudstone-dominated parasequences. The A-2 HST is similar in southern and central Ghawar

is similar, but in northern Ghawar, the HST is made of subaqueous anhydrite cycles, in which the individual anhydrites appear to be lowstand deposits relative to the parasequences . In A-3, the HST in the south and central area is made up of grainstone parasequences fining up into lagoonal mudstone parasequences and then into laminite-dominated parasequences; however in the north, the HST of A-3 is mainly lagoonal mud cycles grading up into peritidal laminite parasequences. The A-4 HST consists of restricted mudstone- and laminite-capped parasequences, which are thrombolitic in the south; the A-4 HST in the south consists of lagoonal limestone passing up and grading northward into dolomite. These are overlain by regional shales and lesser carbonates of the Sudair Formation.

Facies maps of the dominant HST facies of Triassic Khuff A sequences are shown in Figure 2.16 c. Progradation of the highstand of HFS A-1 is to the north with lagoonal muds in northernmost Ghawar, tidal flat facies in north-central Ghawar, and anhydrites over central and southern Ghawar. Progradation direction reverses in A-2 and A-3, and is to the south. Southerly progradation in the HST of sequence A-2, is shown by lagoonal facies over southern and central Ghawar, passing into northernmost Ghawar into tidal flat facies and anhydrite. Southerly progradation in the HST of A-3 is indicated by the lagoonal muds in northernmost Ghawar, passing south into back-shoal packstones and then into oolites in the extreme south.

Reservoir Facies

Late Permian Reservoir Facies: Late Permian reservoir development is limited to UC-7 and rarely to upper UC-6. The potential reservoir facies lower in the section are fully plugged by anhydrite. Reservoir facies are developed in a transgressive ooid grainstone (P-7 TST) and

prograding ooid grainstone/packstone shoal complexes and prograding lagoonal dolosiltites and rare intertidal dolomuddy facies (P-6 and -7). Moldic, interparticle and intercrystalline pores of Choquette and Pray (1970), are developed in the dolograinstone/packstone, and intercrystalline pores in the dolosiltites.

Early Triassic Khuff B Reservoir Facies: Reservoir facies are limited to sequences B-1 and B-2 in south Ghawar. Reservoirs are best developed in transgressive grainstones and prograding highstand ooid lime- and dolograinstone/packstone, and less commonly in prograding lagoonal dolomudstone/wackestone (burrowed/ripple laminated dolosiltites and thrombolitic facies). Moldic pores are only developed in the lime-grainstone/packstone, whereas moldic, interparticle and intercrystalline pores are common in the dolograinstone/packstone. The lagoonal dolomudstone facies contain intercrystalline pores. Anhydrite cementation occluded pores minimizing destroying potential reservoir facies. Anhydrite plugged all the grainstone/packstone reservoir facies in late highstand systems tracts of B-1 throughout Ghawar and in sequence B-2 in central and north Ghawar. Anhydrite also plugs porosity in sequences B-3 and 4 throughout Ghawar.

Early Triassic Khuff A Reservoir Facies: Reservoir development is limited to sequences A-1 and A-2 in southern Ghawar, sequence A-3 in south and central Ghawar and A-4 in a few areas in north Ghawar. There is insufficient core data to evaluate sequence A-4. Reservoir facies are best developed in transgressive- and prograding ooid grainstone/packstone of shoal complexes and sheets, and in prograding lagoonal dolosiltites. Moldic, interparticle and intercrystalline pores are common in the dolograinstone/packstone, whereas in lime-grainstone/packstone, moldic pores are common and interparticle pores are rare.

Intercrystalline pores are developed in the shallow lagoon dolomudstone. Plugging of reservoir grainstone/packstone by anhydrite causes major loss of porosity.

DISCUSSION

Paleogeography and Climate

During the Late Carboniferous to Early Permian, when Pangea spanned the globe, global climate was icehouse with average global temperatures of 12–14º C. The Arabian Plate during the Permo-Carboniferous was between 30ºS and 55ºS, moving northward with Gondwana. Global climate changed to greenhouse conditions from the Mid Permian to Triassic, with surface ocean temperatures of 30º C in the tropics (Scotese, 1999; Parrish 1985 and 1993; Ziegler et al., 1997). By Late Permian, the Arabian Plate had moved from 35 to 10ºS and by the Early Triassic (end of Khuff deposition) its northern margin had reached 5ºS (Fig. 2.2; Konert et al., 2001; Sharland et al., 2001).

Much of the continental area of Pangea adjacent to the tropics (which included Arabia) were arid during the Middle and Late Permian (Fig. 2.17). Humid belts were north and south of 30 degrees latitude and on microplates and arcs in the Far East (Scotese, 1999; 2003). These desert conditions persisted into the Early Triassic and evaporites and redbeds became more widespread. This intensely arid climate was a result of the massive global warming triggered by the Siberian Traps volcanism at the end of Permian, relatively low sea-levels and the assembly of Pangea, which resulted in immense land areas north and south of the equator.

This Pangean paleogeography and greenhouse climate may have generated megamonsoonal atmospheric circulation which resulted in relatively dry tropics and the

absence of the Humid Tropical Belt (Parrish, 1993; Scotese, 1999; Ziegler et al., 1997). Parrish et al. (1986) predicted that the monsoonal circulation reached its maximum strength in the Triassic. During this maximum stage, climates in the tropical zone on the eastern side of the Pangea became dry. In contrast, the tropical western side became relatively humid, similar to present-day west Africa (Parrish, 1993; Loope et al., 2004). The Inter-Tropical Convergence Zone (ITCZ) that generally lies near the Equator is the locus of rainfall in the Humid Tropics on the present globe. However with Pangean paleogeography, strong seasonal monsoons or megamonsoons shifted the ITCZ to middle latitudes, distributing the rainfall over a large area, resulting in generally drier conditions. The strong seasonal monsoons and extreme ITCZ deflection was due to severe seasonal heating of the Pangean landmass which straddled the equator with large landmasses to north and south (Parrish, 1988; Loope, 2004).

This arid setting is evidenced by the common evaporites, mainly anhydrites, in the Khuff succession, and high salinities indicated by the abundance of microbial laminites, restricted biotas of the ramp interior, as well as widespread oolitic facies on the ramp interior. Arid conditions along the present-day evaporitic Arabian Gulf coast are similar to those that existed during the Khuff deposition, with the major difference in setting being the development of immense salinas in the Permian-Triassic, compared to the narrow sabkha evaporites today. Local root-like structures and minor karst in the Khuff deposits, especially on the Latest Permian restricted lagoonal mudstones, may mark short periods of slightly more humid conditions. The overlying Sudair shale and siltstones also indicate ephemeral terrigenous influx during the early Triassic, while the red colors of mudrocks and presence of evaporites indicates prevailing, relatively dry conditions (Alsharhan and Kendall, 1986; Ziegler, 2001).

Tectonics

Khuff deposition was initiated following the Middle Permian break-up unconformity and deposition of pre-Khuff clastics, associated with inception of the Neo-Tethys Ocean in the vicinity of the present-day Zagros suture. This was accompanied by the most extensive transgression of the Paleozoic, when marine waters from Neo-Tethys spread over the Arabian foreland. This led to formation of the immense, east-sloping Khuff ramp that extended to the present Zagros fold-thrust belt (Al-Jallal, 1989; Al-Aswad, 1997; Sharland et al., 2001; Konert et al., 2001). This major transgression caused a change from mainly siliciclastic- to carbonate-evaporite deposition as the Arabian Plate moved northward into warmer and drier, lower latitudes.

During the Permo-Triassic, along with Neo-Tethys sea-floor spreading, syndepositional, wide, broad and gentle structures (folds and domes) formed on the eastern Arabian Plate above re-activated basement faults (Fig. 2.6; Al-Jallal, 1989; Sharland et al., 2001; Abu-Ali and Littke 2005). These gentle structures likely were responsible for the subtle topography (e.g. the southern and central highs of this paper) and the subtle changes in subsidence rate and progradation directions in Ghawar.

Subsidence history plots of Ghawar (Fig. 2.18; Abu-Ali and Littke, 2005) show relatively rapid subsidence from the Late Permian to Middle Triassic (~5 cm/k.y.) probably related to thermo-tectonic subsidence of the relatively young margin. This was followed by slow subsidence to the Early Jurassic (0.2 cm/k.y.) as the margin aged (cf. Bott, 1992), prior to renewed rapid subsidence in the Late Jurassic (Abu-Ali and Littke, 2005). The average subsidence rate of the updip Khuff outcrop belt, was 1.5 cm/k.y. (Al-Aswad, 1997). More rapid subsidence rates typified the Ghawar study area for the Permian, ranging from 2 to 2.5

cm/k.y. (based on thickness of 335-366 m and a duration of 15.5 +/- 0.7 m.y. (Ogg et al., 2008). Early Triassic subsidence rates were relatively high ranging from 5 to 7.5 cm/k.y. based on thicknesses of 80-110m and duration of 1.5 +/-0.7 m.y. Subsidence rates for the seaward edge of the passive margin during the Permo-Triassic (beneath the present-day Zagros fold-thrust belt) were 9 cm/k.y. based on a thickness of 1524 m and duration of 17 +/- 0.7 m.y. The Khuff isopach (Fig. 2.5), the Khuff cross sections and these subsidence rates indicate that the Khuff passive margin was a typical seaward-thickening wedge. These subsidence rates fall within the range of modern and ancient mature passive margins (Steckler and Watts, 1982; Read 1989).

The relatively low rates of rotational subsidence on the passive margin, coupled with the small magnitude greenhouse sea-level changes, resulted in the Khuff ramp top from Saudi Arabia to Iran being aggraded to sea-level for much of the time. Thus the ramp top had a low gradient, implied by the depositional model of Insalaco et al (2006) for the Upper Khuff sequences in Iran. Slopes per cycle (parasequences) for the present study were calculated from the outcrop thicknesses in Saudi Arabia to thicknesses in Ghawar Field using:

Regional gradient per cycle = regional thickening / (number of cycles X distance)

(after Koerschner and Read 1989). Using 155 m of Late Permian-Early Triassic Khuff in Ghawar, thinning to a feather edge onto the Arabian Shield over a distance of ~600 km and 275 cycles in the Late Permian-Early Triassic Khuff in Ghawar gives 0.1 cm/km slope. Even using the 450 m thickening from the Saudi Arabian outcrop to the Iranian Khuff, and a 1000 km distance and divided by a similar number of cycles would still yield a slope per cycle of less than 0.1 cm/km. These slopes are far less than the 4 cm/km slopes on the Bahamas. The slopes would yield maximum water depths in Ghawar of ~6 m, and 10 m on the platform in

Iran. However, the slopes probably increased from the relatively flat topped ramp onto the ramp slope (with subwave-base muds) in Iran. The slopes on the ramp top varied over subtle topographic structures such the large Ghawar structures, as well as over subtle highs within Ghawar (cf Abu-Ali and Littke, 2005),

The broad regional trends shown by the facies maps indicate that progradation directions were to the south and sometimes to the northeast, rather than outward from Ghawar in all directions (Fig. 2.16). This suggests that the broad facies trends were not dominantly influenced by the elongate Ghawar structure. The Triassic cross section (Figure 2.15) shows more regional depositional slopes mainly to the northeast, complicated by subtle warping of the area. For example, when the top of the Khuff D anhydrite is datumed on the PTB, the Khuff-D anhydrite below the study interval shows a gentle slope to the south in southern Ghawar and to the north in northern Ghawar (Fig. 2.14). In contrast, when the top of the Khuff D anhydrite is datumed on the top of the Triassic Khuff Formation, it shows a gentle slope to the south in southern Ghawar, followed by a reversal of slope to the north in the northern 2/3 of Ghawar, in which the northern slope is punctuated by two gentle uplifts (Fig. 2.15). These local reversal of slopes and subtle highs have influenced the overlying facies of the Permian and Triassic carbonates (Figs. 2.14, 2.15) and directions of progradation and offlap, and sites of evaporite deposition (Fig. 2.16 c). Thus the Permian and Triassic Ghawar structure was a relatively subtle topographic feature on which low relief, small ephemeral highs over Ghawar appear to have localized some of the facies such as oolites, tidal flats and breccias. Nevertheless, movement on the Ghawar structure may have been responsible for the reversals in paleoslope seen in the facies maps (Fig. 16).

Duration of Sequences

Likely duration of the various scales of sequences in the Khuff Formation can be estimated from the chronostratigraphic chart; uncertainty in the ages of the stages is +/- 0.7 m.y. although the stage durations determined by cyclostratigraphy agree fairly closely with the estimated ages (Fig. 2.3; Rampino et al 2000). The upper C sequence is a ~2.8 m.y. third order sequence, which may relate to the long term eccentricity cycle of 2.4 m.y. (Matthews and Al-Husseini 2010; Boulila et al 2011). The three small scale 3rd order sequences making up the upper C interval are perhaps ~800 k.y. each. The seven constituent high frequency sequences within the Upper C are each perhaps ~400 k.y. duration based on 2.8 m.y. divided by 7 high frequency sequences; these likely relate to orbital eccentricity (Matthews and Frohlich, 2002). Sequences B and A are each about ~700 k.y. and are thus small scale third order sequences; each has 4 HFSs, which average about 170 k.y. duration each, implying that these are 4th order sequences.

Because of the great thickness variation in the parasequences associated with oolite shoals versus off-shoal settings, spectral analysis was not done on the sections. However, average duration of parasequences can be estimated crudely from the duration of the intervals and number of component parasequences. For the latest Permian Changhsingian, which roughly spans 2.8+/- 0.7 m.y., there are ~125 cycles, which averages out at about ~22 +/-5 k.y. per cycle. For the Induan (Early Triassic) part of the succession, which spans 1.5 +/-0.7 m.y., there are ~150 cycles, averaging out to about 10 +/-5 k.y. per cycle. These crude estimates suggest that the parasequences may be driven by orbital precessional and half precessional forcing of climate that caused small changes in sea-level. Thus most of the cycles are Milankovitch and related to precession, rather than being sub-Milankovitch cycles

of the order of just a few kiloyears, as documented for the Middle Triassic Latemar Formation in the Dolomites (Zuhlke et al 2003; see Hinnov, 2000 and Preto et al., 2001 for a differing opinion).

Eustasy and Accommodation Cycles

Third Order Eustasy

Accommodation (Fischer) plots of the cyclic Khuff succession for three wells are shown in Figure 2.19. The plots track the cumulative departure from average cycle thickness against cycle number, which is used as a proxy for time (Saddler et al., 1993). On the plots, accommodation increase is shown by the limb rising to the left, while the accommodation decrease is shown by the limb fall toward the right. The sequence boundaries based on the lithologic succession and the sequence analysis are shown alongside the Fischer plots. The Permian Chianghsingian Upper C sequence on the Fischer plot is marked by accommodation increase from HFSs UC-1 to 3 which make up a transgressive high frequency sequence set. The falling limb of the Upper C sequence is made up of HFSs UC-4 and 5, with a maximum flood likely lying within UC-4. HFSs UC-6 and 7 appear to mark a turn around, with accommodation starting to increase prior to the PTB (supported by the presence bryozoans, crinoids and brachiopods), although the plot of well 4 differs from the plots of the other two wells in showing increasing accommodation toward the end of UC-6 as well as UC-7; merging of cycles within the sequence bounding paleosols may have masked the accommodation change in well 4. The overall transgression across the PTB is synchronous with the overall increasing C isotope excursion across the PTB, presumably related to increasing global warming.

The Triassic Induan part of the Fischer plot shows increasing accommodation within B-1 in the three wells, followed by decreasing accommodation in upper B-1. However the plots from the 3 wells start to differ. In well 10, the plot shows decreasing accommodation in B-2 and 3, whereas in well 13 the plot shows relatively little accommodation change through B-4; however in well 4, the plot shows a rise in B-2, followed by a fall in B-3 followed by rise and fall in B-4. All the plots then show a significant increase in accommodation but in different parts of the succession. In well 4, the rise is in A-1 through 4; in well 10 the rise is largely in B-4 while in well 13 the rise is mainly in A-2. This apparent diachroneity is probably a result of the plots and the preservation and picking of cycles, rather than being reflection of timing of accommodation increase. Thus the plots show mixed success at picking 3rd order accommodation changes in this highly cyclic succession, probably due to autocycle development (including picking of cycles that are in fact local storm layers or mud drapes in core), merging of cycles within thick grainstones, and loss of cycles within thick paleosols. The plots are poor at picking high frequency sequences, probably because of the small number of cycles within each HFS (Sadler et al., 1993).

The sea-level curve for the Permian-Triassic study interval are shown in Figure 2.20 along with approximate ages of the high frequency sequences LC-1 to 5, UC-1 to 7, B1 to 4 and A-1 to 4. In addition, published 3rd order curves (Haq and Al-Qahtani, 2005; Haq and Schutter, 2008; Markello et al., 2008) also are plotted for comparison. Although the present study interval extends from just above LC-5 to A- 4, the other lower C sequences documented by Al-Dukhayyil et al (2006) and Al Eid (2009) have been included on Figure 2.20. Given that third order sequences are at the limit of biostratigraphic resolution (Miall, 1999), the

following correlations of the Arabian sequences to the global charts should be considered tentative.

Sequence boundary (SB) LC-1 (basal Wuchiapingian) may correlate with Wu-1 SB on Haq and Al-Qahtani (2005), Wu-1 on the Haq and Schutter (2008) and Wuc2 on the Markello et al (2008) curves, all of which are close to the base of the Wuchiapingian. SB LC-2 correlates with Wu 2 on Haq and Al-Qahtani curve and Wuc3 on the Markello et al curve. SB LC-3 does not correlate with either of the Haq and Al-Qahtani or the Haq and Schutter curves, but correlates well with the Wuc4 SB of Markello et al. curve. SB LC-4 does not correlate with either of the Haq and Al-Qahtani, the Haq and Schutter, or the Markello et al. curves. SB LC-5 correlates with Wu2 on Haq and Schutter curve and Wuc3 on the Markello et al curve; it probably correlates with Wu 3 on the Haq and Al-Qahtani Arabian curve, which they probably place too high.

SB UC-1 is basal Changhsingian and correlates well with Chan1 of the Haq and Schutter curve, however it does not correlate with either of the Haq and Al-Qahtani or the Markello et al curves. There are no correlatives with sequence boundaries of UC-2 and 3 on the other sea-level curves suggesting these events are too small or are local. SB UC-4 correlates well with Ch 1 of the Haq and Al-Qahtani curve and Chan2 of the Haq and Schutter curve. SB-5 has no correlatives on the other curves. SB UC-6 does not correlate with either of the Haq and Al-Qahtani or the Markello et al curves, but correlates well with Chan3 SB of the Haq and Schutter curve.

The Permo-Triassic boundary (B-1) correlates well with the In0 SB of the Markello et al. curve, but the other two curves show gradually rising sea-level at this time. The A-1 SB correlates well with In 1 on the Haq and Al-Qahtani curve and In2 on the Markello et al

curve; In1 on the Markello et al curve may correlate with one of the higher frequency cycles in the study area. A-5 correlates well with Ol 1 of the Haq and Al-Qahtani and Haq and Schutter curves. The higher frequency cycles A-2 to 4 and B 2 to 4 are below the resolution of the curves.

Thus of the major 3rd order events (LC-1, LC-5, UC-1, UC-4, B-1, A-1, A-5) all correlate to major events on the published charts. The smaller scale 4th/5th order are either below the resolution of the curves and/or are of more local origin.

Milankovitch Forcing of Climate and Sea-Level

Milankovitch forcing of climate has been well documented from the Permian and early Triassic, starting with the pioneering work of Anderson (1982) who did varve counts on a 250 k.y. record from the deep-water Permian Castille evaporite. He demonstrated a Milankovitch 100 k.y. signal, a distinct oscillation around 20 k.y. marking precession, and a very strong, sub-Milankovitch climate response at 2.7 k.y. marked by freshening of the basin. More recent studies of Permo-Triassic shallow-water, cyclic carbonate sections in the Austrian Alps and South China, have documented a minor 412 k.y., a prominent ~100 k.y., along with ~40 k.y., and ~20 k.y. quasi-periodicities (Yang and Lehrmann 2003; Rampino et al 2000). These studies all support Milankovitch forcing of climate and, in turn, sea-level changes in the Permian and Triassic.

The cyclic successions of the study area are not amenable to spectral analysis given the large range of cycle thickness, associated with the development of thick oolitic units that interrupt the meter-scale cyclicity. Also, locally developed stacked thin cycles that merge laterally with a few thick cycles, could reflect local shallowing by autocyclic processes, or

pinchout of higher frequency cycles onto depositional highs. On the Fischer (accommodation) plots there is a locally well developed bundling of 4 to 8 cycles per bundle, perhaps suggestive of precessional (and half precessional) bundling into 100 k.y. eccentricity bundles, with the added complication of autocycle development associated with local shallowing events. In addition, some thin parasequences in the cores may include interlayered grainstone and mudstone resulting from storm events. The precessional cyclicity is compatible with the crude estimates of 10 to 20 k.y. average durations of the parasequences. Most such Milankovitch driven sea-level fluctuations within the Latest Permian-Early Triassic, which is a time of well documented greenhouse climate (Frakes et al 1992; Fielding et al 2011), would likely be small. They might be driven by Alpine glaciation, storage of water in aquifers and rift basin, and heating/cooling of the oceanic water columns (Jacobs and Sahangian, 1993). However, this does not to exclude possible cooling events at sequence boundaries (associated with breccia development) which might have been associated with larger sea-level falls, perhaps associated with buildup of small ice sheets, sequestering of water into rift basins and aquifers (Jacobs and Sahagian 1995; Elrick et al 2009). Such increased magnitudes of sea-level fall at sequence boundaries have been documented from Middle Devonian greenhouse sequences using oxygen isotopes of conodont apatite (Elrick et al., 2009).

Basin-Scale Controls on Carbonate vs. Anhydrite Deposition

Late Permian and Early Triassic seas were aragonite seas characterized by Mg/Ca ratios similar to today (Hardie1996; Stanley and Hardie, 1998; 1999). For the transition from carbonate to evaporite deposition, sea water volumes need to be reduced to about one third of their original volumes by evaporation, driving salinities above ~90 ppt (Holser, 1979). To generate evaporites over carbonates, evaporation has to greatly exceed seawater inflow plus

rainfall plus riverine influx, and the brine basin needs a hydroseal to prevent them rapidly leaking into the underlying units. For the Late Permian and Early Triassic, precipitation and riverine influx generally were low, given the restriction of siliciclastics to the updip margins of the platform (Ziegler, 2001). In terms of seawater inflow onto the platform, ocean waters could have migrated onto the platform from embayments in the platform margin due east of Ghawar and characterized by open marine carbonates, and possibly to the north (present day Iraq). The platform was bordered by land in western Arabia, the south (Yemen) and southeast (southern Oman). North of Ghawar is a major anhydrite basin with 100 m of evaporites, extending from northern Saudi Arabia into Kuwait and east into Iran (Fig. 2.4). Local highs that also might have limited exchange and characterized by Permian thinning occur in offshore Abu Dhabi (Sharland et al., 2001) and Qatar (data in Abu-Ali 2005).

Given sufficiently arid climate phases, the simplest way to generate evaporites on the Arabian platform would be to lower sea level. This would decrease the water depths over marginal sills (formed by constructional upbuilding of carbonates, and local slowing of subsidence) that may have lain south-east , east and north east of Ghawar (Fig. 2.4). The decreased water depths over the sills would thus have decreased the cross sectional area of the inflow system, decreasing seawater exchange with the interior platform and the open ocean. Lowered sea levels are suggested by occurrence of the evaporites at the tops of Late Permian HFSs UC-1 and 2, and Triassic HFS B-2 and A-1. However, the evaporites in Triassic HFSs B-2 and 4 occur throughout the sequences in northern Ghawar pinching out into carbonates to the south. This suggests that inflow was restricted perhaps by slowing of subsidence to the north, while open marine conditions continued to the south. The

dissappearance of beds of anhydrite in Triassic HFSs A-3 and 4 suggest decreased aridity, perhaps coupled with less restricted inflow.

Deposition of sabkha anhydrite occurred during shallowing of carbonate parasequences into the tidal zone, and with continued subsidence and growth of dominantly displacive anhydrite, extensive units of anhydrite capping units were developed. In contrast, in areas where accommodation still remained off from carbonate shoals, the space was initially filled with subaqueous layered anhydrite (formerly gypsum) followed locally by sabkha anhydrite. Interlayering of the anhydrites with dololaminites suggest that there was substantial migration of the salinoclines across the platform at the parasequence scale.

Sequence Development in the Khuff Upper C, B and A

The late Permian-Early Triassic greenhouse climate had a major control on sequence development in the Khuff Formation, limiting the magnitudes of sea-level falls, and resulting in a very large number of stacked parasequences within sequences.

Sequence Boundary Development

Third Order Sequence Boundaries: Major emergence events with multiple breccias characterize the thick third order sequence boundary zone at the base of the upper C, capping the Lower C sequence at the Wuchiapingian-Changhsingian boundary. This developed during the major global sea-level fall (Fig. 2.20). The smaller scale 3rd order sequence boundaries within the upper Khuff C, which are characterized by more localized breccia zones and or tidal flat exposure surfaces, developed during relative sea-level fall below the resolution of the sea-level curves (Fig. 2.20).

The third order basal sequence boundary of the Khuff B coincides with the Permian Triassic boundary, and is characterized by single- or multiple breccia zones throughout Ghawar, and developed during relative sea-level fall evident on Markello et al (2008) chart. Whether this sea-level fall is a global event or due to local tectonics is not clear, given that it is not shown on some of the global curves (Fig. 2.20). In addition, in many other areas, the PTB occurs during a time of transgression (Erwin, 2006; Insalaco et al., 2006).

The Khuff A basal sequence boundary, which developed on evaporites, formed during global sea-level fall, which terminated evaporite deposition over most of Ghawar, although the lack of exposure breccias suggests only limited exposure (Fig. 2.20).

High Frequency Sequence Boundaries: The sequence boundaries associated with the 4th order sequences of the Khuff succession, which are characterized by relatively limited breccia development and widespread tidal flat deposits and local evaporites, probably resulted from relatively small sea-level falls (less than 10 m) which only exposed local highs, while elsewhere, tidal flats and local evaporites developed. The change in the areal distribution of breccias from sequence boundary to sequence boundary in Ghawar, if not related to local up-building by sedimentation, is suggestive of differential warping of Ghawar. This is evident in breccia distribution in UC-5 to 7. In contrast, the latest HST facies of HFSs B-1 to 4 generally show evidence of marine conditions to the south, suggesting a paleoslope in this direction due to tilting or sediment starvation. However, Khuff HFSs A-1 through 3 show reversals in directions of progradation, strongly suggestive of tilting. The Khuff breccias likely developed on subtle highs, that probably were a combination of sediment up-building and differential warping.

Transgressive Systems Tract Development

Third Order Transgressive Systems Tracts, Upper Khuff C: The 3rd order transgressive systems tract within the upper Khuff C is manifested in three thin HFSs (P-2 to 4), with the 3rd order maximum flooding surface within the overlying thick HFS P-5. This reflects increasing accommodation toward the maximum flood, but the relatively low accommodation rates (combination of low subsidence rate and small sea-level rise rate) did not allow deepening beyond oolite water depths, indicating that sedimentation rates never greatly lagged accommodation.

Transgressive Systems Tracts of High Frequency Sequences, Upper Khuff C: The fourth order TSTs within the Permian Khuff upper C, show an overall upward deepening trend, also resulted from sedimentation only slightly lagging accommodation, with water depths never exceeding that of the oolitic facies. Sea-level rise forming the the TSTs of the high frequency sequences UC-1 through 7 probably was driven by 400 k.y. long term eccentricity, which flooded a relatively uniform paleoslopes to the north, indicated by the facies maps (Fig. 2.16).

Transgressive Tracts of 3rd Order Khuff B: In the Early Triassic, the third order Khuff B TST is defined by the initial Triassic transgressive set of cross-bedded grainstone deposits associated with thrombolites that deepen to distal lime mudstone with subtidal microbial lamination, and thrombolite heads. These distal open lagoonal muds that are thick (up to 10 m) in southern Ghawar, mark maximum flooding of the Khuff B sequence. They likely are contemporaneous with the global MFS Tr10 of Sharland et al. (2001). Low sedimentation rates due to depauperate calcified biotas following the end Permian extinction, coupled with increased accommodation rates, probably favored deepening below wave base. Likely that sea-level rise rates were relatively high compared to the low sedimentation rates.

Transgressive Tracts, High Frequency Sequences, Khuff B: The two and one half, fourth order HFSs within the Khuff B TST thicken upward in response to the increasing accommodation. The low sedimentation rates versus increased accommodation are also reflected in the Early Triassic Khuff B, fourth order TSTS, with the development of widespread lime mudstone parasequences. These however disappear into the later HFSs of the Khuff B, as accommodation decreased.

3rd Order Transgressive Tract, Khuff A: The TST of the Triassic Khuff A third order sequence is defined by the development of three HFSs comprising ooid grainstone, lagoonal mudstone with thrombolites, laminites tidal flats and sub-aqueous anhydrite, that deepen into the maximum flood in HFS A-3, which has evaporite-free, thick grainstone cycles in southern and central Ghawar, and elsewhere lagoonal mudstone. This deepening event marks the maximum flooding surface of the third order Khuff A sequence, and developed during global sea-level Tr 20 of Sharland et al., (2001). The abundant evaporites in most of the TST (at least locally in Ghawar), suggest shallow water depths over the marginal sills, that deepened with maximum flooding, terminating evaporite deposition.

Transgressive Tracts, Khuff A High Frequency Sequences: Within the Triassic Khuff A high frequency sequences, the TSTs in the south remained in the carbonate precipitation fields, reflecting more open conditions, while to the north, except for HFS A1, waters were in the anhydrite precipitation field throughout much of the TSTs, reflecting increasing restriction to the north, at this time. At the parasequence scale,the dominantly subaqueous anhydrites in northern Ghawar in A-2, appear to be late highstand to low stand deposits that filled in remaining accommodation above the thin inter-shoal carbonates.

Highstand Systems Tract Development

Third Order Highstand Tract, Upper Khuff C: The HST within the Permian upper Khuff C, 3rd order sequence, which is characterized by part of a thick HFS UC-4, overlain by 3 thin HFSs (UC-5 to 7) that contain progressively shallower water carbonate facies, marks decreasing accommodation toward the Permo-Triassic unconformity. This resulted from sedimentation slightly exceeding accommodation. However near the end of the Permian, there was a slight increase in accommodation and salinity lowering, evidenced by bryozoan-crinoidal oolitic facies within the uppermost HFS UC-7, which anticipates the major flood back in the earliest Triassic.

Highstands of High Frequency Sequences, Upper Khuff C: Within the HFSs of the Permian upper Khuff C, the HSTs all shallow from oolite to lagoon to tidal flat and only minor anhydrite facies, marking decreased accommodation exceeded by sedimentation. Waters stayed mainly within the carbonate precipitation field, probably due insufficient restriction to waters inflowing onto the platform; the small amounts of anhydrite present do indicate that climate remained arid. The 400 k.y. durations of these HFSs is suggestive of long term eccentricity driving the sea-level falls.

Third Order Highstand Tract, Khuff B: The HST of Triassic Khuff B, third order sequence, (upper B-1 to B4) shallows up from open lagoon to oolite to peritidal facies, then anhydrite, the anhydrites becoming more abundant northward. The decrease in accommodation was due to eustatic sea-level fall. During the HST, waters remained within the carbonate precipitation field for much of the time in the south, while downdip to the north, waters for much of the late HST were in the anhydrite precipitation field, indicating marked restriction north of Ghawar

and into the evaporite basin (Fig. 2.4). Loading by anhydrite in north Ghawar probably increased accommodation resulting in thicker deposits in the north.

Highstands of High Frequency Sequences, Khuff B: The fourth order Triassic Khuff B HSTs show upward shallowing trends, that mark decreased accommodation (relative to TSTs) exceeded by sedimentation. Facies shallow from open lagoonal mud to oolite, to restricted peritidal facies to anhydrite and show progradation to the south in sequence B-1a to B-4, resulting in thick anhydrites in central and northern Ghawar (Fig. 2.15).

Third Order Highstand of Khuff A Sequence: The 3rd order highstand systems tract of the Triassic Khuff A-Sudair small-scale sequence is characterized by prograding shallowing upward succession of thin oolite, restricted lagoonal mud with thrombolites. The marked decrease in anhydrite probably reflects both decreasing aridity (heralding the subsequent influx of Sudair fine clastics) as well as increase in lagoonal facies at the expense of restricted supratidal and salina facies.

Highstands of High Frequency Sequences, Khuff A: The HSTs of Triassic Khuff A HFSs or parasequence sets contain successively shallower water facies that resulted from sedimentation slightly exceeding accommodation. The southward development of anhydrites capping the carbonate portion of HFS A-1, reflect restriction to the south, while the north remained open marine. In contrast, the HST of sequence A-2 is dominated by development in the north of subaqueous anhydrite that filled remaining accommodation above the thin carbonates within parasequences, and parasequence-sets lapped out onto highstand carbonates to the south. At the parasequence scale, these A-2 anhydrites are late highstand to low-stand facies. The presence of a paleosol at the top of these A-2 anhydrite parasequences indicates that at the HFS scale, the A-2 anhydrites overall are highstand deposits.

Parasequence Development – Milankovitch vs Autocyclic Controls

The 10 to 20 k.y. durations of the parasequences which is suggestive of precession and half precessional Milankovitch orbital forcing (Hinnov, 2000), indicates that high frequency sea-level changes, although small, were an important driver of parasequence development in the Permian-Triassic greehouse world. However, because some of the thinner parasequences appear to be local in extent, suggests that there could have been considerable autocyclic processes involved. Local autocycle development also is compatible with the expected small scale sea-level changes under greenhouse conditions, in which most of the high frequency sea-level falls were unable to completely expose the platform after each cycle. Autocyclic processes would have been related to subtle changes in local sedimentation rates, complicated by subtle warping which changed local accommodation rates and depositional topography. Depositional lows on this shallow platform were likely to develop more cycles than on depositional highs, with already filled accommodation. Rapid filling of accommodation by oolite units caused few parasequences to be developed within areas of the thicker shoals, whereas off the shoals within areas of unfilled accommodation, numerous parasequences developed.

Implications for Khuff Reservoirs

The sequence framework indicates that reservoirs developed in both transgressive and highstand systems tracts. These were associated with grainstone facies with oomoldic and minor interparticle porosity, dolomitized lagoonal muds and rare tidal flat facies (both with fine intercrystal porosity). Dolomitized and leached grainstone/packstone facies that

preserved much of their interparticle pores and lack anhydrite or calcite cements, make the best reservoirs quality.

Anhydrite cementation was the most influential factor in reducing and destroying porosity in the Khuff (Fig. 2.21). Anhydrite cementation took place when grainstone/packstones were deposited downdip of, and were overlain by tidal flat laminites and prograding anhydrites. Dense brines from supratidal flats, subaqueous salinas and tidal flats moved downward and seaward through originally highly permeable grainstone/packstone to deposit pore-filling anhydrite destroying porosity. Where grainstone/packstone facies were distant from evaporitic tidal flats/sabkhas or near open marine lime mudstones, porosity was commonly preserved.

Impact of P/T Event and Biotic Changes on Khuff Sequence Development

The Permian-Triassic boundary represents the greatest biotic extinction in the earth history, with a massive (up to 96%) decrease in marine and terrestrial species (Raup, 1979; Erwin, 1993; Sepkoski, 1996; Retallack, 1995). It was an interval of profound change in tectonics, climate and geochemistry. The Permian skeletal carbonate factory was rapidly replaced in the Early Triassic by a non-skeletal carbonate factory, with widespread development of microbial stromatolites and thrombolites. This accompanied increased abundance of cyanobacteria immediately after the mass extinction globally. Biotic recovery was largely delayed until the Middle Triassic (Erwin, 2006; Baud et al., 2007; Yin et al., 2007).

Diversity of biotic groups in thin sections of core plugs across the PTB in Ghawar (Fig. 2.22), show that in the Permian, the Changhsingian Khuff Formation had a diverse biota

dominated by foraminifera, calcareous (green and red) algae, bivalves, gastropods, and minor ostracods. Bryozoans, crinoids, and brachiopods are only present in the last HFS (UC-7), 3 to 5 m below the PTB. These groups were not encountered in the more restricted facies in the studied cored well from northern Ghawar. Gastropods and bivalves extend through the end-Permian extinction into the Early Triassic and minor ostracods reappeared around 15 m above the PTB.

The aftermath of the P-T extinction was manifested in the early Triassic sequences in Ghawar by the slowing down of carbonate production, and development of numerous muddy flood units containing thrombolites with limited biotas. The microbialite abundance significantly increased in the upper Khuff Formation following the end-Permian extinction. Microbial laminites within the Permian part of the Khuff Formation occur only as stratiform microbial laminites within tidal flat successions. Thrombolites are not present in the Permian Khuff probably due to the diverse grazing and burrowing biota, which caused a noncompetitive ecologic restriction.

The first appearance of abundant heads of stromatolites and thrombolites occurs above the PTB in outcrops in central Saudi Arabia (Al-Dukhayyil and Al-Tawil, 2006) outcrops in UAE (Strohmenger et al, 2002), Oman and Iran (Heydari et al., 2000; Koehrer et al., 2010). This resulted from extinction of many of the grazers, browsers and burrowers, allowing subtidal microbial heads to proliferate (Schubert and Bottjer, 1992; Erwin, 2006). In Ghawar, thrombolites are more dominant than columnar stromatolites in the Triassic Khuff, because calcified coccoid microbes replaced filamentous sediment-trapping and -binding within microbial structures (Kennard and James, 1986). That browsing by gastropods was important on the heads, is supported by the numerous gastropods entombed within thrombolites, a

feature observed as far back as the Cambrian (Bova and Read, 1987). In fact, there is a striking resemblance between the Triassic facies and many Cambrian shallow shelf facies that predate the Middle Ordovician biotic diversification.

Subtidal microbial head growth in the Early Triassic also was promoted by high carbonate supersaturation (Riding 2005), due to the lack of widespread metazoan calcareous biotas extracting Ca and bicarbonate ions from the seawater. These increased supersaturation states may be reflected in increased abundance of ooid grainstone/packstone in Triassic sequences A and B (Groves and Calner, 2004; Calner, 2005) but this is difficult to separate out from the effects of high salinities promoting supersaturation.

CONCLUSIONS

Detailed logging of selected cores throughout Ghawar, eastern Saudi Arabia, has allowed a comprehensive depositional model, and high resolution sequence stratigraphic framework to be generated for the Upper Permian and Lower Triassic Khuff Formation, along with a more refined relative sea-level curve for the region. It also allowed time slice maps of the facies distribution within sequences in Ghawar to be developed. Ages were constrained by published biostratigraphy and by new C isotope data. The resultant cross sections and maps should provide a framework for a new generation of 3-D geological reservoir models.

Several scales of depositional sequences are developed, that include the 3rd order sequences of the Permian upper Khuff C, and the Early Triassic Khuff B and the Khuff A sequences, and their correlation with the global curves suggest that they were driven by global eustasy. The 3rd order sequences contain several high frequency sequences, which in the Khuff C are ~400 k.y. duration and probably driven by long term eccentricity, but those in the Khuff B and A, appear to be ~100 to 200 k.y. duration and not easily tied to Milankovitch

orbital eccentricity forcing. The high frequency sequences are in turn composed of parasequences, which appear to be 10 to 20 k.y. average durations, suggesting orbital precessional and half precessional forcing. However, many thin locally developed cycles may be autocycles or subprecessional cycles.

The sequence stratigraphic cross sections and facies maps of systems tracts illustrates the subtle interplay between the Ghawar structure and regional paleoslopes. This is evidenced by changes in directions of progradation from one high frequency sequence to the next. Southward progradation is evident in the Khuff B, while the Khuff A shows initial northward progradation, followed by southward progradation. These trends also could reflect regional changes in areal restriction of platform waters.

Anhydrites are rare in the Permian Upper Khuff C except near the base of the studied interval, and as anhydrite cement within grainstones. Anhydrite units are well developed in the Triassic Khuff B and Khuff A. They mark times of arid climate and restriction over marginal sills. Some anhydrites form transgressive deposits within anhydrite-dominated high frequency sequences, but others are highstand deposits of high frequency sequences although at the parasequence scale, the subaqueous anhydrites appear to be late highstand to lowstand fills of accommodation remaining after carbonate deposition.

This study indicates that the Permian-Triassic boundary on the Arabian Platform was synchronous with a significant relative sea-level drop that exposed at least the inner half of the platform (from the outcrop belt to east of Ghawar). This contrasts with the conformable PT boundary in many other areas, which is characterized by overall transgression. Thin sections of core plugs across the PTB document the mass extinction with a major decrease in biotic groups. Within the Triassic sequences, the extinction was followed by widespread

development of subtidal thrombolites, marking decimation of grazing and burrowing faunas, and increased microbial calcification due to decreased bioskeletonization.

The oolite facies are the dominant reservoirs occurring in the uppermost high frequency sequence of the Permian Khuff C, and especially in the Triassic Khuff B and A. Reservoir facies are best developed when non-dolomitized oolitic facies were associated with open lagoon facies and were distant from evaporitic tidal flats. Within dolomitized units, best reservoirs are associated with oomoldic porosity. Anhydrite plugging destroys reservoir porosity, apparently reflecting proximity to sabkhas or salinas.

FIGURES AND FIGURE CAPTIONS

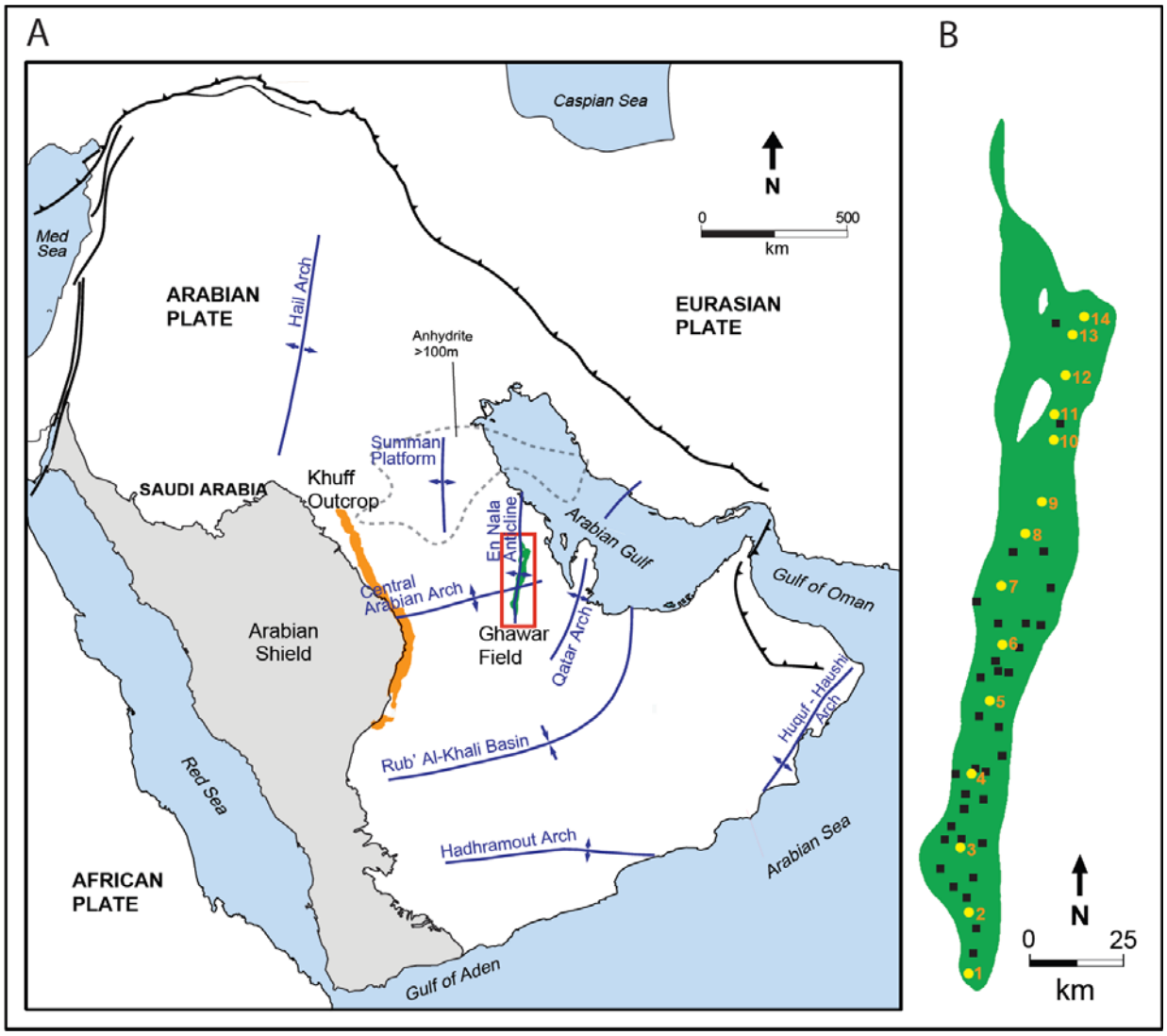

Figure 2.1: (**a)** Map of Arabian Plate showing the plate boundaries, major structural elements, location of Ghawar Field (study area; red rectangle), and the Permian-Triassic Khuff outcrop belt (orange); (**b).** Map of Ghawar Field showing approximate location of the studied wells including numbered wells used for cross-sections (yellow circles), and additional wells used for facies maps (black squares).

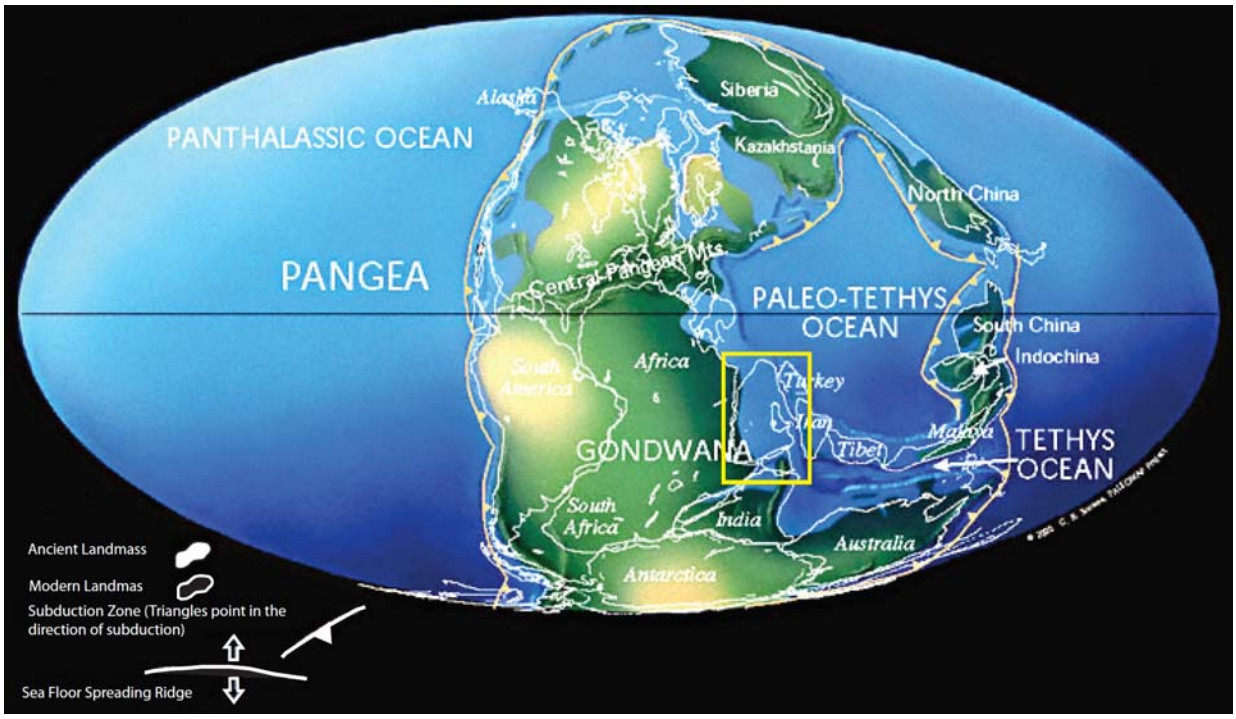

Figure 2.2: Regional plate tectonic and paleogeographic map showing the position of the Arabian Plate (outlined with yellow rectangle) during Late Permian (modified after Scotese 2003).

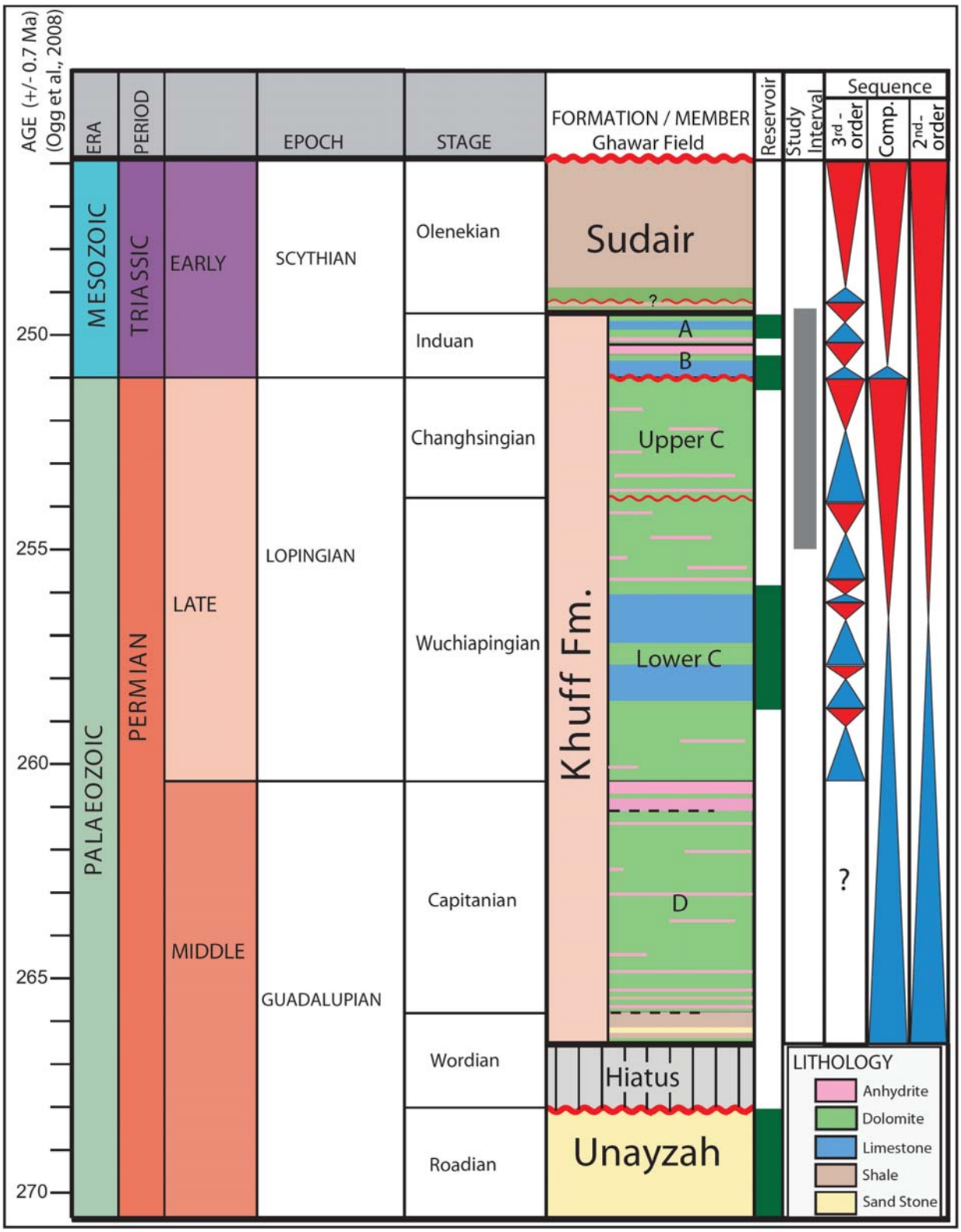

Figure 2.3: Chronostratigraphic chart showing the subdivision of the Khuff Formation, Saudi Arabia, as used in this paper. Modified from Ogg et al. (2008) and Al-Jallal (1995).

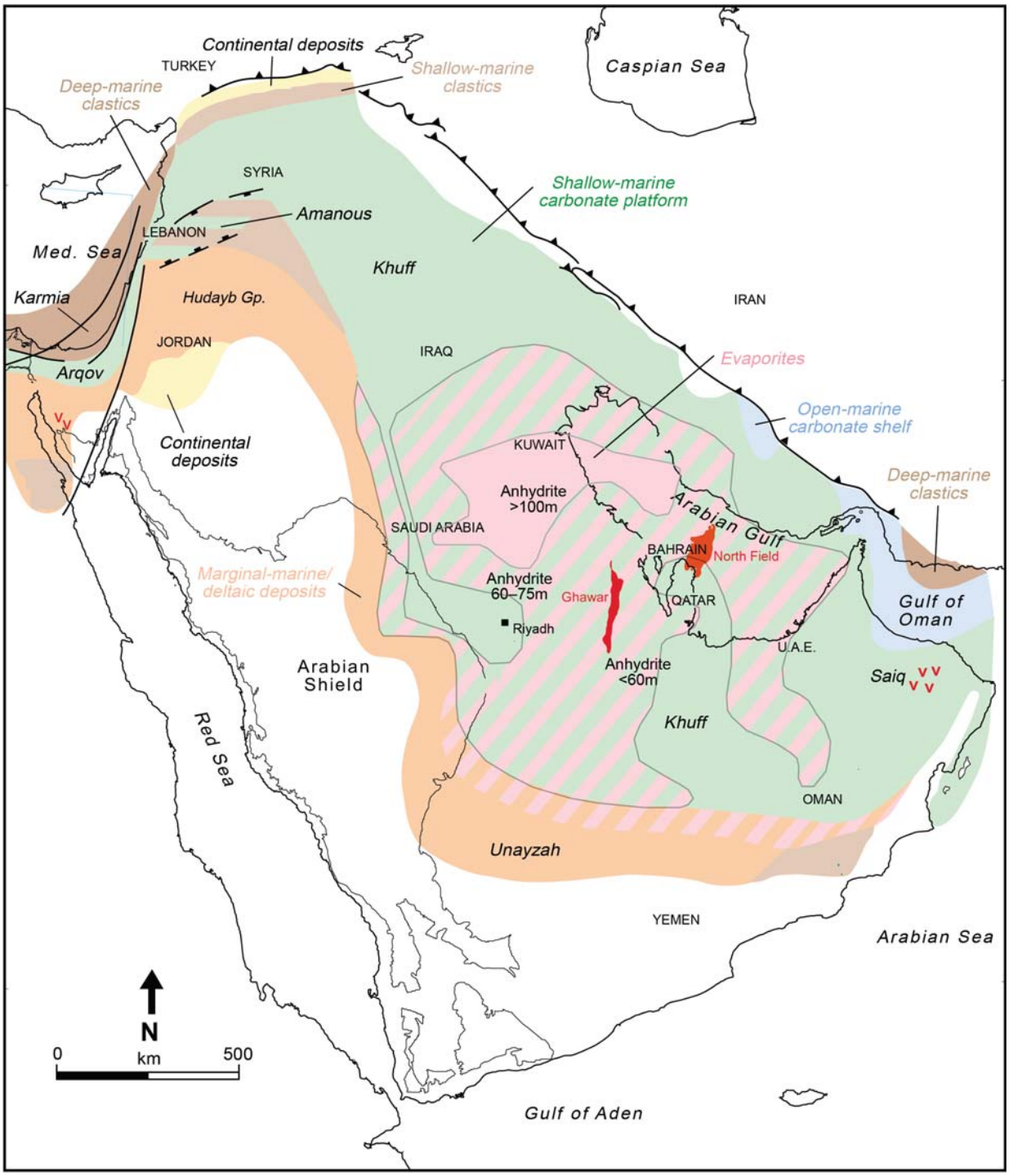

Figure 2.4: Map of Arabian Plate showing broad scale depositional facies of the Khuff carbonates and evaporites during Middle-to-Late Permian; Ghawar study area and North Field are shown in red (modified after Ziegler, 2001).

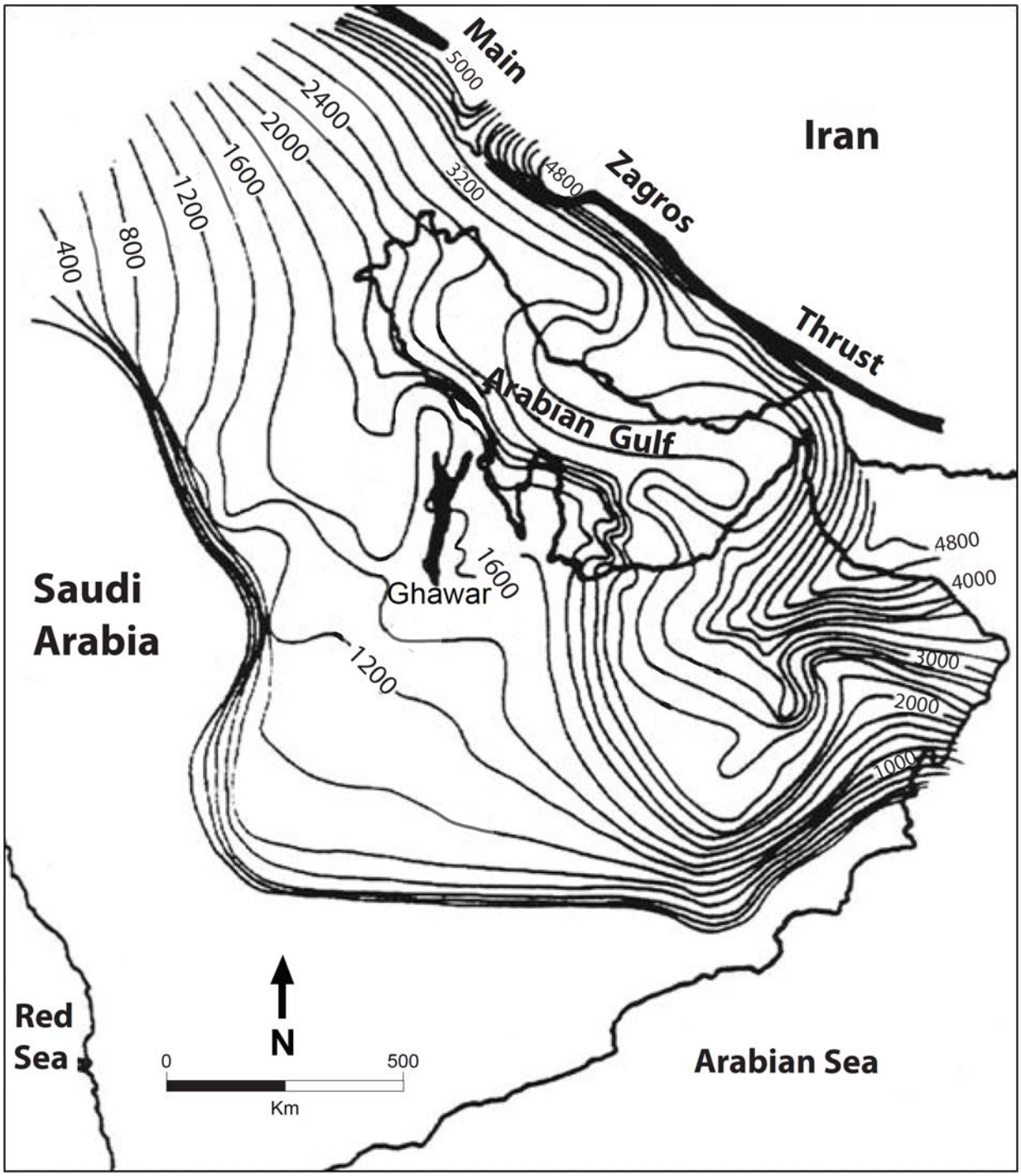

Figure 2.5: Regional isopach map of Permian-Triassic Khuff Formation in the Middle East (contour interval = 200 ft; ~ 60 m) (modified after Al-Jallal, 1995).

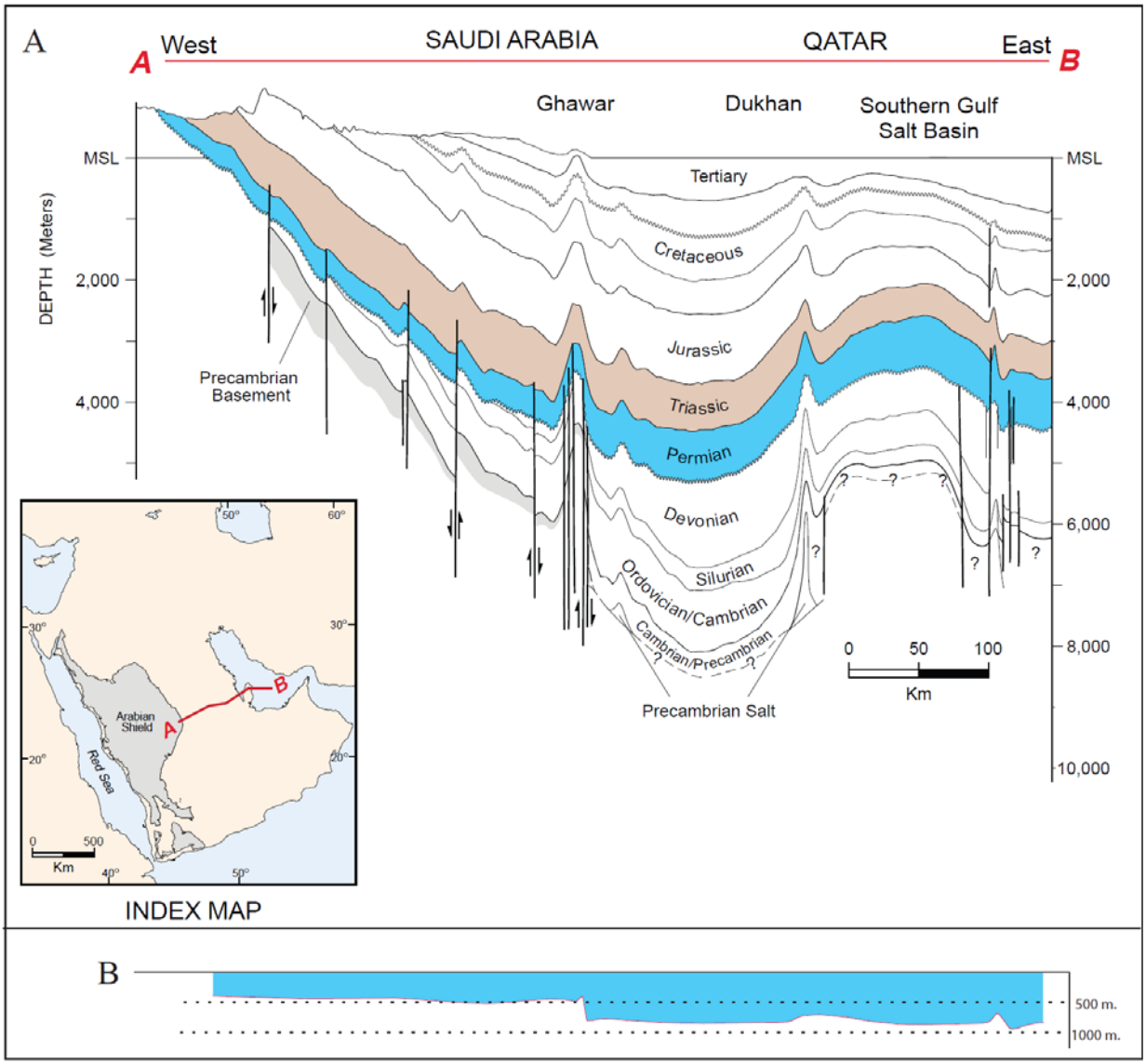

Figure 2.6: (a) Regional geologic cross section through the Middle East showing the gross stratigraphy and major structures; inset map shows cross section location (modified after Konert et al., 2001); (b) Restored cross section of the Permian succession including the underlying Unayzah Formation clastics, showing major thickening across faults beneath the Ghawar structure, which subdivide the area into a more slowly subsiding inner platform and a more rapidly subsiding outer platform.

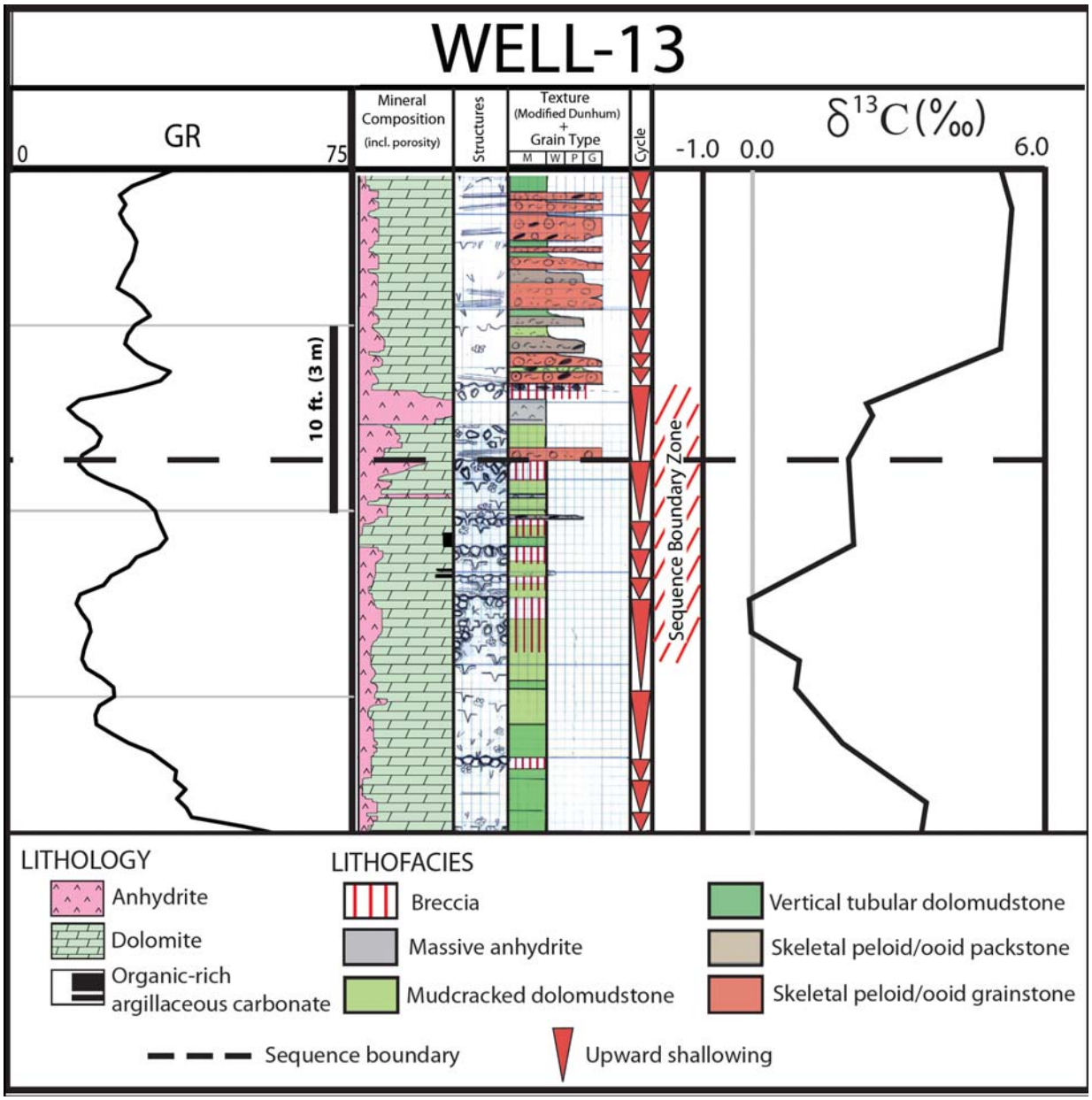

Figure 2.7: Detail lithologic column spanning the Wuchiapingian-Changhsingian boundary in Ghawar, along with gamma ray log and Carbon isotope profile. On core log, left hand column is mineralogy, central column is sedimentary structures, and right hand column is Dunham rock type. See legend for color coded rock types.

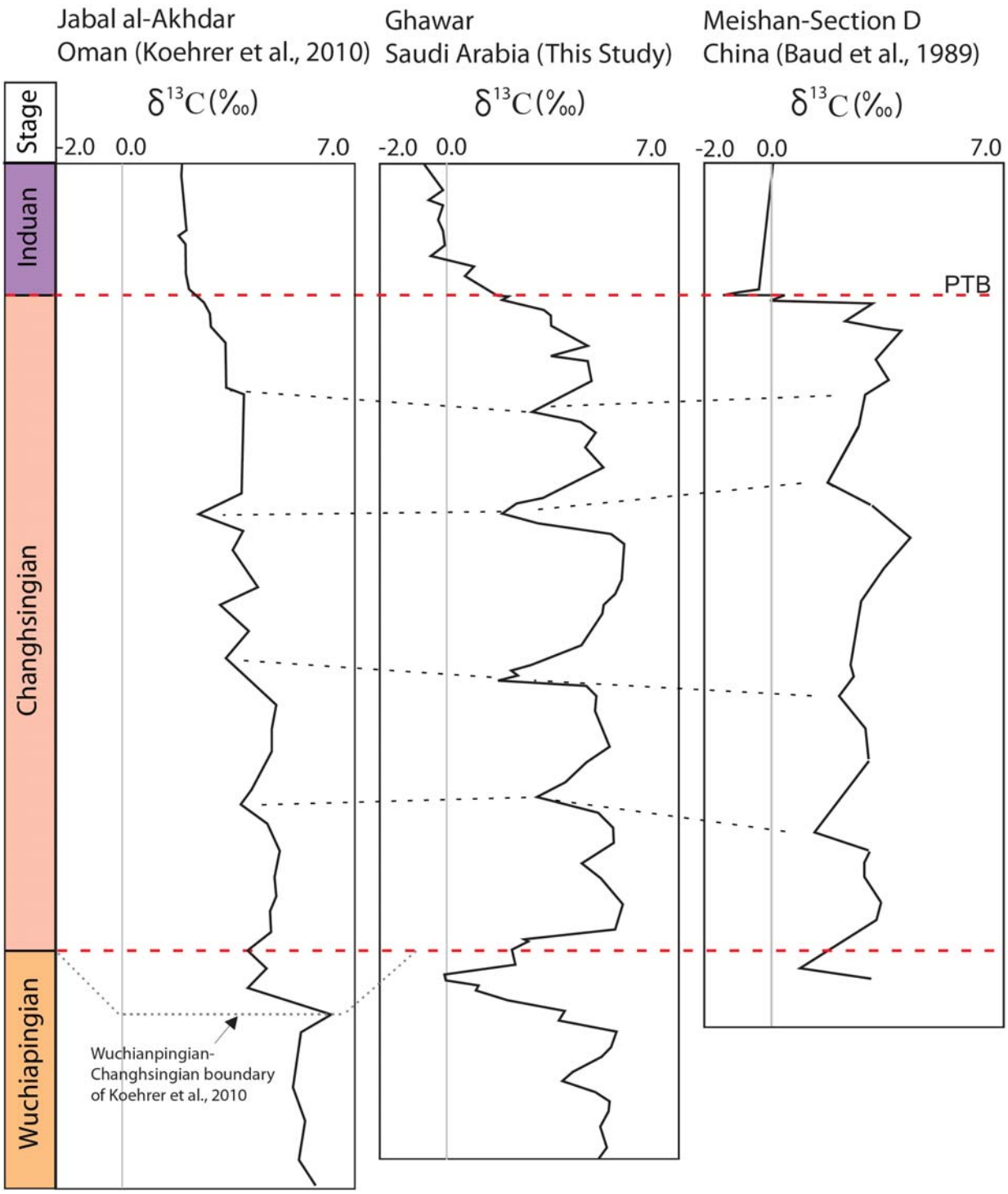

Figure 2.8: C-O isotope profiles through latest Permian and Early Triassic units. Well 13, Ghawar (central profile) is compared to those from Oman (left) and China (right). There are two major excursions, one in the latest Wuchiapingian-Changhsingian and one across the Permian-Triassic boundary.

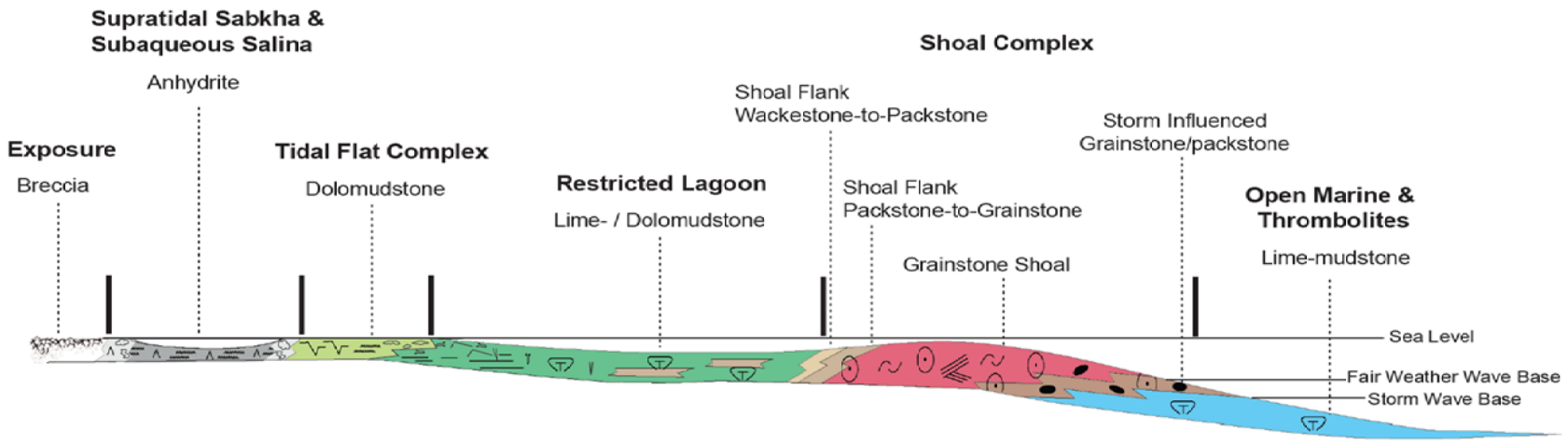

Figure 2.9: Depositional profile showing the relative water depths and facies on the ramp for the Upper Permian-Early Triassic Khuff Formation (modified after Al-Dukhayyil and Al-Tawil, 2008).

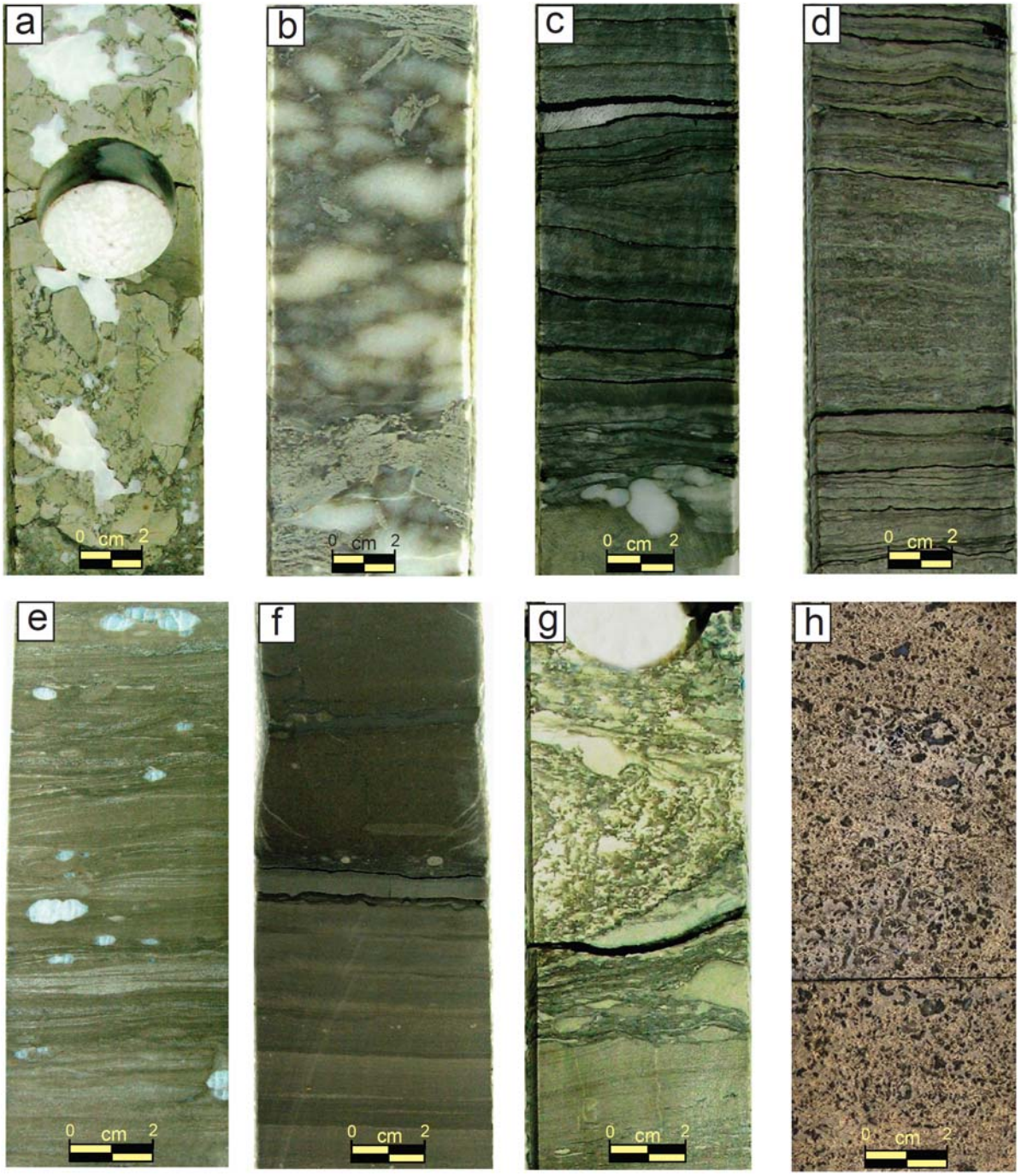

Figure 2.10: Slab photos of facies, Upper Khuff Formation (a) Fitted-fabric breccciated dolo-mudstone typical of the paleosols capping cycles; (b) Displacive nodular anhydrites within dolomite matrix (supratidal sabkha); (c) Subaqueous anhydrite showing typical layering (salina); (d) Mudcracked microbial laminite (tidal flat), with some burrow mottles;. (e) Horizontally burrowed ripple laminated dolo-mudstone (shallow subtidal carbonate sand-flat); (f) Carbonate mudstone ranging from structureless to layered (lagoon); (g) Thrombolite head with clotted fabric from restricted lagoonal facies (Early Triassic); (h) Brown skeletal peloid dolo-packstone (lagoonal sand sheets) with slightly later greenish gray anhydrites filling the pore spaces;

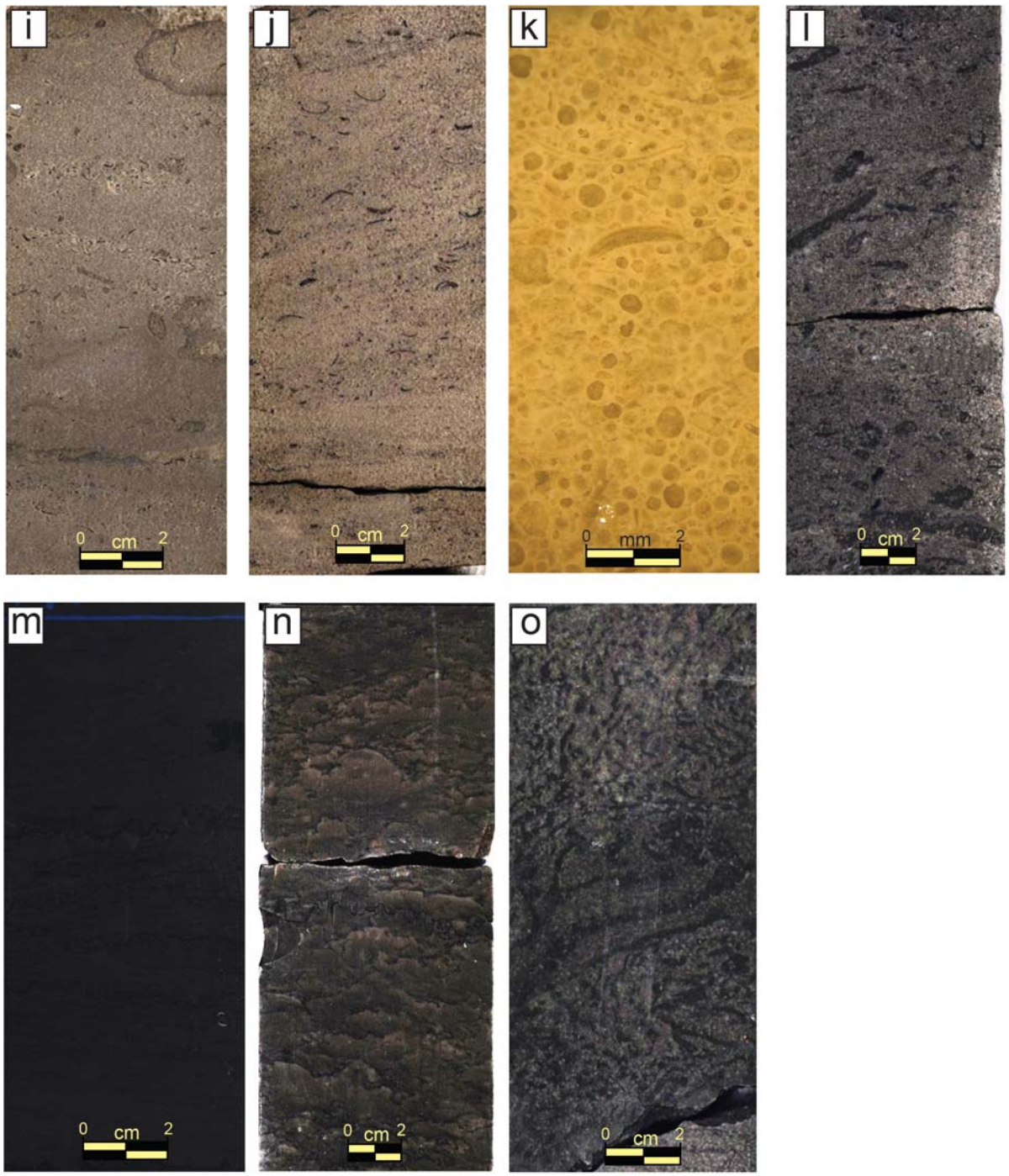

Fig. 2.10 continued: (i) Ooid peloid packstone to wackestone (back shoal facies); (j) slab and (k) binocular photo of cross-bedded skeletal peloid/ooid grainstone reservoir facies (oolitic shoal), (l) Flat-pebble- intraclast skeletal ooid/peloid grainstone (storm bed within fore-shoal facies); (m) Massive dark lime-mudstone (open lagoon, Early Triassic); (n) Microbially laminated/thrombolotic lime-mudstone (open lagoon, Early Triassic); (o) Clotted thrombolite fabric within lime mudstone (open lagoon, Early Triassic).

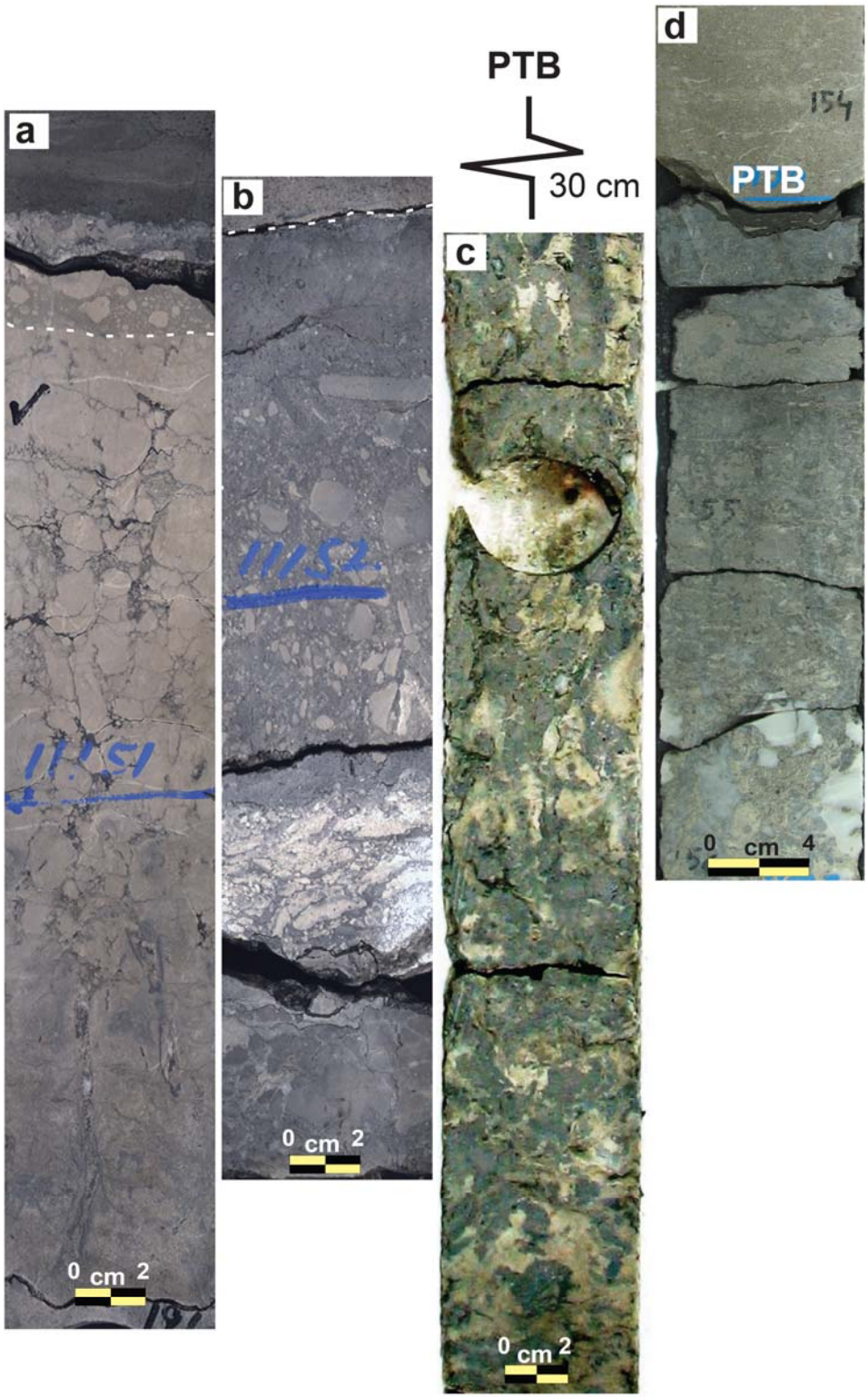

Figure 2.11: Close-up of slabs of paleosols, and breciated and/or rooted dolomudstone: (a) Fitted fabric breccias roots from the sequence boundary zone of UC-5, Well-4; (b) Reworked paleosols from 20 cm beneath previous slab; (c) Breciated and rooted dolomudstone at PTB, Well-4; (d) Breccias underlying the PTB, overlain by thin shale parting at PTB, Well-5.

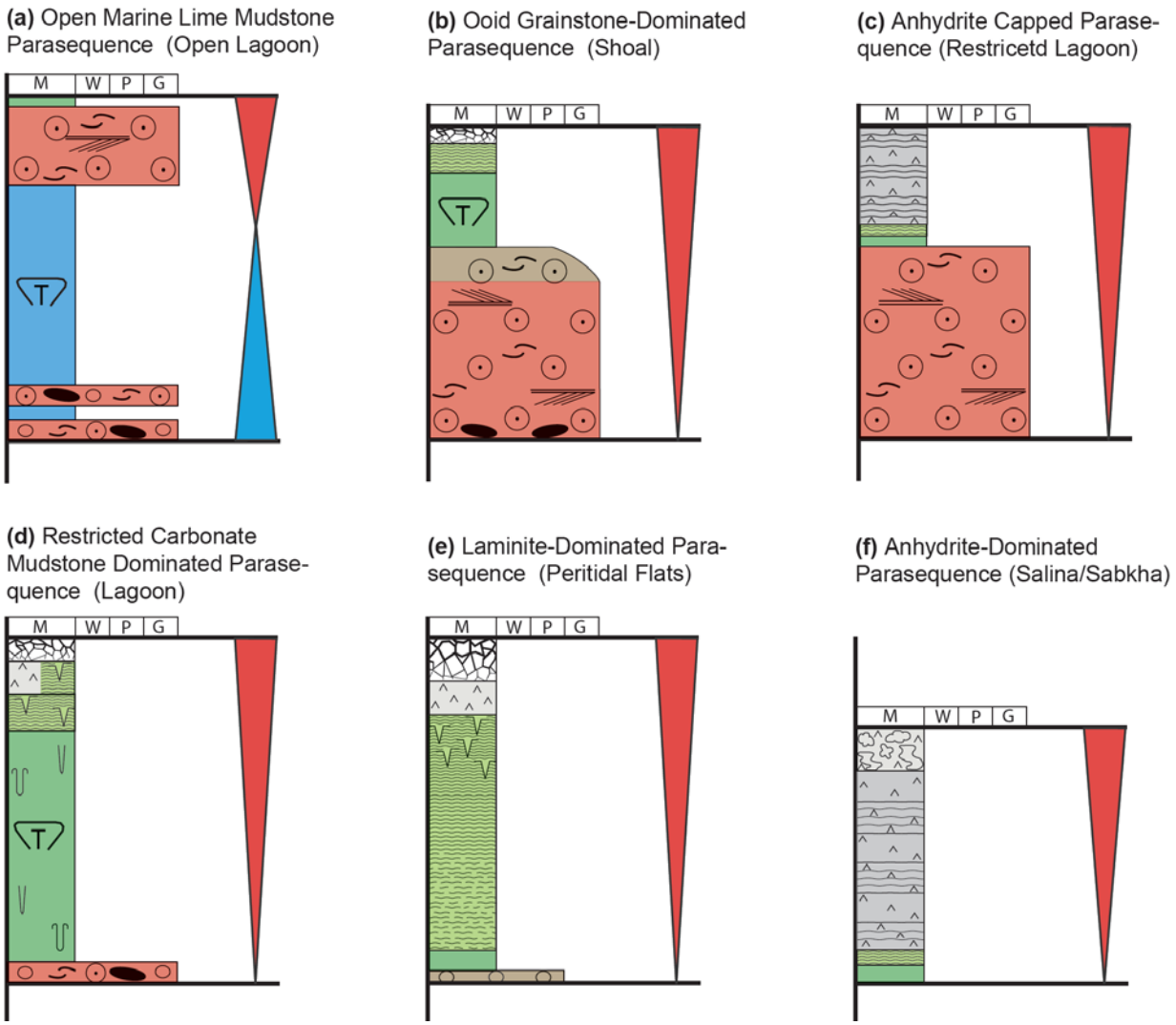

Figure 2.12: Types of Upper Khuff parasequences.

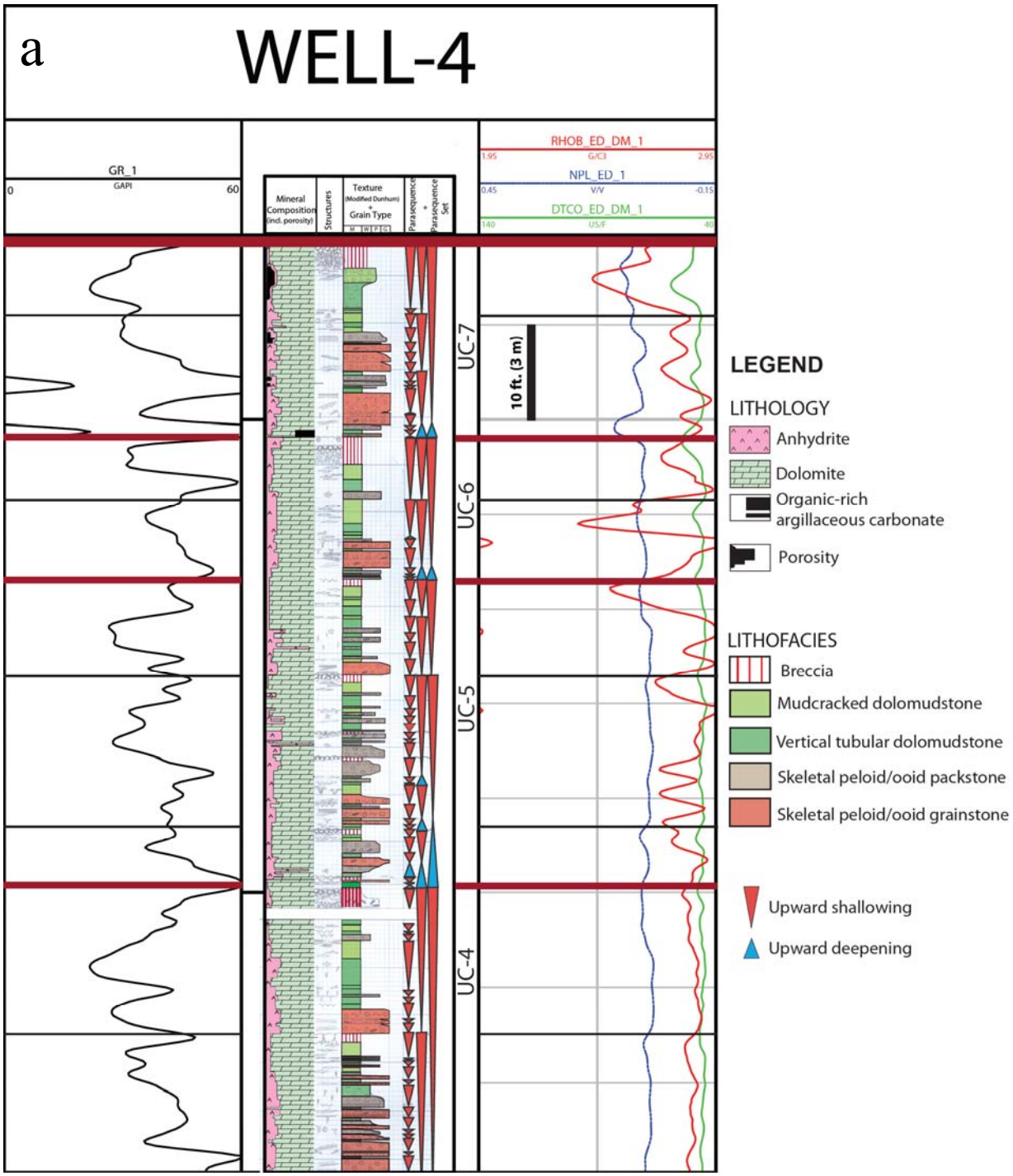

Figure 2.13 a: Representative core log description, Latest Permian section, Well-4. Sequence boundaries are marked by heavy dark red line and parasequence set boundaries are black lines. Left hand column is mineralogy, central column is sedimentary structures and right hand column is Dunham rock type. See legend for color code.

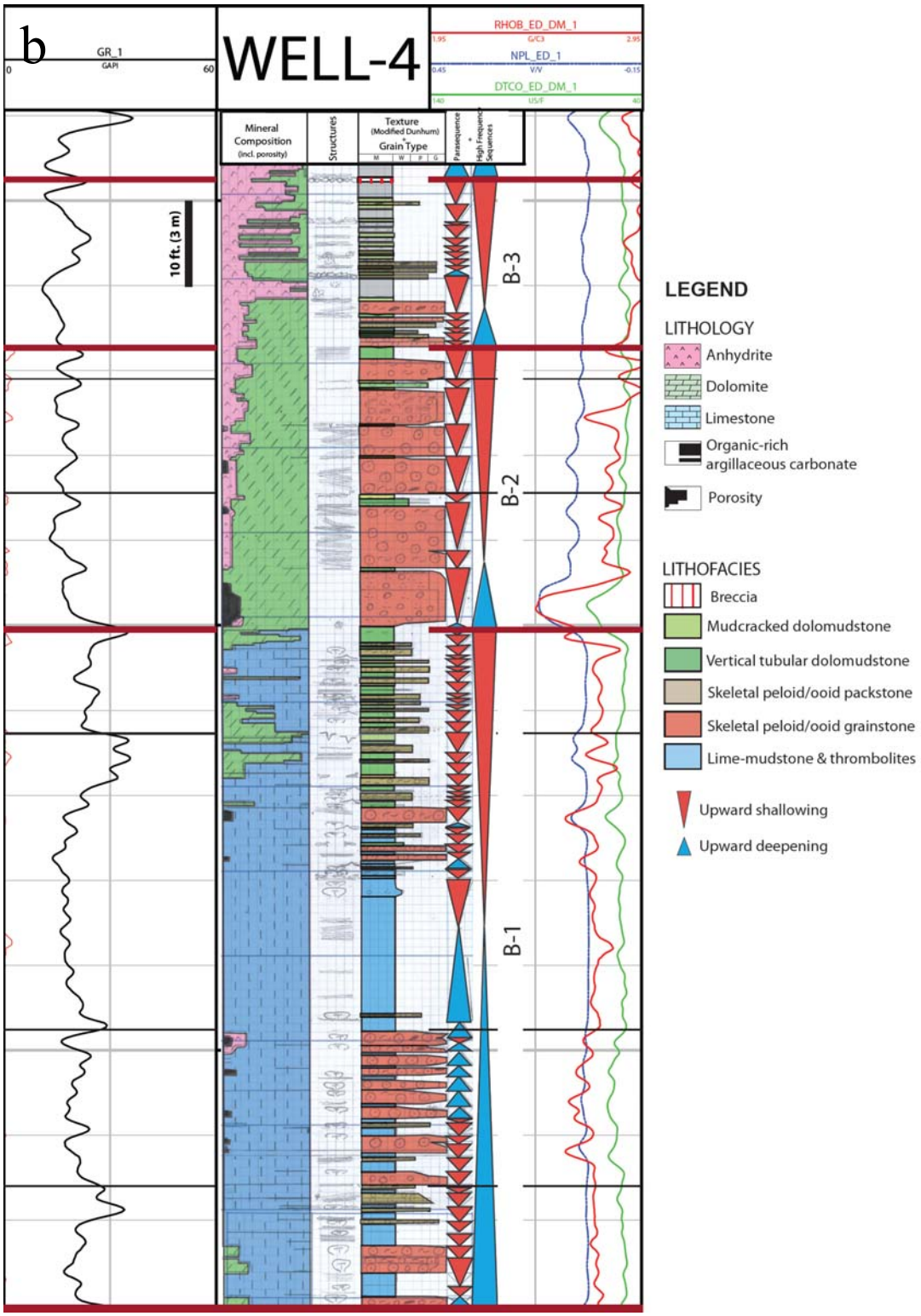

Figure 2.13 b: Representative core log description, Early Triassic section, Well-4. Sequence boundaries are marked by heavy dark red line and parasequence set boundaries are black lines. Left hand column is mineralogy, central column is sedimentary structures, and right hand column is Dunham rock type. See legend for color code.

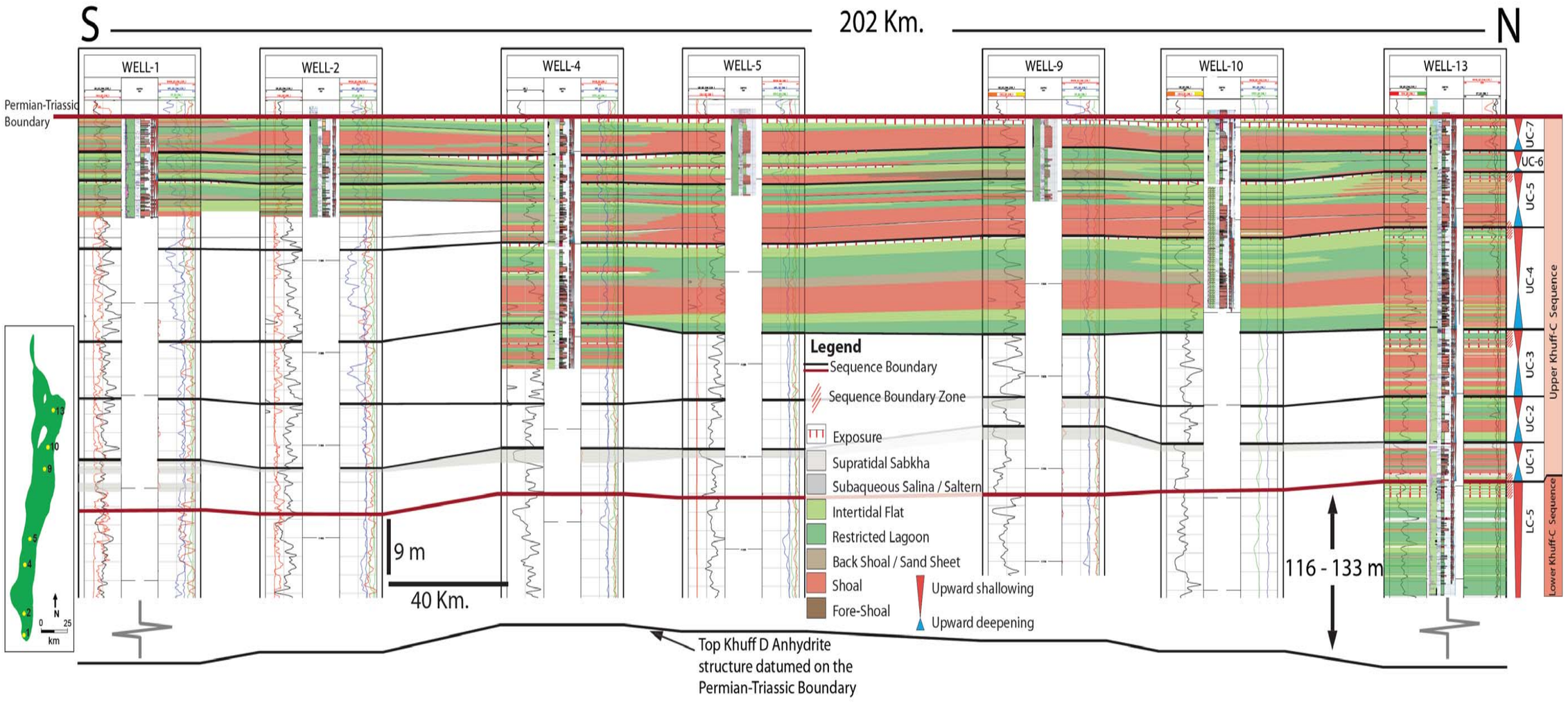

Figure 2.14: Cross section showing the facies distribution and interpreted sequence stratigraphy of the latest Permian Khuff Formation. Inset map shows location of logged cores used for the cross section. Lithologies are only shown in areas of well control.

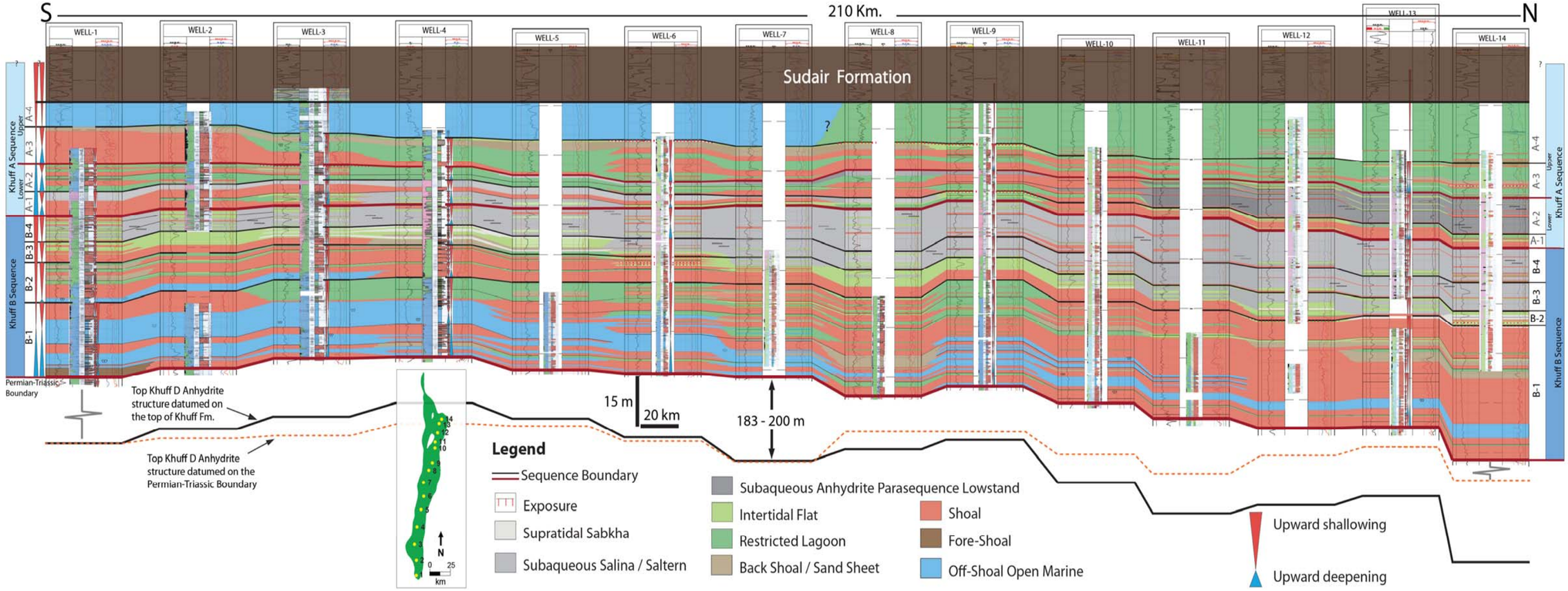

Figure 2.15. The Early Triassic Khuff cross-section showing facies distribution and interpreted sequence stratigraphy. Inset map shows the core locations used in the cross section.

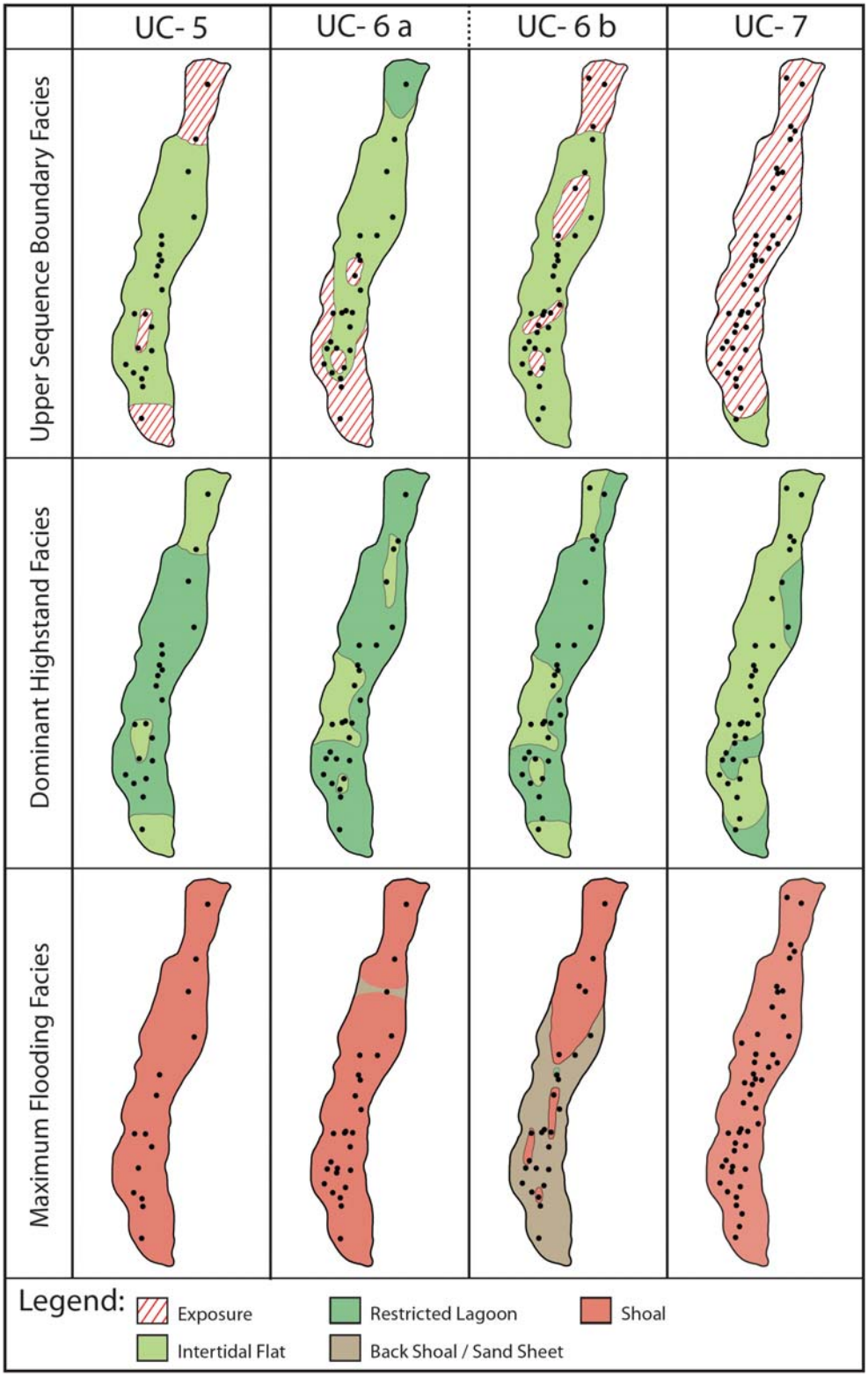

Figure 2.16 a: Facies maps of high frequency sequences, showing maximum flooding facies, the dominant highstand facies and the facies immediately underlying the upper boundaries, for Upper Permian Khuff C member. The black circles show the approximate location of the cored wells.

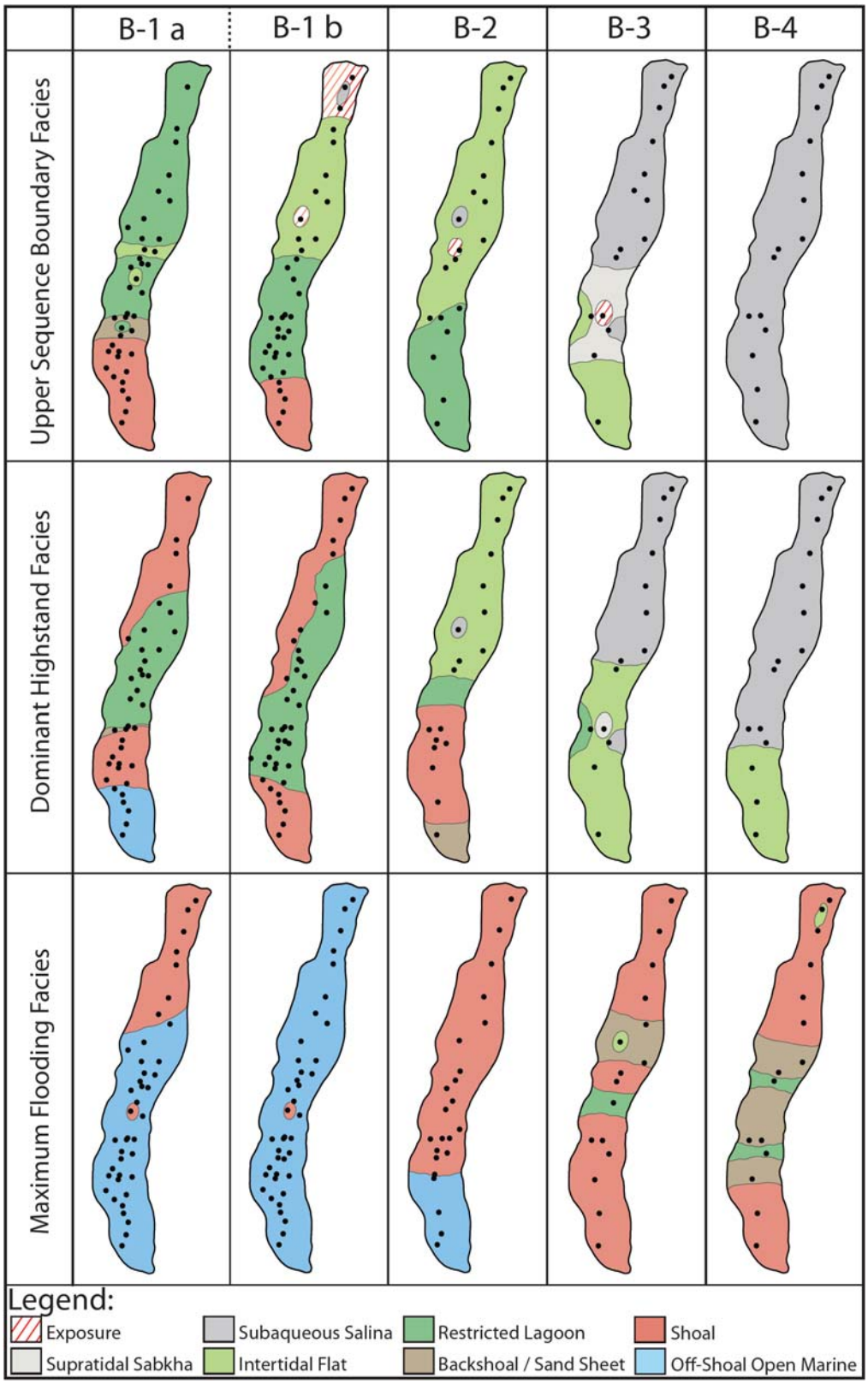

Figure 2.16 b: Facies maps of high frequency sequences, showing maximum flooding facies, the dominant highstand facies and the facies immediately underlying the upper boundaries Early Triasic Khuff B. The black circles show the approximate location of the cored wells.

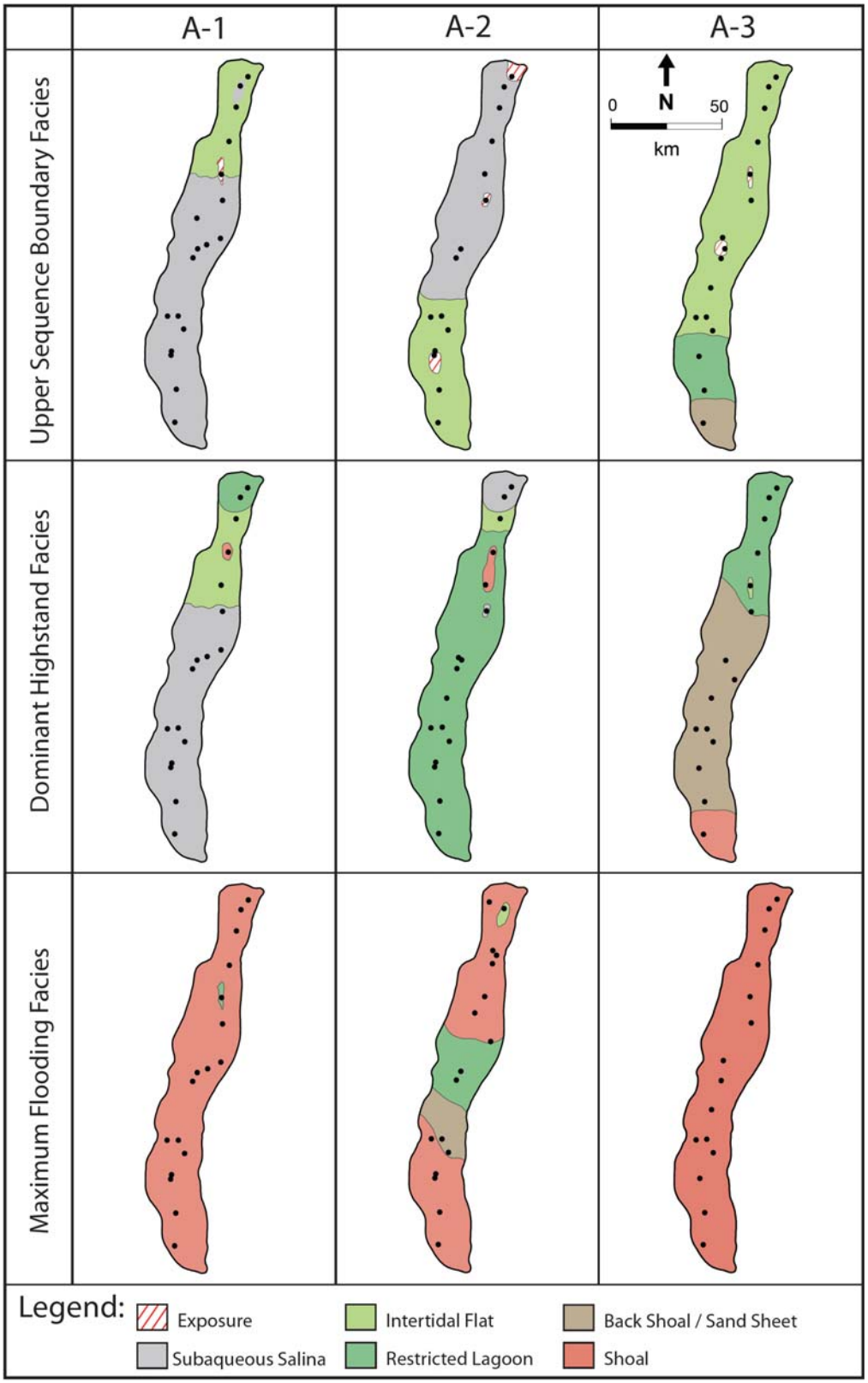

Figure 2.16 c: Facies maps of high frequency sequences, showing maximum flooding facies, the dominant highstand facies and the facies immediately underlying the upper boundaries Early Triassic. The black circles show the approximate location of the cored wells.

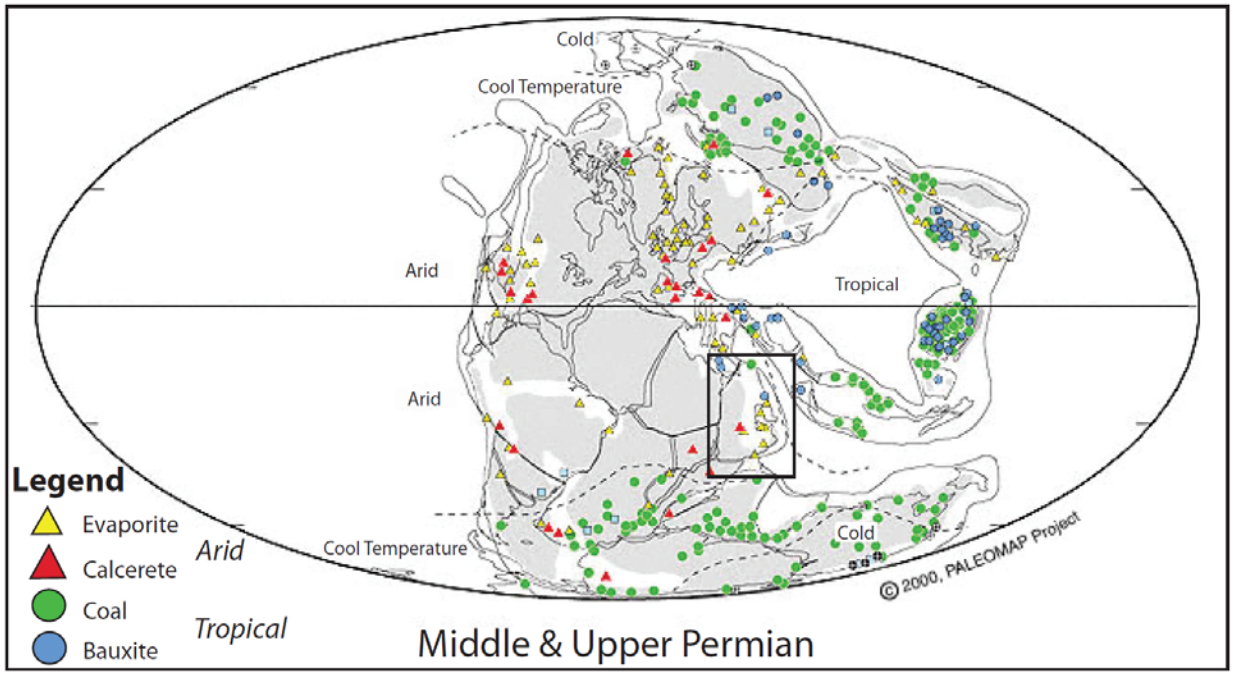

Figure 2.17: Global paleoclimate map for the Late Permian (modified after Scotese, 2003). Arabia (outlined by rectangle) lies within an extensive desert belt, even though it was situated at 5 to 20 degrees south, reflecting the Pangean megamonsoon system which kept the tropics dry. This situation continued into the Early Triassic.

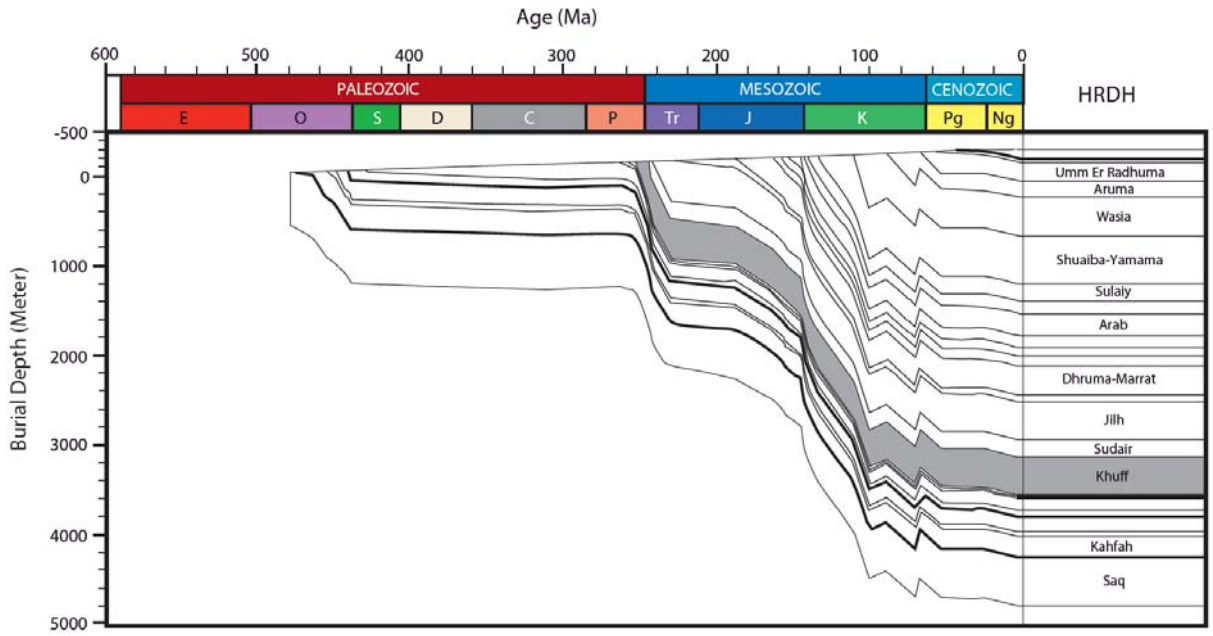

Figure 2.18: Burial history plot for a well from Haradh area, Ghawar; Khuff Formation is shaded grey. Late Permian and Early Triassic mark a significant increase in subsidence rate (modified after Abu-Ali, M. and R. Littke, 2005).

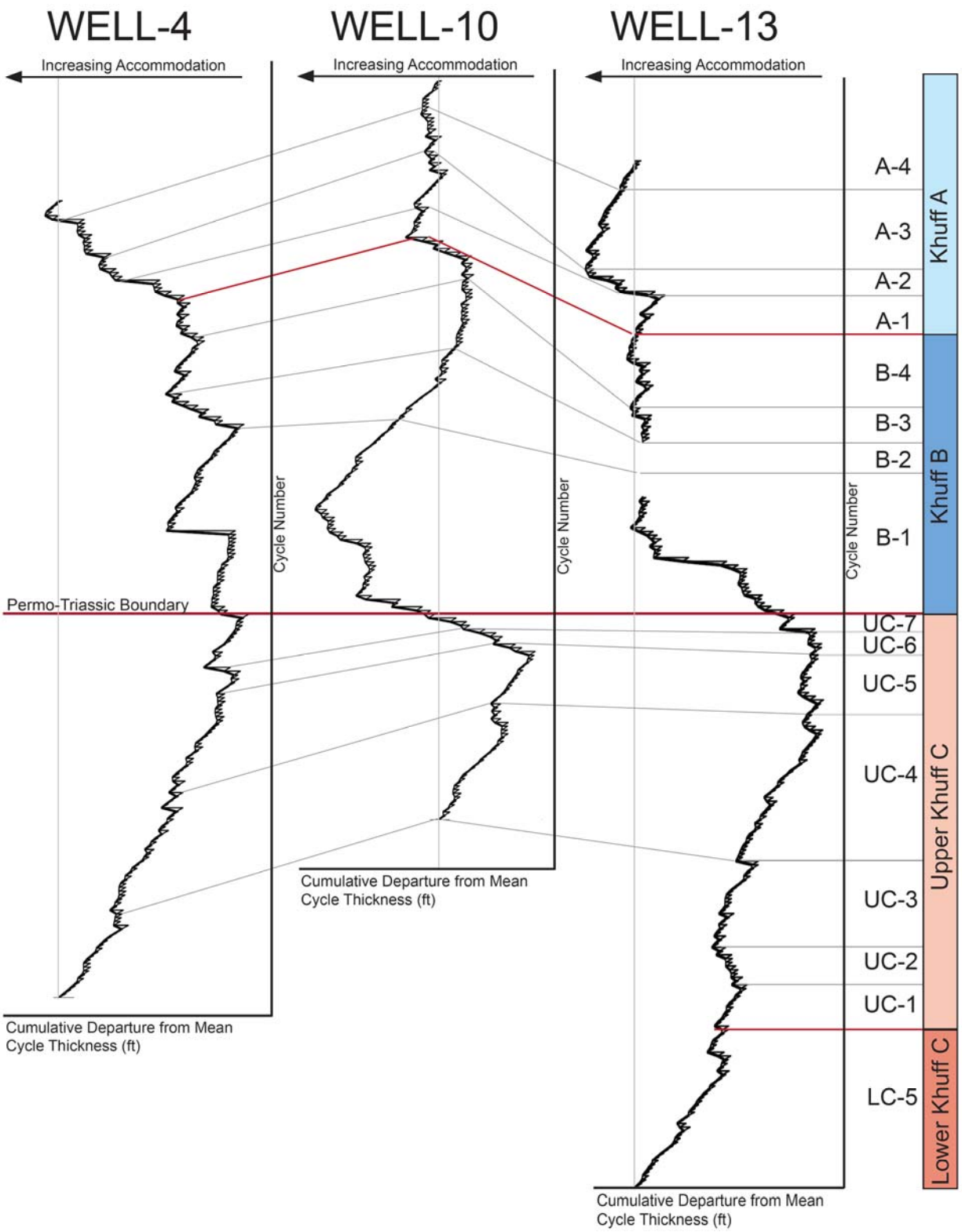

Fig. 2.19: Fischer plots of cyclic successions of three wells: Well-4, Well-10 and Well-13.

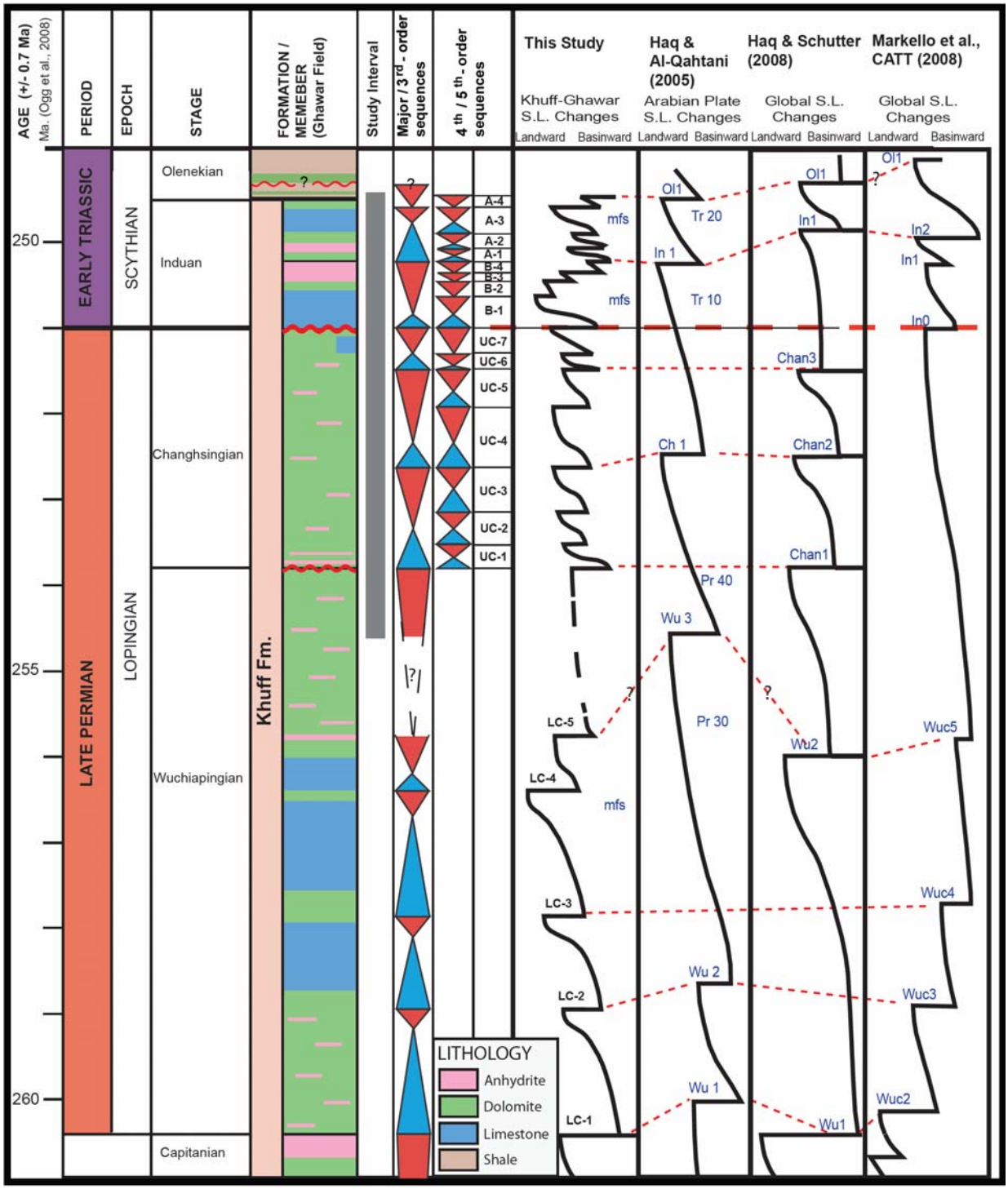

Figure 2.20: Khuff coastal onlap curve from the study interval (left hand curve) compared to coastal onlap curves from the Arabian Plate of Haq and Al-Qahtani (2005), the global curve of Haq and Schutter (2008) and the global CATT chart of Markelle et al. (2008). Thin dotted lines link possible correlative sequence boundaries; temporal position of these is uncertain in many cases, given the limits on the biostratigraphic control at this high resolution. Sequence boundaries on Haq and Qahtani curve were labeled by the author to simplify discussion.

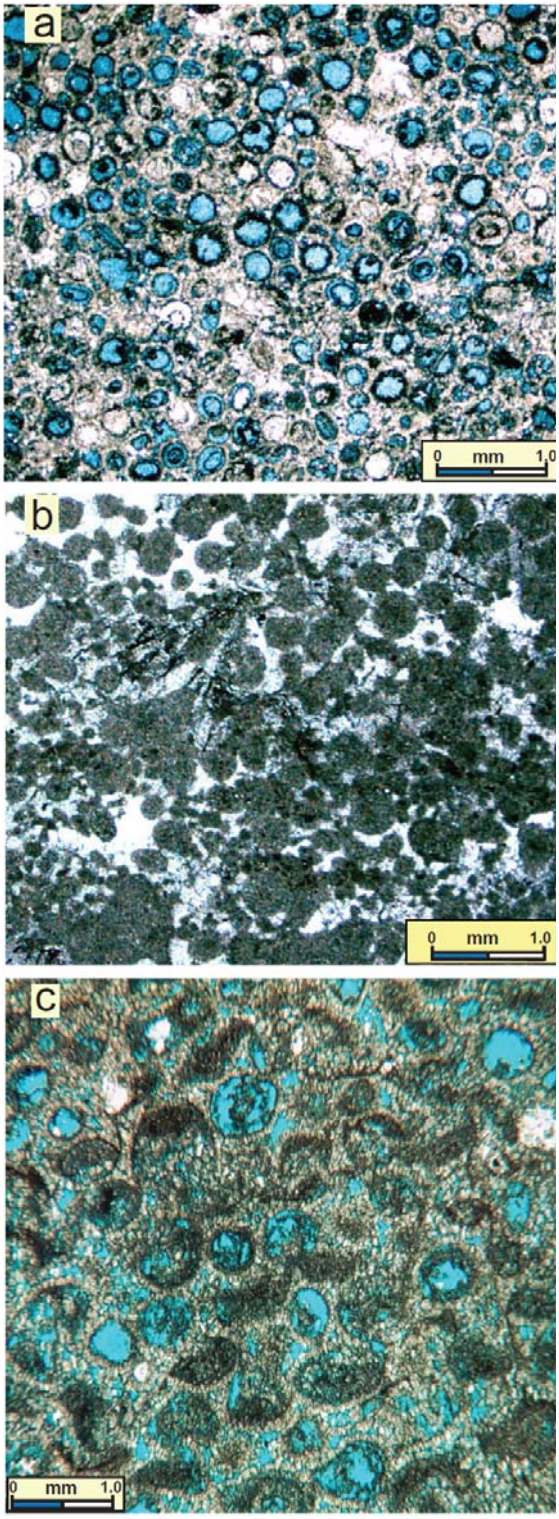

Figure 2.21: Lime-grainston/packstone reservoir facies (a) Undolomitized moldic ooid grainstone with minor interparticle porosity; (b) Dolomitized grainstone with porosity plugged by anhydrite cemen; (c) dolomitized moldic ooid grainstone with oomoldic pores surrounded by dolomitized cement rims bordering interparticle pores; these are the best reservoir quality in the Upper Khuff Formation.

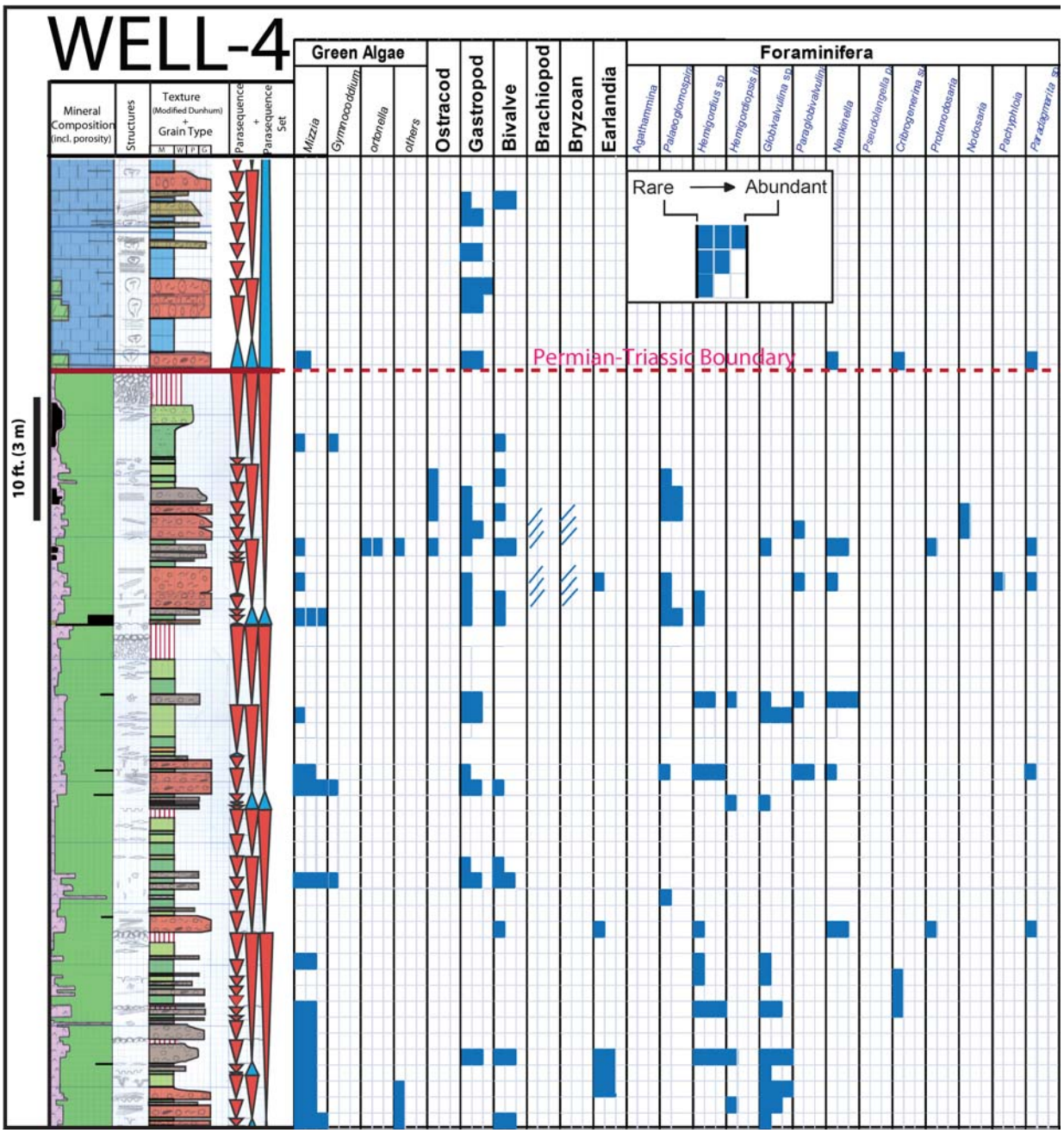

Figure 2.22 a: Plot of biodiversity of major taxonomic groups across the PTB, using petrographic diversity as determined from thin sections. Note that bryzoans and brachiopods although they are present in northern Ghawar, were not observed in this well; reworked Permian faunas (see Fig. 2.22 b) are observed in the thin grainy bed sitting on the PTB in a few wells, but are not observed above this level.

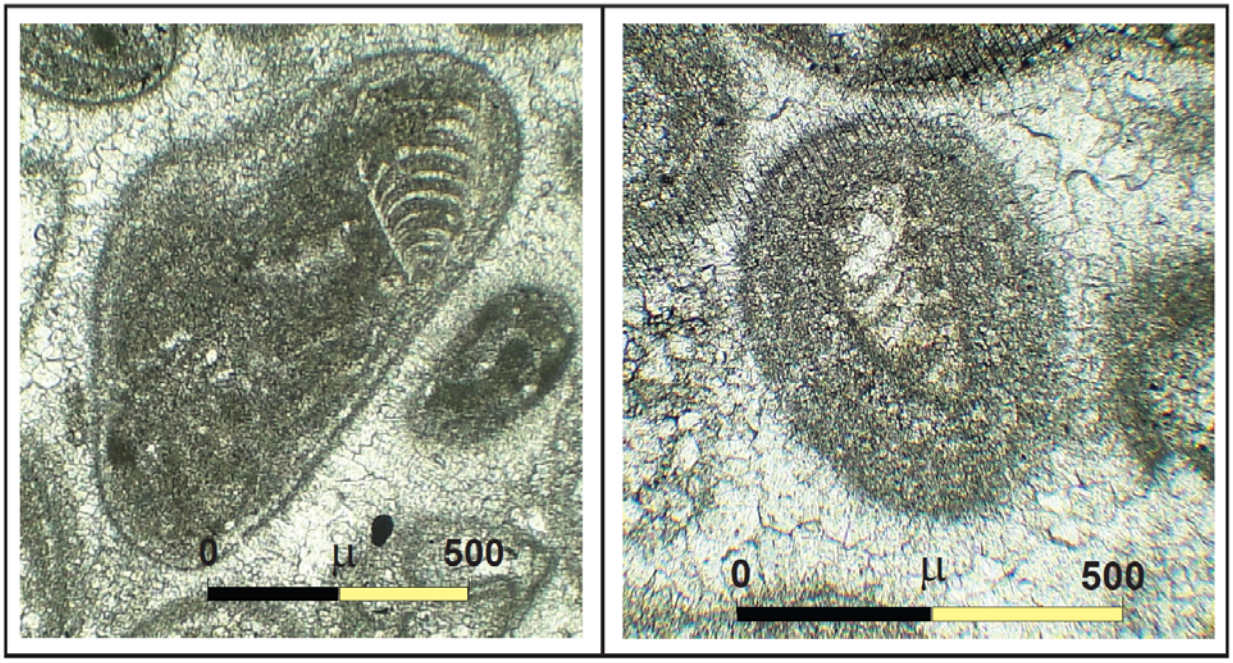

Figure 2.22 b: Examples of the reworked Permian foraminifera; *Cribrogenerina sumatrana* (left) and *Paradagmarita* sp. (right).

TABLES AND TABLE CAPTIONS

Table 2.1. Permo-Triassic Khuff carbonates and evaporites facies

Depositional Environment	**Exposure/ Emergent Terrane**	**Supratidal Sabkha**	**Subaqueous Salina/ saltern**	**Tidal Flat Complex**	**Lagoon**			**Back-Shoal-Sand Sheet** (rare; in Triassic only)	**Ooid/Peloid Shoal Complex**			**Subtidal Off-shoal/Open Marine**
					Hypersaline Shallow Subtidal	Hypersaline Peritidal to subtidal	Less Restricted		Back Shoal	Shoal Crest	Storm Influenced Fore-shoal	
Energy/Depth		Low-energy supratidal flats	Low-energy salinas	Low-energy tidal flats	Low-energy		Low-energy subtidal	Moderate; behind the shoal (above fair-weather wave base)	Moderate-to-low energy; behind the shoal (above fair-weather wave base)	High-energy; within fair-weather wave base (~10 meters depth)	Intermittent high-energy: above storm wave base, and below fair-weather wave base (~15.0 meters depth)	Low-energy: below storm wave base (> 15 meters depth
Rock Type	**Breccias**	**White nodular-to-massive anhydrite**	**Black laminated-to-massive anhydrite**	**Crinkly laminated dolomudstone**	**Ripple laminated dolosiltites**	**Vertical tubular dolomudstone -to-wackestone**	**Massive-to-laminated muddy carbonates and thrombolites**	**Skeletal peloid packstone/ grainstone**	**Wackestone-to-packstone**	**Oolitic grainstone**	**Intraclast ooid packstone/ grainstone**	**Lime mudstone**
Thickness (meter)	0.15 – 2 m	0.05 - 1.5 m	0.1 – 4 m	0.03- 2 m	0.03- 1 m		0.5 - 3.5 m	1.0- 2 m	0.3 - 1.5 m	0.3 to 12 m	0.3 to 2 m	0.1 – 8 m
Color	Gray-to-tan	White-to-grayish white	Black, dark-to-white gray-to-white	Light-to-medium grey	Tan-to-brown		Gray-to-dark gray	Brown and greenish gray	Brown	Light-to-medium brown.	Medium-to-dark brown	Dark gray-to-dark brown
Sedimentary Structure	Fitted fabric breccias, karstic collapse features, and root traces	Massive-to-nodular-to bedded with fine laminations	Laminated, massive and minor nodular fabrics with microbial laminations	burrow-mottled crinkly (microbial) laminated and fenestrae-to-crinkly laminated-to-mud-cracked	Extensively horizontally burrowed with ripple laminations	Vertical tubes (burrows or roots?)	Vertical and horizontal burrows (many anhydrite filled) millimeter-to-centimeter planer or wavy mechanical lamination, hardgrounds, and structureless beds. Sub-aqueous microbial heads and thrombolites in Triassic.	Structureless, with rare horizontal-to-sub horizontal lamination	Sub horizontal lamination-to-horizontally burrowed-to-massive.	Sub horizontal-to-low angle cross-laminated, and rare high angle cross-bedded	Horizontal-to-sub horizontal lamination	In Permian: minor horizontal burrows-to-non-burrowed. In Triassic: sub-aqueous microbial lamination, and thrombolites;
Mineralogy	Dolomite with anhydrite	Anhydrite with dolomite	Anhydrite with dolomite	Dolomite and anhydrite	Dolomite	Anhydrite fills burrows	Dolomite and limestone with diagenetic anhydrite	Dolomite with diagenetic anhydrite	Dolomite and limestone	Dolomite and limestone	Limestone and dolomite	Limestone
Texture (Dunham + grain type)	Mud-to-wackestone composed of angular-to-sub angular gravel size intraclasts	Mud supported size	Mud supported size	Mudstone composed of clay-to-silt size mud.	Pellet mudstone-to-packstone (dolosiltite/ fine sucrosic dolomite)		Mudstone-to-mud clast peloidal skeletal wackestone composed of fine size peloids	Skeletal peloid packstone/ grainstone composed of fine-to-coarse sand size, and rare very coarse peloids; and common gravel size mud clasts.	skeletal peloid/ooid packstone-to-wackestone, composed of fine-to-medium sand size, and rare coarse peloids and ooids; and rare gravel size mud clasts.	Skeletal peloid/ooid grainstone composed of fine-to-medium sand size, and rare coarse peloids and ooids; and rare gravel size mud clasts.	Flat-pebble conglomerate-to-intraclastic skeletal grainstone-to-Packstone composed of fine-to-medium sand size, and rare coarse peloids and ooids, and common gravel size mud clasts.	Mudstone; skeletal wackestone-to-packstone and thrombolites composed of clay-to-silt size.

Fossils Permian Triassic	None	None	None	None	None	Foraminifera, green algae gastropods, bivalves and ostracods. .	Foraminifera, green algae gastropods, bivalves.and ostracods. Gastropods and bivalves.	Bivalves and gastropods	Foraminifera, green algae gastropods, bivalves and rare ostracods. Gastropods and bivalves.	Foraminifera, gastropods, bivalves and rare ostracods, brachiopods, bryozoans and crinoids. Gastropods, bivalves and rare ostracods.	Foraminifera, gastropods, bivalves and rare brachiopods, bryozoans and crinoids. Gastropods and bivalves.	Rare bryozoans, crinoids, and brachiopods. Subaqueous mats and gastropods.
Reservoir Quality	None	None	None	Fair intercrystalline porosity + fair perm. (rare)	Fair-to-good intercrystalline porosity + medium-to-high-perm.	None	None	None-to-fair moldic, interparticle and intercrystalline porosities + very low-to-medium perm.	None-to-fair moldic and intercrystalline porosities + low-to-medium perm.	None-to-high Moldic, fair-to-low interparticle and intercrystalline porosities + Low-to-high perm.	Fair Moldic porosity + low perm.	None

Table 2.2. Brief description of the Permian Khuff sequences

Sequences	Thickness	Basal Sequence Boundary	LST	TST	MFS	HST
LC-5 Based on one cored well (cut in the upper 60 ft.	38 to 42 m ft (?) thick	On a regional supratidal anhydrite capping the Khuff C reservoir.	Not recognized	Restricted lagoonal dolomudstone-dominated parasequences with some thin grainstone/packstone beds base of cycles.	Developed above uppermost grainstone.	Dominated by thick of peritidal dolomuddy carbonate; shallows up to breccias and/or supratidal anhydrite.
UC-1 Based on one cored well.	7 to 11 m thick	Includes several exposure surfaces (sequence boundary zone)	Not recognized	Dolo-laminite-dominated parasequence deepening up into parasequences of peloid dolograinstone-dominated.	Developed above grainstone-dominated cycles.	Thick parasequences of dolograinstone and lagoonal mudstone-dominated parasequences.
UC-2 Based on one cored well.	6.5 to 10 m thick	Placed above regional supratidal anhydrite	Not recognized	Peritidal dolomudstone parasequence that deepens up into ooid dolograinstone-dominated cycle.	Placed above regional ooid grainstone	Parasequences of lagoonal dolomuddy carbonate grading to tidal flat laminites.
UC-3 Based on two cored wells.	9.5 to 12 m thick	Erosional surface with thin incipient breccia	Not recognized	Four parasequences of thick dolograinstone up into laminite with supratidal anhydrite capping parasequence 2; thin paleosol caps uppermost oolite of TST.	Placed above top thick grainstone	Thinning upward parasequences of thin dolograinstone and peritidal muddy carbonates.
UC-4 Based on three cored wells.	14 to 17 m thick	Placed above fitted fabric breccia in the north (up dip, and burrowed laminites in south (down-dip)	Not recognized	Consists of thin interbedded dolograinstone- and laminite-dominated parasequences deepening up into thick ooid grainstone-dominated parasequences.	Placed above the ooid grainstone-dominated cycles	Parasequences of thin dolograinstone overlain by lagoonal dolomuddy carbonates that grade up into laminite-dominated parasequences.
UC-5	9 to 11 m thick	Basal sequence boundary is an erosional surface on slightly brecciated carbonates	Not recognized	Parasequences of ooid dolograinstone and minor muddy peritidal dolomudstone deepening into thick grainstone.	Placed above the thick ooid-grainstone complex	Subordinate dolograinstone parasequences grading up into peritidal mudstone and laminate-dominated parasequences locally with breaccia caps.
UC-6	3 to 5 m thick	Basal sequence boundary is either hardground or erosional surface with breccia or laminite	Not recognized	Dolograinstone-dominated parasequences.	Developed on basal thin to thick ooid grainstone and lesser packstone	Restricted lagoonal dolomudstone-dominated parasequences shallow up into laminite-dominated cycles.
UC-7	5 to 6.5 m thick	Erosional surface on burrowed laminate or breccia	Not recognized	Dolograinstone parasequences with bryozoans, crinoids and brachiopods lime-dolostone in northern Ghawar	Developed on grainstone.	Interbedded grainstone- and lagoonal mudstone-dominated parasequences capped by tidal flat laminite and some localized breccia. Grainstones are dolomitic limestone in northern Ghawar.

Table 2.3. Brief description of the Triassic Khuff sequences

Sequences	Thickness	Basal Sequence Boundary	LST	TST	MFS	HST
B-1	26 to 41 m thick	Permian Triassic boundary; on regional emergence breccias and paleosols over much of Ghawar, and mud cracked laminites in southernmost Ghawar.	Not recognized	Consists of open marine lime mudstone parasequences and lesser oolite-dominated parasequences in southern Ghawar. In northern Ghawar, oolite-dominated parasequences and lesser open marine lime mudstone parasequences; thrombolites are common.	Developed at the top of interval of open marine lime-mudstone	Dominated by ooid grainstone facies in southern Ghawar. In northern Ghawar, the grainstone facies shallow up to lagoonal mud and laminites. Lagoonal mudstone parasequences become more dominant over subtle highs in south and central Ghawar.
B-2	5 to 12 m thick	Placed above fitted fabric breccia and laminites in the north (up dip), and lagoonal mudstone and ooid grainstone in south (down-dip).	Not recognized	Consists of open marine lime mudstone -dominated parasequences in southern Ghawar. From south center-to-north central Ghawar TSTs of oolite-dominated parasequences, passing northward into black anhydrite capped- and black anhydrite dominated parasequences. Thrombolites are common in southern Ghawar.	Placed on open marine lime-mudstone in southern Ghawar and on ooid grainstone over much of Ghawar.	Consists of ooid grainstone dominated parasequences in southern Ghawar that grade up into laminite- and subaqueous anhydrite-dominated parasequences.
B-3	5.5 to 10 m thick	Placed above laminites and lagoonal mudstone; rarely on emergence breccias and subaqueous anhydrite.	Not recognized	Dominated by oolite parasequences in southern Ghawar, passing up dip into black subaqueous anhydrite dominated parasequences.	Developed on the ooid grainstone over much of Ghawar, peloid/ooid packstone back shoal in north central Ghawar and lagoonal mudstone in south central Ghawar.	Dominated by parasequences of laminite in southernmost Ghawar, capped by supratidal anhydrite up dip, that grade northward into black subaqueous anhydrite dominated parasequences.
B-4	10 to 14 m thick	On subaqueous and supratidal anhydrites, laminites and breccia	Not recognized	Consists of thin ooid grainstone parasequences and thin black anhydrite parasequences in southern Ghawar passing northward into thick anhydrite- and lesser thin oolite parasequences	MFS on ooid/peloid grainstone over much of Ghawar. MFS placed on packstone backshoal and lagoonal mudstone in central Ghawar.	Dominated by anhydritic laminite -dominated parasequences in southern Ghawar, that grade northward into thick black anhydrite-dominated parasequences
A-1	3 to 8 m thick	Placed above regional subaqueous anhydrite.	Not recognized	Dominated by ooid grainstone parasequences in southern and northern Ghawar; restricted mudstone-and subaqueous anhydrite dominated parasequences in central Ghawar.	Developed on ooid grainstone shoal.	Dominated by anhydrite-capped parasequences in south and central Ghawar, grading northward into laminite dominated parasequences in north central Ghawar, with lesser ooid grainstone dominated parasequences developed in subtle lows. Restricted mudstone parasequences in northernmost Ghawar
A-2	3.5 to 11 m thick	Commonly a planar surface on regional subaqueous anhydrite and laminites; locally an erosional surface on breccia.	Not recognized	Dominated by lagoonal mudstone over much of Ghawar; oolite parasequences are common in southern Ghawar, and are dominant in central northern Ghawar, passing northward into black subaqueous anhydrite parasequences.	Developed on ooid grainstone in southern, north central and northern Ghawar, with packstone back- shoal and lagoonal mudstone in central Ghawar.	Dominated by restricted mudstone parasequences over much of Ghawar; become increasingly oolitic in north central Ghawar. In northern Ghawar, subaqueous anhydrite- and lesser laminite dominated parasequences.
A-3	6.5 to 13 m thick	On subaqueous anhydrite, laminites and locally fitted fabric breccias.	Not recognized	Consists of thick ooid grainstone parasequences in southern, central, and north central Ghawar. Lagoonal mud- and lesser ooid grainstone parasequences in south central and northern Ghawar. Thrombolites are common in lagoonal mudstone	Developed on the ooid grainstone.	Oolite dominated parasequences in southern and central Ghawar; in south central Ghawar dominated by restricted mudstone parasequences shallowing up into regional packstone sand shoal and laminites. In north Ghawar, dominated by restricted mudstone- with thin oolite- and lesser laminite dominated parasequences. Thrombolites common in southern Ghawar.
A-4	5 to 6.5 ft thick	Placed on packstone and lagoonal mud in the south, and on laminites with local breccias in north.	Not recognized	Lagoonal mudstone parasequences with minor thin grainstones. Digitate stromatolites and thrombolites widespread near base of TST; thrombolites range upward throughout TST.	Developed on thin ooid/peloid grainstone and packstone.	Dominated by restricted mudstone- and laminite-capped parasequences with thrombolite in the south. Grades up into shales of lower Sudair Formation.

REFERENCES

Abu-Ali, M. and R. Littke 2005. Paleozoic petroleum systems of Saudi Arabia: a basin modeling approach. GeoArabia, v. 10, no. 3, p 131-168.

Al-Aswad, A.A. 1997. Stratigraphy, sedimentary environment and depositional evolution of the Khuff Formation in south-central Saudi Arabia. Journal of Petroleum Geology, v. 20, p. 307.

Al-Dukhayyil, R.K. 2007. High-resolution sequence stratigraphy of the Khuff A and B carbonates in the subsurface of Haradh Area, Southern Ghawar, Saudi Arabia. MS Thesis, King Fahd University of Petroleum and Minerals, 93 p., (unpublished).

Al-Dukhayyil, R. K. and A. A. Al-Tawil 2006. Reservoir architecture of the Triassic Khartam carbonate sequence, Khuff outcrop analogue in Al-Qasim, central Saudi Arabia. 7th Middle East Geosciences Conference, Geo 2006 in Bahrain, abstract.

Al-Dukhayyil, R. K. and A. A. Al-Tawil 2008. High-resolution sequence stratigraphy of the Triassic Khuff A and B carbonates in the subsurface of Haradh Area, southern Ghawar Field, Saudi Arabia. AAPG Annual Conference in San Antonio, abstract.

Al-Dukhayyil, R.K., G.A. Al-Eid and A.A. Al-Tawil 2006. Core-and-log signature of high-resolution sequence-and-cycle stratigraphy of Permian Khuff C Reservoir; implications for reservoir characterization and development, Ghawar Field, Saudi Arabia. AAPG Annual Conference in Houston, extended abstract.

Al-Dukhayyil, R., J. Read and A. Al-Tawil 2012. Permo-Triassic upper Khuff carbonate sequences, Ghawar Field, Saudi Arabia. 10th Middle East Geosciences Conference, Geo 2012 in Bahrain, abstract.

Al-Eid, G.A. 2009. High-resolution sequence stratigraphy of the late Primary Khuff C carbonates central Ghawar Field, Saudi Arabia. Ph.D. Thesis, University of Tübingen, Germany, 158 p., (unpublished).

Al-Husseini, M.I. 2000. Origin of the Arabian Plate structures: Amar Collision and Najd Rift. GeoArabia, v. 5, no. 4, p. 527-542.

Al-Jallal. I.A. 1989. Depositional environments, diagenesis and reservoir characteristics of the late Permian Khuff Formation in eastern Saudi Arabia: Ph. D. Thesis, University of London, (unpublished).

Al-Jallal, I.A. 1995. The Khuff Formation: Its regional reservoir potential in Saudi Arabia and other Gulf countries; depositional and stratigraphic approach. In M.I. Al-Huseini (Ed.), Middle EastPetroleum Geosciences Conference, GEO'94. Gulf PetroLink, Bahrain, v. 1, p. 103-119.

Alsharhan, A.S. 2006. Sedimentological character and hydrocarbon parameters of the Middle Permian to Early Triassic Khuff Formation, United Arab Emirates. GeoArabia, v. 11, no. 3, p.121-158.

Alsharhan, A.S. and C.G.St.C. Kendall 1986. Precambrian to Jurassic rocks of the Arabian Gulf and Adjacent Areas; their facies, depositional setting and hydrocarbon habitat. American Association of Petroleum Geologists Bulletin, v. 70, p. 977-1002.

Anderson, R.Y. 1982. A long geoclimatic record from the Permian. Journal of Geophysical Research, v. 87, p. 7285-7294.

Angiolini, L., M. Balini, E. Garzanti, A. Nicora, A. Tintori, S. Crasquin-Soleau and G. Muttoni 2003. Permian climatic and palaeogeographic changes in Northern Gondwana: The Khuff Formation of Interior Oman. Palaeogeography, Palaeoclimatology, Palaeoecology, v. 191, nos 3-4, p. 269-300.

Baud, A., W.T. Holser and M. Magaritz 1989. Permian-Triassic of the Tethys: carbon isotope sudies. Geologische Rundschau, v. 78/2, p. 649-677.

Baud, A., S. Richoz and S. Pruss 2007. The lower Triassic anachronistic carbonate facies in space and time. Global and Planetary Change, v. 55, p. 81–89.

Bott, M.H.P. 1992. Passive margins and their subsidence. Journal of the Geological Society, London, v. 149, p. 805-812.

Boulila, S., B. Galbrun, K.G. Miller, S.F. Pekar, J.V. Browning, J. Laskar and J.D. Wright 2011. On the origin of Cenozoic and Mesozoic “third-order” eustatic sequences: Earth Science reviews, v. 109, p. 94-112.

Bova, J.A. and J.F. Read 1987. Incipiently drowned facies within a cyclic peritidal continental ramp sequence, Chepultepec interval, Virginia Appalachians. Geological Society of America Bulletin, v. 98, p. 714-727.

Calner, M. 2005. A Late Silurian extinction event and anachronistic period. Geology, v. 33, p. 305-308.

Choquette, F. W. and L.C. Pray 1970. Geologic nomenclature and classification of porosity in sedimentary carbonates. AAPG, v. 54, p. 207-250.

Demicco, R.V. and L.A. Hardie 1994. Sedimentary structures and early diagenetic features of shallow marine carbonate deposits. SEPM Atlas Series 1, p. 255.

Dunham, R.J. 1962. Classification of carbonate rocks according to depositional texture, in Ham, W.E. (ed.), Classification of carbonate rocks: AAPG Memoir 1, p. 108-121.

Elrick, M., S. Berkyova, G. Klapper, Z. Sharp, M. Joachimski, J. Fryda 2009. Stratigraphic and oxygeni sotope evidence for My-scale glaciation driving euastasy in the Early-

Middle Devonian greenhouse world. Palageography, Palaeclimatology, Palaecology, v. 276, p. 170-181

Embry, A.F. and J.E. Klovan 1971. A Late Devonian reef tract on northeastern Banks Island, Northwest Territories. Bulletin of Canadian Petroleum Geology, v.19, p. 730-781.

Erwin, D.H. 1993. The Great Paleozoic Crisis: Life and Death in the Permian. Columbia Univ. Press, New York, 327 p.

Erwin, D.H. 2006. Extinction: How life on Earth nearly ended 250 million years ago: Princetone, Princetone University Press, 296 p.

Esteban, M. and C.F. Klappa 1983. Subaerial exposure environment. In Scholle, P.A., Bebout, D.G and Moore, C.H. (Eds), Carbonate Depositional Environments. AAPG Mem., no. 33, p. 1-54.

Evans, G. 1975. Intertidal flat deposits of the wash, Western Margin of the North Sea. In: R.M. Ginsburg (Editor), Tidal Deposits. Springer, New York, N.Y., p. 13-20.

Fielding, C.R., T.D.Frank, L.P. Birgenheier, M.C. Rygel, A.T. Jones, J. Roberts 2008. Stratigraphic imprint of the Late Palaeozoic Ice Age in eastern Australia: a record of alternating glacial and nonglacial regime. J. Geol. Soc. Lond., vol. 165, p. 129–140.

Frakes, L.A., J.E. Francis and J.I Syktus 1992. Climate modes of the Phanerozoic: the history of the Earth's climate over the past 600 million years. Cambridge University Press, Cambridge, UK, 274 p.

Groves, J.R. and M. Calner 2004. Lower Triassic oolites in Tethys: a sedimentologic response to the end-Permian mass extinction. Geological Society of America Abstracts with Programs, v. 36, no. 5, p. 336.

Handford, C.R. 1988. Review of carbonate sand-belt deposition of ooid grainstones and application to Mississippian reservoir. Damme Field, southwestern Kansas. AAPG, v. 72, p. 1184-1199.

Hinnov, L.A. 2000. New perspectives on orbitally forced stratigraphy. Annual Review of Earth and Planetary Sciences, v.28, p. 419-475.

Haq, B.U. and A. Al-Qahtani 2005. Phanerozoic cycles of sea-level change on the Arabian Platform. GeoArabia. V. 10, no. 2, p. 127-158.

Haq, B.U. and S.R. Schutter 2008. A chronology of Paleozoic sea-level changes. Science, v. 322, p. 64-68.

Hardie, L.A. 1967. The gypsum-anhydrite equilibrium at one atmosphere pressure. American Mineralogist, v. 52, p. 171-200.

Harris, P.M. 1983. The Joulters ooid shoal, Great Bahama Bank. In Peryt, T.M. (ed.), Coated Grains. Springer-Verlag, Berlin, p. 132-141.

Harris, P. M., C. Kerans and D. G. Bebout 1993. Ancient outcrop and modern examples of platform carbonate cycles—Implications for subsurface correlation and understanding reservoir heterogeneity. In R. G. Loucks and J. F. Sarg, eds., Carbonate sequence stratigraphy-Recent developments and applications: AAPGMemoir 57, p. 475–492.

Heydari, E., J. Hassanzadeh and W.J. Wade 2000. Geochemistry of central Tethyan Upper Permian and Lower Triassic strata, Abadeh region, Iran. Sedimentary Geology, v. 137, p. 85-99.

Hughes, G.W. 2005. Saudi Arabia Permo-Triassic biostratigraphy, micropalaentology and palaenvironment. Micrpaleontological Society, Special Publications, p. 91-108.

Hughes, G.W. 2009. Micropaleontology and paleoenvironments of Saudi Arabian Upper Permian carbonates and reservoirs. In Geologic Problem Solving with Microfossils: A volume in Honor of Garry D. Jones. SEPM Special Publication, no. 93, p. 111-126.

Husinec, A., D. Basch, B. Rose and J.F. Read 2008. Fischerplots: an excel spreadsheet for computing Fischer plots of accommodation change in cyclic carbonate successions in both the time and depth domain. Computers & Geosciences, v. 34, p. 269-277.

Insalaco, E., A. Virgone, B. Courme, J. Gaillot, M. R. Kamali, A. Moallemi, M. Latfpour and S. Monibi 2006. Upper Dalan Member and Kangan Formation between the Zagros Mountains and offshore Fars, Iran: depositional system, biostratigraphy and stratigraphic architecture. GeoArabia, v. 11, no. 2, p. 75-176.

Jacobs, D.K. and D.L. Sahagian 1993. Climate-induced fluctuations in sea level during non-glacial times: Nature, v. 361, p. 710-712.

Jahnert, R.J. and L.B. Collins 2012. Characteristics, distribution and morphogenesis of subtidal microbial systems in Shark Bay, Australia. Marine Geology, v. 303-306, p.115-136.

James, N. P. 1979. Shallowing-upward seqences in carbonates. In Walker, R.G., ed., Facies Models: Geoscience Canda Reprint Series 1, p. 109-119.

Jin, Y.G., Y. Wang, W. Wang, Q.H. Shang, C.Q. Cao and D.H. Erwin 2000. Pattern of marine mass extinction near the Permian–Triassic boundary in South China. Science 289, 432– 436.

Kendall, A. C., 1979a. Continental and supratidal (Sabkha) Evaporites. In facies models, R. G. Walker, ed. Geoscience Canada, Reprint Series 1, p. 145-157.

Kendall, A. C.,, 1979b, "Subaqueous Evaporites. In facies models, R. G. Walker, ed. Geosci ence Canada, Reprint Series 1, pp. 159-174.

Kennard, J. M. and P.N. James 1986. Thrombolites and stromatolites: two distinct types of microbial structures. Palaios, v. 1, p. 492-503.

Koehrer, B., M. Zeller, T. Aigner, M. Poeppelreiter, P. Milroy, H. Forke and S. Al-Kindi 2010. Facies and stratigraphic framework of a Khuff outcrop equivalent: Saiq and Mahil formations, Al Jabal al-Akhdar, Sultanate of Oman. GeoArabia, v. 15, no. 2, p. 91-156.

Koerschner, W.F. and J.F. Read 1989. Field and modeling studies of Cambrian carbonate cycles, Virginia Appalachians, Journal of Sedimentary Petrology, v. 59, p. 654-687.

Konert, G., A. Al-Afifi, S. Al-Hajri and H. Dorste 2001. Paleozoic stratigraphy and hydrocarbon habitat of the Arabian Plate. GeoArabia, v. 6, no. 3, p.407-442.

Krull, E.S., and G.J. Retallack 2000. δ13C depth profiles from paleosols across the Permian-Triassic boundary: evidence for methane release. GSA Bulletin, v. 112, p. 1459-1472.

Logan, B. W., P. Hoffman, and C.D. Gebelein 1974. Algal mats, cryptalgal fabrics, and structures, Hamelin Pool, Western Australia. In Evolution and diagenesis of Quaternary carbonate sequences, Shark Bay, Western Australia, Logan, B.W., J.F. Read, G.M. Hagan, P. Hoffman, R.G. Brown, P.J. Woods and C.D. Gebelein (eds.). AAPG Memoir, no. 22, p. 140-194.

Loope, W.L., T.G. Fisher, H. M. Jol, R.J. Goble, J.B. Anderton and W.L. Blewett 2004. A Holocene history of dune-mediated landscape change along the southeastern shore of Lake Superior. Geomorphology, v.61, p. 303-322.

Markello, J.R., R.B. Koepnick, L.E. Waite and J.F. Collins 2008. The carbonate analogs through time (CATT) hypothesis and the global atlas of carbonate fields – a systematic and predictive look at Phanerozoic carbonate systems. SEPM Special Publication, v. 89, p. 15-45.

Miall, A.D. 1999. In defense of facies classifications and models. Journal of Sedimentary Research, v. 69, p. 2-5.

Manivit, J., D. Vaslet, A. Berthiaux, P. Le Strat and J. Fourniguet 1986. Geologic map of the Buraydah quadrangle, sheet 26G, Kingdom of Saudi Arabia (with explanatory notes). Saudi Arabian Deputy Ministry for Mineral Resources, Geoscience Map GM114, Scale 1:250,000.

Mitchum, R.M. Jr. and J.C. Van Wagoner 1991. High-frequency sequences and their

stacking patterns: sequence stratigraphic evidence of high-frequency eustatic cycles, in: K.T. Biddle and W. Schlager, eds., The record of sea-level fluctuations. Sedimentary Geology, v. 70, p. 131-160.

Montañez, I.P. and D.A. Osleger 1993. Parasequence stacking patterns, third-order accommodation events and sequence stratigraphy of Middle to Upper Cambrian platform carbonates, Bonanza King Formation, southern Great Basin. In: Loucks, R.G., and F.R. Sarg, eds., Carbonate sequence stratigraphy: recent developments and applications. AAPG Memoir, no. 57, p. 305-326.

Matthews, R.K. and C.F. Frohlich 2002. Maximum flooding surface and sequence boundaries: comparisons between observation and orbital forcing in the Cretaceous and Jurassic (65-190 Ma). GeoArabia, v. 7, no. 3, p. 503-538.

Matthews, R.K. and M.I. Al-Husseini 2010. Orbitalforcing glacio-eustasy: A sequence-stratigraphic time scale: GeoArabia, v. 15, p. 155–167.

Ogg, J.G., G. Ogg and F.M Gradstein 2008. The concise geologic time scale. Cambridge, UK, Cambridge University Press, 177 p.

Parrish, J. T. 1985. Latitudinal distribution of land and shelf and absorbed solar radiation during the Phanerozoic: U.S. Geol. Survey Open-File Rept. 85-31, 21 p.

Parrish, J.T. 1993. Climate of the supercontinent Pangea. Journal of Geology, v. 101, p. 215-233.

Parrish, 1.M., J.T. Parrish and A.M. Ziegler 1986. Permian-Triassic paleogeography and paleoclimatology andimplications for therapsid distributions. In Hotton, N.H., P.D. MacLean, J.J. Roth and E.C. Roth, eds., The ecology and biology of Mammal-like reptiles. Washington, D.C., Smithsonian Press, p. 109-132.

Preto, N., L.A. Hinnov, L.A. Hardie, and V. De Zanche 2001. Middle Triassic orbital signature recorded in the shallow-marine Latemar carbonate buildup (Dolomites, Italy). Geology, v. 29, p. 1123–1126.

Rampino, M.R., A. Prokoph and A. Adler 2000. Tempo of the end-Permian event: high-resolution cyclostratigraphy at the Permian-Triassic boundary. Geology, v. 28, p. 643-646.

Rankey, E.C., B. Riegl, and K. Stefen 2006. Form, function and feedbacks in a tidally dominated ooid shoal, Bahamas. Sedimentology, v.53, p.1191-1210.

Raup, D.M. 1979. Size of the Permo-Triassic bottleneck and its evolutionary implications. Science, Wash. 206, p. 217-218.

Read, J.F. 1989. Controls on evolution of Cambrian-Ordovician passive margin, U.S. Appalachians. In Crevello, P.D., J.L. Wilson, J.F. Sarg,and J.F. Read, eds., Controls

on carbonate platform and basin development. Society for Sedimentary Geology Special Publication 44, p. 147–166.

Retallack, G.L. 1995. Permian-Triassic life crisis on land. Science, v. 267, p. 77-80.

Riding, R. 2005. Phanerozoic reefal microbial carbonate abundance: Comparisons with metazoan diversity, mass extinction events, and seawater saturation state. Revista Española de Micropaleontología, v. 37, p. 23–39.

Sadler, P.M., D.A. *Osleger* and I.P. *Montanez* 1993. *On the labelling, length and objective basis of Fischer plots.* Journal of Sedimentary Petrology, v. 63, p. 360-*368*.

Sarg, J. F. 1988. Carbonate sequence stratigraphy. In: Sea-level changes: An integrated approach , edited by Wilgus, C.K., B.S. Hastings, H. Posamentier, J. van Wagoner, C.A. Cross and C.G.St.C. Kendall. Society of Economic Paleontologists and Mineralogits, Special Publication, vol. 42, p. 155-181

Schubert, J.K. and D.J. Bottjer 1992. Early Triassic stromatolites as post-mass extinction disaster forms. Geology, v. 20, p. 883-886.

Scotese, C. R., A.J. Boucot and W.S. McKerrow 1999. Gondwanan palaeogeography and palaeoclimatology. Journal of African Earth Sciences, v. 28, no. 1, p.99-114.

Scotese, C.R. 2003. PALEOMAP, Earth History and Climate History, Late Permian. Paleomap, Permian Earth, URL http://www.scotese.com

Senalp, M. and A. Al-Duaiji 2001. Sequence stratigraphy of the Unayzah reservoir in central Saudi Arabia. Saudi Aramco Journal of Technology, Summer, p. 20-43.

Sharief, F. A. 1983. Permian and Triassic geological history and tectonics of the Middle East: Journal Petroleum Geology, v.6, p. 95-102.

Sharland, P.R., R. Archer, D.M. Casey, R.B. Davies, S.H. Hall, A.P. Heward, A.D. Horbury and M.D. Simmons 2001. Arabian Plate sequence stratigraphy. GeoArabia Special Publication 2, 371 p.

Stanley, S.M. and L.A. Hardie 1998. Secular oscillations in the carbonate mineralogy of reef-building and sediment-producing organisms driven by tectonically forced shifts in seawater chemistry. Palaeogeography, Palaeoclimatology, Palaeoecology, 144, 3–19.

Stanley, S.M. and L.A. Hardie 1999. Hypercalcification: paleontology links plate tectonics and geochemistry to sedimentology. GSA Today 9, 2 – 7.

Sepkoski, J.J. 1996. Patterns of Phanerozoic extinction: a perspective from global data bases. In Global bio-events and event-stratigraphy (ed. O. H. Walliser). Springer, Berlin, pp. 35-51.

Steckler, M.S. and A.B. Watts 1982. Subsidence history and tectonic evolution of Atlantic-type continental margins, Amer. Geophys. Union, Geodynamics Series 8, 184-196

Seilacher, T. and T. Aigner 1991. Storm deposition at the bed, facies, and basin scale: the geological perspective. In Einsele et al. (eds.). Cycles and Event in Startigraphy,Springer-Verlag, p. 249-267.

Strohmenger, C.J., R.H. Alway, R.W. Broomhall, R.F. Hulstrand, A. Al-Mansoori, A.A. Abdalla and A. Al-Aidarous 2002. Sequence stratigraphy of the Khuff Formation comparing subsurface and outcrop data (Arabian Plate, UAE): SPE paper no. 78535, p. 558-568.

Vail, P.R., R.M. Mitchum Jr. and S. Thompson III 1977. Seismic stratigraphy and global changes of sea-level, Part 4: Global cycles of relative changes of sea-level. In C.E. Payton (Ed.), Seismic Stratigraphy - Applications to Hydrocarbon Exploration. American Association of Petroleum Geologists Memoir 26, p. 83-98.

Vaslet, D., Y.-M. Le Nindre, D. Vachard, J. Broutin, S. Crasquin-Soleau, J. Gaillot, M. Berthlen, M. Halwani and M.I. Al Husseini 2005. The Khuff Formation of central Saudi Arabia. GeoArabia, v. 10, no. 4, p.77-134.

Warren , J. K. 2006. Evaporites: sediments ,resources and hydrocarbons. Springer , Berlin , 1035 p.

Warren, J.K. and C.G.St.C. Kendall 1985. Comparison of sequences formed in marine (subaerial) and salina (subaqueous) settings-modern and ancient. American Association of Petroleum Geologists Bulletin 69, 1013– 1023.

Wender, E. L., J. W. Bryant, M. F. Dickens, A. S. Neville and A. M. Al-Moqbel 1998. Paleozoic hydrocarbon geology of the Ghawar Area, Eastern Saudi Arabia. GeoArabia, v. 2, no. 2, p.273-302.

Wilson, J. L., and C. Jordan 1983. Middle shelf environment. In: Scholle, P.A., D.G. Bebout and C.H. Moore (Eds.), Carbonate depositional environments. AAPG Memoir, no. 33, p. 298-343.

Yin, H., Q. Feng, X. Lai, A. Baud and J. Tong 2007. The protracted Permo-Triassic crisis and multi-episode extinction around the Permian-Triassic boundary. Global and Planetary Change, v. 55 (1–3), p. 1–20.

Yang, W. and D.J. Lehrmann 2003. Milankovitch climate signals in Lower Triassic (Olenekian) peritidal carbonate successions, Nanpanjiang Basin, South China. Palaeogeography, Palaeoclimatology, Palaeoecology, v. 201, p. 283-306.

Zühlke, R., T. Bechstadt and R. Mundil 2003. Sub- Milankovitch and Milankovitch forcing on a model Mesozoic carbonate platform—The Latemar (MiddleTriassic, Italy): Terra Nova, v. 15, p. 69–80.

Ziegler, M.A., M.L. Hulver and D.B. Rowley 1997. Permian world topography and climate. In: I.P. Martini (ed.), Late glacial and postglacial environment changes-Quaternary, Carboniferous-Permian, and Proterozoic. New York: Oxford University Press, p.111-146.

Ziegler, M. A., 2001. Late Permian to Holocene paleofacies Evolution of the Arabian Plate and its hydrocarbon occurrences. GeoArabia, v. 6, no. 3, p.445-504.

CHAPTER 3

CARBON AND OXYGEN ISOTOPE CHEMOSTRATIGRAPHY ACROSS THE PERMIAN-TRIASSIC BOUNDARY, GHAWAR FIELD, SAUDI ARABIA

ABSTRACT

Carbon and oxgyen isotope profiles up to 150 m long were sampled across the Permian-Triassic boundary from cored wells of the Khuff Formation, Ghawar Field, Saudi Arabia. Major global excursions are at the Wuchiapingian-Changhsingian - and the Permian-Triassic boundary (PTB), but several smaller excursions also appear to correlate with excursions elsewhere. The presence of the negative C-isotope excursions globally in both $\delta^{13}C_{carbonate}$ and $\delta^{13}C_{organic}$ as well as in deeper water sections lacking emergence surfaces, strongly supports the idea of these excursions being global phenomena related global C cycling.

Over 75% of the negative carbon isotope excursions in Ghawar occur beneath emergence surfaces, including the two major excursions at the Wuchiapingian and Changhsingian stage boundaries. The $\delta^{13}C$ profiles beneath the boundaries resemble those associated with early diagenesis associated with isotopically light soil gas. The $\delta^{18}O$ profiles beneath the surfaces are variable, perhaps reflecting variable effects of evaporation on the meteoric input, mixing or overprinting by burial diagenesis. This suggests that the C-isotope excursions on the Arabian Platform, although global in origin, appear to have been modified by early diagenesis.

U depletion across the boundary is compatible with the postulated origins of the PTB event with bottom waters becoming stagnant and reducing, as a result of warming induced by volcanogenic CO_2 released by Siberian trap volcanism, methane release from thermal metamorphism of coals, and destabilization of clathrates in the deep sea due to ocean

warming. The global extent of the C-isotope and U excursions provides a high resolution correlation tool for Late Permian and Early Triassic successions.

INTRODUCTION

Carbon isotope chemostratigraphy has shown well developed negative- followed by positive C isotope excursions within the Permian-Triassic succession worldwide, one associated with the Permian Wuchiapingian-Changhsingian boundary (Baud et al 1989; Erwin, 2006, Jin et al 2006) and the other associated with the Permian-Triassic boundary or PTB (e.g. Baud et al., 1989; Heydari et al., 2001; Holser et al., 1989; Jin et al., 2000; Korte and Kozur, 2010; Xu et al., 1986). It has been suggested that the negative excursions relate to introduction of light C from exhalation of volcanic CO_2 during eruption of the immense flood basalts of the Siberian Traps, liberation of light C tied in coal beds that were intruded by the volcanic units, and destabilization of methane clathrates as a result of rising temperatures, perhaps coupled with falling sea level (Erwin 2006; Grasby et al., 2011; Knoll et al., 1996; Krull et al., 2000).

In terms of the Arabian Plate, C-O isotope chemostratigraphy among other indicators, has been examined by Richoz (2006), Richoz et al. (2010) and Koherer et al. (2010) across the PTB in Oman and by Insalaco et al. (2006) across the boundary in Iran. In Ghawar, Saudi Arabia (Fig. 3.1), C and O isotopes profiles from the Permian Triassic Khuff Formation (Fig. 3.2) have been studied by Markello (1988) and Al-Jalall (1989); both workers noted that the $\delta^{13}C$ values decrease from the Permian Khuff-C into the Triassic Khuff-B and A, although at this time there was some confusion concerning the position of the Permian-Triassic boundary in the region. Swart and McKenzie (2001a, b) gathered C-O isotope data from the Permian-Triassic of Ghawar, Saudi Arabia, but interpreted the C shift across the PTB as related to

diagenetic overprinting. However, Hughes (2005) reinterpreted this shift as reflecting the global event regardless of the mineralogical change from dolomite in Late Permian to limestone in Early Triassic that occurred across the PTB in Ghawar (Fig. 3.2).

The present study takes advantage of continuous cores across the PTB in Ghawar Saudi Arabia (Figs. 3.1, 3.2), and is part of a high resolution sequence stratigraphic study of the subsurface Permian-Triassic Khuff Formation in Ghawar, Saudi Arabia. This project is part of a larger project on Khuff reservoirs throughout Saudi Arabia. Samples were taken for C and O isotope analysis to help constrain the chronostratigraphy. In conjunction, the downhole wireline logs were collated and studied to examine the marked decrease in U in carbonates spanning PTB. The present study provides a detailed C-O chemostratigraphic framework tied to the high resolution sequence stratigraphic framework for Ghawar, along with a synthesis of the gamma ray log data across the boundary. It evaluates the impact of the PTB events within the sequence framework, its effect on the accumulating sedimentary facies succession, and implications with regard to paleoceanography and paleoclimate.

STRATIGRAPHIC FRAMEWORK

Paleogeography, Regional Setting and Structure

During the Permo-Carboniferous ice age, the Arabian Plate was between 30ºS and 55ºS, moving northward with Gondwana (Sharief, 1983; Ziegler et al., 1997; Konert et al., 2001). By Late Permian, and onset of greenhouse conditions (Frakes et al., 1992; Fielding et al., 2008), the Arabian Plate lay at 10ºS to 35ºS. By the end of Khuff deposition in the Early Triassic, northernmost Arabia had reached 5ºS (Konert et al., 2001; Sharland et al., 2001).

A major unconformity underlies the Khuff Formation, and is a Middle Permian break-up unconformity, termed the "Pre-Khuff Unconformity" (Fig. 3.3). Its age is approximately 268 Ma (Ogg et al. 2008 time chart), and it marks inception of the Neo-Tethys Ocean along the present day Zagros-Oman suture, as well as the major Permian transgression and expansion of the Neo-Tethys Ocean (Al-Aswad, 1997; Sharland et al., 2001; Konert et al., 2001). This caused shallow marine carbonates and evaporites to be deposited over much of the Arabian Plate as it moved N into drier warmer latitudes (Fig. 3.4; Al-Jallal, 1989 and 1995; Ziegler, 2001).

The Permian-Triassic Khuff Formation was deposited on a huge, east-facing, arid ramp (Al-Dukhayyil et al., 2006; Insalaco et al., 2006) that formed an eastward thickening wedge, up to 450 m in the Ghawar study area, and up to 1500 m in Iran in the fold thrust belt (Al-Jallal, 1995). The Khuff succession terminates to the west in the outcrop belt near the Arabian Shield (Fig. 3.1). Between Arabian Shield and Ghawar the Khuff units thicken slowly, but across Ghawar there is a major increase in thickness, after which the Khuff then thickens gradually into eastern Arabia and offshore. Outer-shelf and shelf edge facies are exposed in Oman and Iran (Angiolini et al., 2003; Heydari et al., 2001; Insalaco et al., 2006; Koehrer et al., 2010).

Subtle syn-depositional growth of structures, mostly folds and domes, formed during the Precambrian-Early Paleozoic along the eastern part of the Arabian Plate within the Zagros Foreland (Al-Husseini, 2000). These domal features with 4 way closure, set the stage for some of the world's best oil and gas reservoirs (Al-Jallal, 1989 and 1995; Konert et al., 2001).

The Ghawar structure which makes up the study area, forms the southern part of the 500 km long En Nala anticline (Fig. 3.1; Al-Husseini, 2000). Ghawar is located on the

interior of the Khuff platform, some 650 km from the platform margin in Iran. It is 240 km long by 30 km wide, and is an elongate dome with 4-way closure. The structure likely was active in the Permian and Triassic, perhaps as a subtle positive area on the regional platform. The structure has continued to increase in structural relief throughout the Mesozoic and Cenozoic (Al-Husseini, 2000; Wender et al., 1998).

Stratigraphy and Age

In the subsurface of Ghawar Field, eastern Saudi Arabia, the Khuff Formation lies at depths of 3000 m (10,000 ft), and overlies Permo-Carboniferous Unayzah siliciclastics (Fig. 3.2). It is 450 m thick and is overlain by Triassic Sudair Shale. The subsurface Khuff Formation (Fig. 3.2) is divided into the Khuff D, including the Basal Khuff Clastics (BKC) or "Khuff E" of Al-Jallal (1995), the lower Khuff C, upper Khuff C of Permian age and Khuff B and Khuff A of Triassic age (Al-Dukhayyil et al., 2006; Hughes 2005 and 2009). The best porosity in developed in the Khuff A, B, and C units.

The Khuff Formation across the Arabian Plate ranges from Middle Permian, Wordian stage to Early Triassic Induan stage (Sharland et al 2001; Hughes, 2005; Alsharhan, 2006; Insalaco et al., 2006). In the Saudi Arabian subsurface (Fig. 3.2), Khuff D Carbonates (including the Basal Khuff Clastics) are possibly late Wordian (?) to Capitanian. The Lower Khuff C Carbonate Member is Wuchiapingian to Changhsingian (?) and the upper Khuff C is Changhsingian (Alsharhan, 2006; Hughes, 2009). The Khuff B and A Carbonates are early Triassic Induan stage (Al-Jallal, 1995; Hughes, 2009). In the present study the Khuff Formation C, B and A units have been divided into high frequency sequences labelled LC-5, UC-1-7, B1-4 and A1-4 (Fig. 3.2).

METHODS

For this study, 256 samples were collected from the Latest Permian through the Early Triassic Khuff Formation from cored wells 3, 4 and 13 in Ghawar (Fig. 3.1). Twenty kilometers separate Wells-3 and 4 while 150 km separates Well-4 and 13 (Fig. 3.1). Samples were obtained from two wells sampling the Permian through Triassic interval, and from a 15 m interval from one well covering the upper part of the Khuff into the Sudair Shale that was not sampled by the other wells. Carbon and oxygen-isotope analyses were done at the Saudi Aramco Research and Development Center, Dhahran, Saudi Arabia. These whole-rock samples were drilled using masonry bits from butts of cores to obtain powder samples at 50 cm to 1 m intervals, and at decimeter scale across some critical intervals such as breccia zones and the PTB. The powder samples were preferentially taken from carbonate mud fraction and from some of the grainstones, avoiding anhydrite intervals.

Powdered whole-rock carbonate samples were analyzed by Aramco on a Thermo-Fisher Gas Bench II headspace gas analyzer interfaced to a Delta Plus XP stable isotope ratio mass spectrometer (Peter Jenden, written comm., 2010). The samples were allowed to react for 2 hours at 70^{o}C before initiating the analysis sequence. Total run time was approximately 13 hours. Error is about +/-0.2 permil for both carbon and oxygen. Values are given in terms of Vienna Peedee Belemnite Standard (V-PDB) (Coplen, 1994). Chemostratigraphic profiles were constructed for C and O alongside the stratigraphic columns, which show emergence surfaces. C and O isotopes also were cross plotted to evaluate diagenetic effects. The chemostratigraphic profiles then were compared with profiles from elsewhere to constrain local and inter-regional correlations.

Downhole gamma ray logs were studied for variation in total gamma through the section. Spectral gamma (U, Th and K) was done on cores at the Aramco Core Laboratory, Dhahran, although the results were disappointing, compared to the downhole spectral gamma ray logs.

RESULTS

The C and O isotope data are shown on the chemostratigraphic profiles plotted alongside the cored lithostratigraphy (Fig. 3.3) and are summarized in Table 3.1 tied to the sequences. The chemostratigraphic profiles from Ghawar are compared to those from elsewhere in Figure 3.4. The Ghawar C and O isotope data are cross plotted in Figure 3.5. Short C and O isotope profiles extending down beneath emergence surfaces are compiled on Figure 3.6, to examine the effects of emergence on the isotope record.

Carbon Isotope Profiles

Permian

The $\delta^{13}C$ values of the cored section of the Permian units have peak positive values of around +4 to +5 (Fig. 3.3). This trend is interrupted by significant negative excursions that are rapidly followed by a return to the previous positive values over a distance of 3 to 10 meters. These negative excursions (abbreviated Exc. 1, 2 etc.) include a small one (Exc. 0) within sequence LC 5, followed by a major one (Exc. 1, -5 permil shift) in the upper part of sequence LC 5, a smaller one (Exc. 2, ~-2 permil shift) spanning the UC-1/UC-2 boundary, significant excursions (Exc. 3 and 4, of -3 permil) at the top of sequences UC-2 and top of UC-3. There is another excursion (Exc. 5, with -4 permil shift) just below the top of UC-4. Negative shifts (Exc. 6, -2 permil shift) also occur near the top of UC-5, and at the top of UC-

6 which is best developed in Well-4 (Exc. 7, shift of -3 permil) whereas it only has a -1 permil shift in Well-13. The major negative excursion (Exc. 8, shift of over -4.5 per mil) spans the PTB, from the latest Permian sequence UC-7 into the base of Triassic sequence B-1 over a distance of 7 m. This major negative shift started in Well-4 around 3 m below the PTB immediately after the last appearance of the Permian fauna. The last appearance of the Permian fauna occurred at 2.4 m below the PTB in Well-13. This major negative excursion at the PTB marks the strongest, negative C excursion observed on the profiles.

Triassic

The $\delta^{13}C$ values of the Triassic are around 0 permil$_{VPDB}$ with several negative excursions that are variably developed from well to well (Fig. 3.3). Excursions within sequence B-1, include Exc.9 (shift of -1 permil), and Exc. 10, with a shift of -1.5 to -3 permil from well to well. Excursion 11 (-1.5 to -2 per mil shift) occurs in sequence A-1, and major Exc. 12, with a shift of from -1 to -4 permil$_{VPDB}$ depending on which well is used, occurs at the sequence A-2/A-3 boundary. Above this, there is little fluctuation of the $\delta^{13}C$ values up to the base of the Sudair Formation.

Correlation of Carbon Isotope Profiles with Profiles from Europe, Middle East and Asia

Figure 3.4 compares C-isotope profiles from this study in Saudi Arabia, with profiles from platform sections in Austria (Hosler at al., 1989), platform and offshelf sections in Iran (Heydari et al 2001; Insalaco at al., 2006) and platform and deep shelf sections in China (Baud et al 1989; Shen et al., 2011). Of the negative excursions evident in the Saudi Arabian cores (this study), only excursions 2 and 3 are difficult to correlate to the Austrian section of Holser et al (1989). The major excursions 1 (at the Chianghsingian-Wuchapingian boundary) and excursion 8 across the PTB are clearly evident in all the long profiles. Most workers

appear to have put the PTB *within* the major negative C isotope excursion (Fig. 3.4), but Shen et al. (2012), who utilized high resolution radiometric dating, appear to place the boundary slightly above the excursion (although in terms of time, this probably is only about 100 k.y.).

Oxygen Isotope Profiles

Permian and Triassic Oxygen Isotope Profiles

In terms of $\delta^{18}O$ values, dolomite commonly is commonly is 3 permil heavier than co-existing limestone, which needs to be taken into account in scanning the oxygen isotope values of the Khuff cores. Some of the $\delta^{18}O$ values up the cores covary with the $\delta^{13}C$ values (Fig. 3.3). Excursions with covarying C and O isotopes in Well-13 include excursions 0, 2, 3, 4, 7, 8 (poorly), and 9. However, within well-4, only excursions 4, 7 and 8 covary in terms of C and O in common with Well-13, although excursions 5 and 10 show covariance within well-4 only. In terms of $\delta^{18}O$ isotopic shifts, much of the Permian shows a 2.5 permil fluctuation, but across the PTB there is a large negative shift of -6 to -7.5 permil$_{VPDB}$ (depending on the well), part of which reflects the change from Permian dolomite up into limestone (the dolomite typically being up to 3 permil heavier than co-existing limestone). In the top of the cored interval of well-13, there is a $\delta^{18}O$ shift of about -3 permil$_{VPDB}$, which is not present in Well-4.

Carbon-Oxygen Cross Plots

Cross plots of C and O isotopes for the Permian and Triassic carbonates are shown in Figure 3.5. The field of Permian marine calcite ($\delta^{13}C$ values of 0 to +6.0 permil and $\delta^{18}O$ values of -6.5 to -3.8 permil $_{VPDB}$) was taken from Viezer et al. (1999), because there were no undolomitized Permian limestones in the cores studied (Fig. 3.5 a). The Late Permian Khuff

dolomites have $\delta^{13}C$ values ranging from 0 to +5 permil$_{VPDB}$, and the bulk of the $\delta^{18}O$ values are from just below +2.8 to -1 permil $_{VPDB}$, with a few samples extending to below -3 permil $_{VPDB}$.

For the Triassic, the Khuff limestones have $\delta^{13}C$ values from +1 to -3 permil $_{VPDB}$ and $\delta^{18}O$ values of -5 to about -6.5 permil $_{VPDB}$ (Fig. 3.5 b). For comparison, the field for Early Triassic marine calcite (Veizer et al., 1999) and Triassic marine calcite (Schauer and Aigner, 1997) also are shown. The Triassic dolomites have $\delta^{13}C$ of +1.8 to -1.8, with a few samples extending to -3.6 permil $_{VPDB}$, and $\delta^{18}O$ values ranging from -5.5 to -2.4 permil $_{VPDB}$. Triassic coarse grained dolomite (probably of burial origin) has $\delta^{13}C$ values of +0.6 to +1.2 and very light $\delta^{18}O$ values of -6.3 to -8.4 permil $_{VPDB}$.

Variation of Stable Isotope Profiles Beneath Sequence Boundaries

For selected intervals below emergence surfaces in the cores, $\delta^{13}C$ and $\delta^{18}O$ profiles were constructed by using the emergence surfaces as a common datum, from which to hang the mini-profiles (Fig. 3.6). Two types of $\delta^{13}C$ profiles emerge. One type (Fig. 3.6 a) shows very negative $\delta^{13}C$ values below the surface that rapidly become heavier downward in the section reaching background values about 2 to 3 m below the surface. The second type of $\delta^{13}C$ profile (Fig. 3.6 b) shows relatively heavy values at the surface, which decrease downward between about 1 and 2 m below the surface, and then a rapid increase with depth to more positive values.

The $\delta^{18}O$ mini-profiles when hung from the emergence surfaces are more complex, and appear to form four trends (Fig. 3.6 c). One has heavy $\delta^{18}O$ values at the surface which decrease downward in a zigzag fashion to more negative values. A second type appears to

have relative positive values at the surface, but then values show decreasing zigzag like fluctuations that decrease in range downward. A third type seems to show heavy $\delta^{18}O$ values at the surface, followed by a rapid decrease, and then an increase with depth. The final type shows positive $\delta^{18}O$ values at the surface, which then decrease, and then gradually become more positive via one or more zigzags.

Gamma Ray Profiles

Gamma ray profiles across the PTB are shown on the regional gamma ray cross section from Saudi Arabia into Iran (Fig. 3.7) with a close up of the transition across the boundary, in Ghawar, shown in Figure 3.8. The gamma ray profiles in the Permian sections below the PTB averages about 40 API with elevated values commonly associated with sequence boundaries, which tend to have increased clay content (Fig. 3.7). Across the PTB, the gamma ray signal shifts to lower values of 10 to 20 API which are then maintained up through the early Triassic section until the Sudair Shale (Figs. 3.7, 3.8). This decrease in gamma ray can be seen in all the wells from Saudi Arabia to Iran.

Downhole spectral gamma ray logs were not available for the wells examined in this study. Spectral gamma ray profiles done on the cores for this study were of poor quality, and were not able to demonstrate which element (K, U, Th) was causing the major variation in the profiles. However downhole spectral gamma ray profiles from Pars Field, Iran, clearly show that the variation in the signal is largely related to U, which shows a significant decrease across the PTB up into the Early Triassic (Insalaco et al. 2006).

DISCUSSION

Evaluation of Diagenetic Signal in the C-O Data

Interpretation of the C-O Isotopic Compositions of the Limestones and Dolomites

Permian C-Isotopes: The relatively heavy $\delta^{13}C$ values of the Permian dolomites (Fig. 3.5), which are similar to the inferred values for Permian marine calcite, suggests that the C isotope system was rock buffered, thus maintaining the carbon isotope signature even during burial.

Permian Oxygen Isotopes: Using the upper range of $\delta^{18}O$ for, late Permian marine calcite of about -3 $permil_{VPDB}$ would imply that evaporative early dolomites should have mean values of about 0 $permil_{PDB}$ or heavier, given the arid evaporitic setting of the Khuff platform and the Δdolomite-calcite fractionation of about +2.6 to +3 permil (Budd, 1997; Vasconcelos et al., 2005). Assuming conservative temperatures of 25 to 35 degrees C for the formation of the Permian dolomites, and the -1 to +3 $permil_{VPDB}$ of the Permian dolomites (excluding the latest Permian samples) would imply that waters forming the dolomites on the Khuff platform had $\delta^{18}O$ values in the range of -1 to +5 $permil_{smow}$ using the dolomite-water equation of Vasconcelos et al. (2005). These generally positive $\delta^{18}O$ water values thus are enriched relative to Permian ocean water. This is compatible with an arid evaporative setting within the carbonate precipitation field and hypersaline salinities (Lloyd, 1966) using the present day gulf analog (Mckenzie et al., 1980). Thus the $\delta^{18}O$ values of the bulk of the Permian dolomites (Fig. 3.5) may have undergone only minor modification by burial fluids, shifting them to slightly lighter $\delta^{18}O$ values. This reflects the lack of reservoir zones in the Permian sections of the cores studied. Thus they were tight relative to warm burial waters, thus retaining relatively pristine values. The latest Permian dolomites have slightly lighter $\delta^{18}O$

values (-1 to below -3) than the bulk of the Permian dolomites in part reflecting the overall decrease in $\delta^{18}O$ values across the Permian Triassic boundary up into the Early Triassic, coupled with any diagenetic overprint associated with proximity to reservoir zones.

Triassic C-Isotopes: For the Triassic, marine calcite $\delta^{13}C$ values are +1.5 to +3 $permil_{PDB}$ according to Veizer et al. (1999) which are heavier than the field for the Triassic limestones of the study area (Fig. 3.5). Since the shallow platform waters would tend to be warmer than open ocean waters, temperature effects on C-isotope fractionation could not explain the difference, since calcite-bicarbonate fractionation increases slightly with increasing temperature (Anderson and Arthur, 1983). This suggests that the marine platform waters had lighter $\delta^{13}C$ values than open ocean waters at the time. Also, the Triassic limestones in the cores may have been *slightly* reset to lighter values during burial. Within the study area, the similarity between the $\delta^{13}C$ values of the Triassic dolomites and the Triassic limestones suggests that the dolomite $\delta^{13}C$ values have been buffered by the coexisting calcites.

Triassic O-Isotopes: The Triassic limestones of the study area have lighter $\delta^{18}O$ values than the inferred open marine calcite values (-3 to -4.5 $permil_{PDB}$) of Veizer et al. (1999; Fig. 3.5). This could suggest a burial diagenetic shift of the limestone $\delta^{18}O$ values relative to open marine calcite values although many of these rocks are tight and were little affected by burial fluids. It would be unlikely that the Triassic Khuff platform waters had lighter $\delta^{18}O$ values than open ocean waters, given the widespread presence of evaporites in the Triassic. Using the dolomite $\delta^{18}O$ values of -2 to -4 $permil_{PDB}$ and 25 to 35 deg. C temperatures would suggest that the dolomitizing waters were from -4 to -1 $permil_{SMOW}$, using the equation of Vasconcelos et al., 2005) which would be compatible with an evolved, slightly evaporated early Triassic marine water. If temperatures were a conservative 5 deg. C higher in the

Triassic (Korte and Kozur, 2010) then waters would have ranged between -3 and +1 $permil_{SMOW}$ compared to the -1 to +5 $permil_{SMOW}$ waters that formed the Permian dolomites. Thus the dolomite data supports the idea that there was a significant negative shift in $\delta^{18}O$ values of the seawater across the PTB, as suggested by Ehrenberg et al. (2008).

C-O Excursions and Emergence Surfaces

Of the negative C-isotope excursions observed within the studied sections in Ghawar, 75% are associated with emergence surfaces. In Ghawar, even the major excursions across the Wuchiapingian-Changhsingian boundary and the PTB are associated with emergence surfaces. This suggests that *at least a part* of the negative excursion in Ghawar may be diagenetic, or in other words, any global negative excursion affecting Ghawar may have been amplified by the effects of diagenesis below the emergence surface.

The plots of the C-O isotope variation beneath the emergence surfaces may provide information on near-surface diagenetic resetting of the carbonates beneath the surface (Fig. 3.6). Buffering of the C-isotope signal by rock carbon probably has limited the effects of burial diagenesis on the δ^{13} values, so that the signal is either primary and related to global C cycling or is in part near surface diagenetic, related to exposure. The light C values observed at or slightly beneath the emergence surfaces in the studied cores (Fig. 3.6 a) is a common feature of subaerial exposure surfaces (Allan and Matthews, 1982; Joachimski, 1994; Saller et al., 1994; Dickson and Saller, 2006). This is related to light soil gas which is enriched in light C. Those profiles in which the C isotope depletion is just below the surface (Fig. 3.6 a) is suggestive of the depletion being associated with the position of the water table during lowered sea level, or it may be unrelated and due to a global C signal (cf. Dickson and Saller, 2006).

It is possible that the oxygen isotope compositions of these rocks has been reset due to burial diagenesis. However, assuming that at least some of the $\delta^{18}O$ signal is primary, then those profiles in which the $\delta^{18}O$ values tend to be relatively heavy at the exposure surface (Fig. 3.6 b) is compatible with an arid climate, which would cause evaporation of the pore waters in the vadose zone and increase the $\delta^{18}O$ values (James and Choquette, 1990). At the other extreme, the profiles whose $\delta^{18}O$ values are lighter at the surface might reflect the effects of meteoric waters on the vadose zone sediments, given the tropical position of the Arabian plate and the likely slightly depleted $\delta^{18}O$ values of the tropical rainfall (Anderson and Arthur, 1983). Those with intermediate $\delta^{18}O$ values (neither depleted nor enriched) are suggestive of meteoric waters that have only been slightly modified by evaporation or had undergone mixing with isotopically heavy continental waters. The zigzag shapes to the curves could relate to positions of the ground water tables at various times during development of the emergence profiles.

Heydari et al. (2001) suggested that C and O isotope compositions across the PTB were in part diagenetic based on covariance of C and O isotopes. However, this is hardly a fool-proof test of diagenetic overprinting because Pleistocene and Olig-Miocene deep sea carbonates show highly covariant C and O isotope variations at the Milankovitch scale when plotted against depth in the core (Zachos et al., 2002). These fluctuations are primary signals related to productivity increase for positive C isotope excursions, coincident with positive $\delta^{18}O$ shifts due to increase in ice volume, and vice versa for the decreases. Thus when C and O data are retained within a time series (proxy for depth) covariation between C and O does not allow evaluation of the extent of diagenetic overprinting. Also, when these data are plotted on a cross plot (removed from their time-series) they may appear to show no co-

variation. In the present study, $\delta^{13}C$ and $\delta^{18}O$ profiles beneath emergence surfaces are highly variable in terms of co-variation of C and O isotopes, suggesting that this not be used as a test of early diagenetic modification of the isotope signal. However, negative C and O isotope shifts in dolomites beneath anhydrites in the Permian and Triassic sections could result in part from biogenic sulfate reduction as in the Pleistocene of the Arabian Gulf (Chafetz et al., 1999).

In conclusion, it is possible that at least some of the negative C isotope excursion that are associated with the emergence surfaces may be related to near-surface diagenesis, but the globally correlative character of most of the excursions suggests that it is at least in part a global signal related to global C-cycling. The recording of the negative C-isotope excursions within the stacks of parasequences below exposure surfaces could be due to the associated warming of the globe, which was associated with marine flooding of the platform, thus preserving the negative excursion in the sedimentary record. Concerning the PTB excursions, the fact that the $\delta\ ^{13}C_{org}$ and $\delta\ ^{13}C_{carb}$ covary across the PTB boundary almost everywhere (Magaritz et al., 1992; Erwin, 2006) indicates that this is primarily a global signal rather than a diagenetic one. It is significant that the latest Permian Khuff stratigraphy in Ghawar suggests a transgressive pulse at the end of the Permian, apparently synchronous with the negative global C isotope excursion. This would appear to indicate warming coupled with sea level rise, which resulted in transgression, prior to emergence at the PTB.

Origin of Global Carbon-Oxygen Isotope Excursions and U-Depletion

Major negative followed by positive C-isotope excursions of global extent are commonly associated with oceanic anoxic events; processes associated with these events have

been outlined by Jenkyns (2010). The major forcing behind these oceanic anoxic events is an abrupt rise in temperature related to a rapid influx of CO_2 into the atmosphere, associated with volcanism and/or methane release The negative C isotope excursion across the PTB thus likely reflects the input of large amounts of light C from exhalation of volcanic CO_2 during eruption of the immense flood basalts of the Siberian Traps, liberation of light C tied up in coal beds that were intruded by the volcanic magmas, and destabilization of methane clathrates as a result of rising temperatures, perhaps coupled with rising oceanic temperatures and tectono-eustatically lowered sea level (Knoll et al. 1996; Krull et al., 2000; Erwin 2006; Grasby et al., 2011; Korte and Kozur, 2010). In addition, Jin et al. (2000) have suggested, on the basis of the occurrence of microspherules (many of which may be volcanic), and a possible Iridium anomaly, that bolide impact also may have been implicated in the extinction event.

The relative role of volcanism versus methane release in forming the C-isotope excursion is controversial. Even though the Siberian trap eruptions were immense, they probably released insufficient carbon dioxide (2,500 Gigatons) to completely explain the C isotope excursion (which would require 40,000 Gigatons of carbon dioxide; Erwin, 2006). This would be supplemented by oxidation of organic material from the land (1,000 Gigatons only). However, only 2,500 Gigatons of methane are needed to cause the observed 4 permil shift in $\delta^{13}C$ values across the PTB. However, to destabilize the methane clathrates either major sea level fall would be needed (which is not likely, since long term sea level was rising across the boundary, or it would require major heating of the deep ocean or warming of permafrost areas (Erwin, 2006). A significant and largely overlooked source of methane is the large Siberian coal deposits underneath the Siberian traps. These could have provided

methane as a result of conversion of CO_2 at elevated temperatures associated with the volcanism and is borne out by the discovery of fly ash in some of the PTB sediments (Erwin 2006; Grasby et al., 2011).

This resulted in increasing warming and stagnation of the deep oceans, decrease in oxygen levels and redox, and buildup of carbon dioxide and bicarbonate levels. Upwelling of these waters onto shallow platforms caused the accompanying extinction. Shut down of the biological pump due to collapse of primary productivity in surface waters, may have caused the negative isotope anomaly (Korte and Kozur, 2010). The extinction resulted in loss of calcifying metazoans, causing default microbial precipitation of carbonates (Heydari et al., 2001 and 2003; Lehrmann et al., 2003; Weidlich and Bernecker, 2011). These microbial carbonates are common in many of the Early Triassic carbonate successions worldwide.

The warming event probably resulted in an accelerated hydrologic cycle, and increased continental weathering. Sequestration of CO_2 in black shales and by reaction with silicate rocks on continents ultimately restored the climatic equilibrium, accompanied by a positive C isotope excursion.

Lowering of sea levels at the PTB has been controversial. Erwin (1993), Yang et al. (1993), Heydari et al. (2001), Sakar et al. (2003), Yin et al. (2007) and Sheng et al. (2010) proposed that there was a regression at end of Permian. A slight lowering of sea level has been identified in the latest Permian by Tong et al. (1999). Conversely, Wignall and Hallam (1992), Hallam and Wignall (1999), Brookfield et al. (2003) and Lehrmann et al. (2003) suggested that the PTB occurred during a continuous sea level rise.

On the Arabian Plate, lowered sea levels at the PTB are indicated by emergence surfaces on the Arabian Platform, from outcrops of central Saudi Arabia and United Arab Emirates (Al-Dukhayyil and Al-Tawil, 2006; Alsharhan, 2006; Strohmenger et al., 2002), to the subsurface in Ghawar. However, in the relatively deeper settings of Oman and west Iran, the PTB occurred during a continuous transgression, started in latest Permian, with no major sedimentation gap (Angiolini et al., 2003; Weidlich and Bernecker , 2003; Insalaco et al., 2006). The dispute suggests that global sea level fall may have occurred but that tectonics on some platforms resulted in continued submergence across the PTB. It has been suggested that the emergence of the Arabian plate at this time may have been related to tectonics (Heydari et al., 2001).

The U depletion with decrease of the gamma ray signal across the PTB has been tied to oceanic anoxia and lowering of redox in the deep oceans, thus sequestering U on the deep sea floor (Erwin 2006; Insalaco et al. 2006; Ehrenberg et al 2008). Thus shallow marine waters circulating onto the early Triassic platforms were depleted in soluble U species, resulting in carbonates with lowered U concentrations. This supports the postulate of poorly oxygenated oceans after the PTB based on the models for C isotope excursions (cf Holser et al., 1989; Baud et al., 1989; Jenkyns, 2010).

The significant negative shift in $\delta^{18}O$ values across the boundary appears to be a primary, rather than a later diagenetic signal borne out by the dolomite oxygen isotope compositions of this study. It is far too large to be related to melting of ice sheets, of which there were few by the latest Permian time anyway (Fielding et al., 2008). Perhaps part of the depletion could be associated with warming of the oceans, resulting in decreased fractionation between carbonate-water but this would hardly account for the amount of the shift by itself, as

5 degrees C warming would only decrease the $\delta^{18}O$ value by 1 $permil_{SMOW}$. As $\delta^{18}O$ values of ocean water in equatorial regions are dependent on salinity, with dilution related to local rainfall (5 ppt salinity decrease would result in a decrease of about 0.5 permil; Swart et al., 2005), global dilution of the surface ocean waters due to increased precipitation caused by ocean warming might add to the $\delta^{18}O$ depletion. Thus it would seem that the $\delta^{18}O$ depletion across the PTB is the product of multiple causes, all of which shifted $\delta^{18}O$ of the precipitated carbonates to more negative values.

CONCLUSIONS

Carbon isotope profiles sampled from cored wells of the Khuff Formation, spanning 150 m of section across the Permian-Triassic boundary in Ghawar Field, Saudi Arabia were studied to evaluate their use in local and global correlation, and to evaluate the possible influences of early diagenesis versus global processes. The two major excursions are at the Wuchiapingian-Changhsingian boundary and the Permian-Triassic (PTB). However there are several smaller excursions that also appear to correlate with excursions elsewhere. These smaller excursions, many of which correlate to emergence events in Ghawar, may be due to a combination of early diagenetic and global mechanisms. Their global extent provides a high resolution correlation tool for the Late Permian and Early Triassic succession.

Over 75% of the negative carbon isotope excursions occur beneath emergence surfaces, including the two major excursions at the Wuchiapingian and Changhsingian stage boundaries. The $\delta^{13}C$ profiles beneath the boundaries resemble those associated with early diagenesis associated with isotopically light soil gas. The $\delta^{18}O$ profiles beneath the surfaces are variable, perhaps reflecting variable effects of evaporation on the meteoric input, mixing or overprinting by burial diagenesis.

The presence of the negative C-isotope excursions globally in both $\delta^{13}C_{carbonate}$ and $\delta^{13}C_{organic}$ as well as in deeper water sections lacking emergence surfaces, strongly supports the idea of these excursions being global phenomena related global C cycling, although on the Arabian Platform they appear to have been modified by early diagenesis. U depletion across the boundary is compatible with the postulated origins of the PTB event with bottom waters becoming stagnant and reducing, as a result of warming induced by volcanogenic CO_2 released by Siberian trap volcanism, methane release from thermal metamorphism of coals, and destabilization of clathrates in the deep sea due to ocean warming.

FIGURES AND FIGURE CAPTIONS

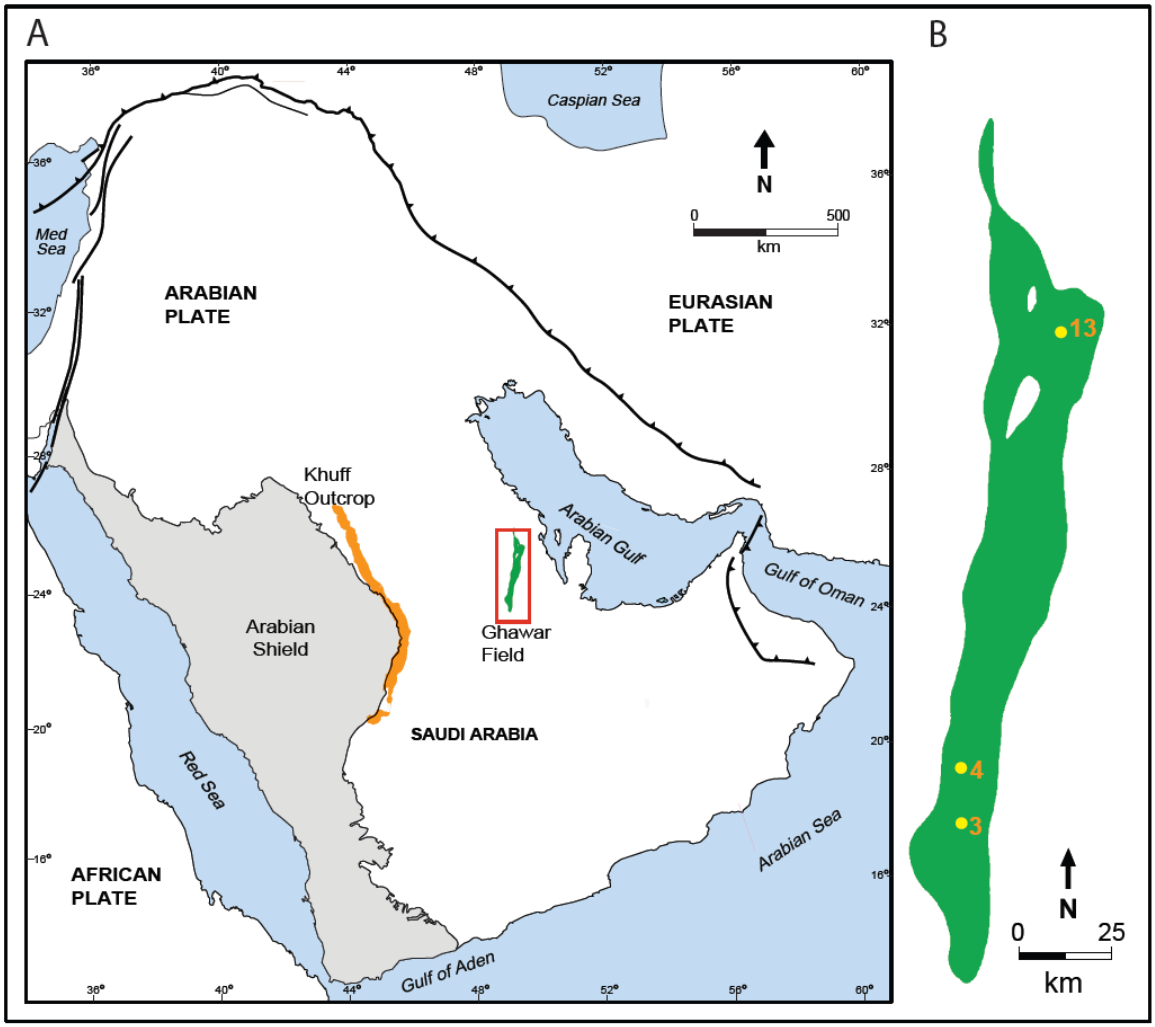

Figure 3.1: (**a)** Map of Arabian Plate showing the plate boundaries, location of Ghawar Field (study area; red rectangle), and the Permian-Triassic Khuff outcrop belt (orange); **(b).** Map of Ghawar Field showing approximate location of the studied wells.

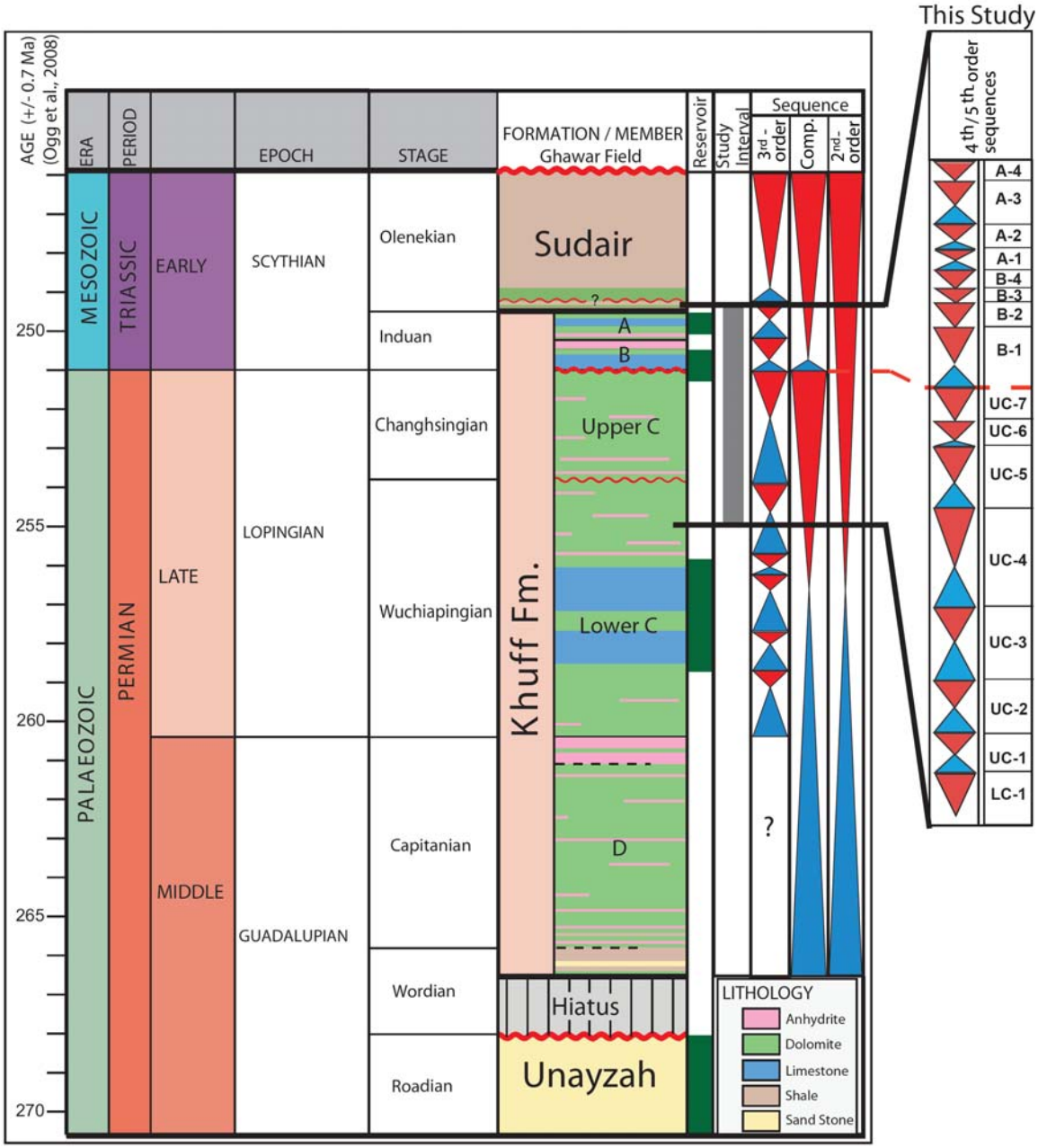

Figure 3.2: Chronostratigraphic chart showing the subdivision of the Khuff Formation in Saudi Arabia. Modified from Ogg et al. (2008) and Al-Jallal (1995).

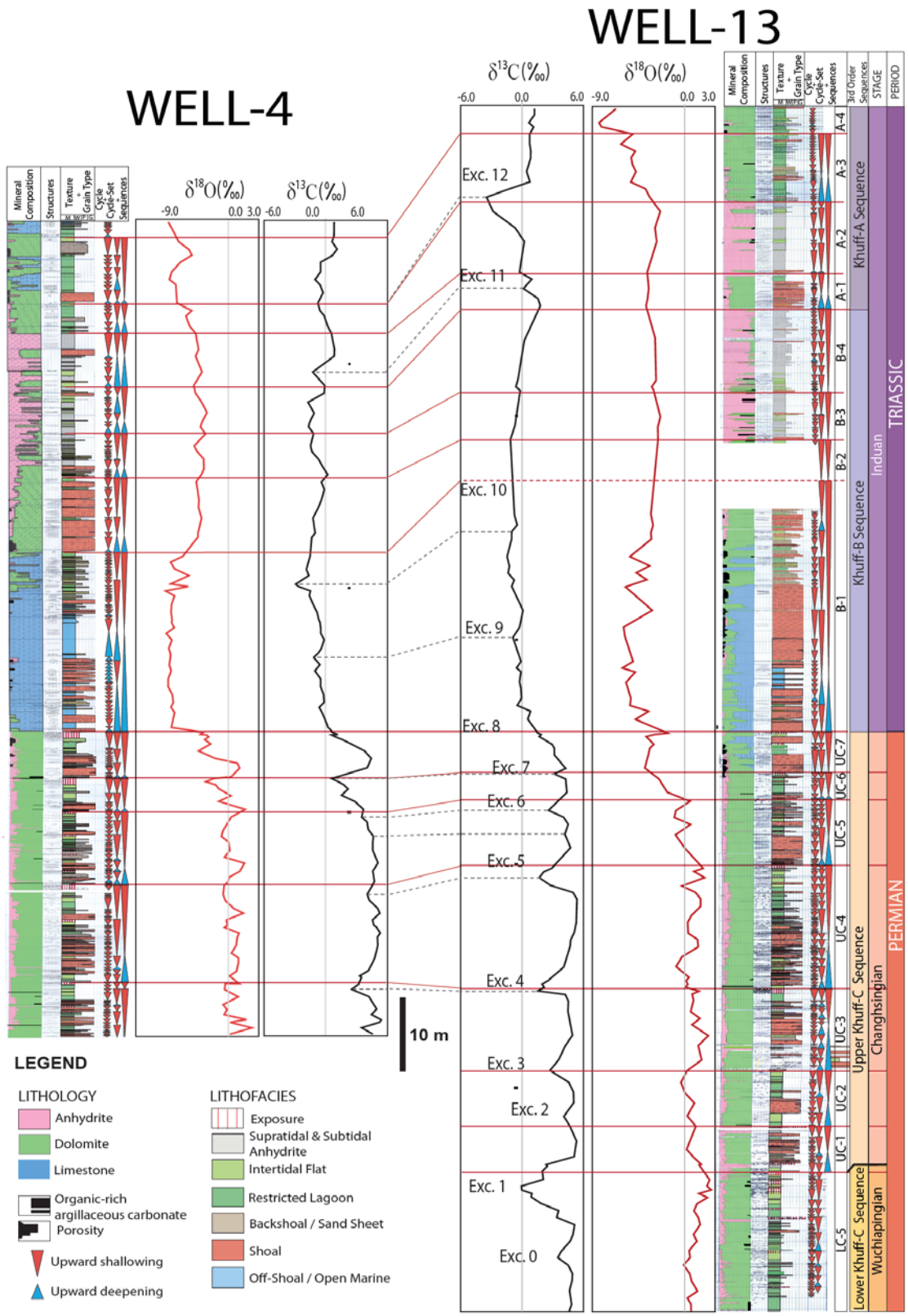

Figure 3.3: Carbon (black) and oxygen (red) isotope profiles for the studied wells alongside the core logs for the wells 4 and 13. Correlation of negative excursions (Exc. 0 to 12) are labeled and shown in dotted lines.

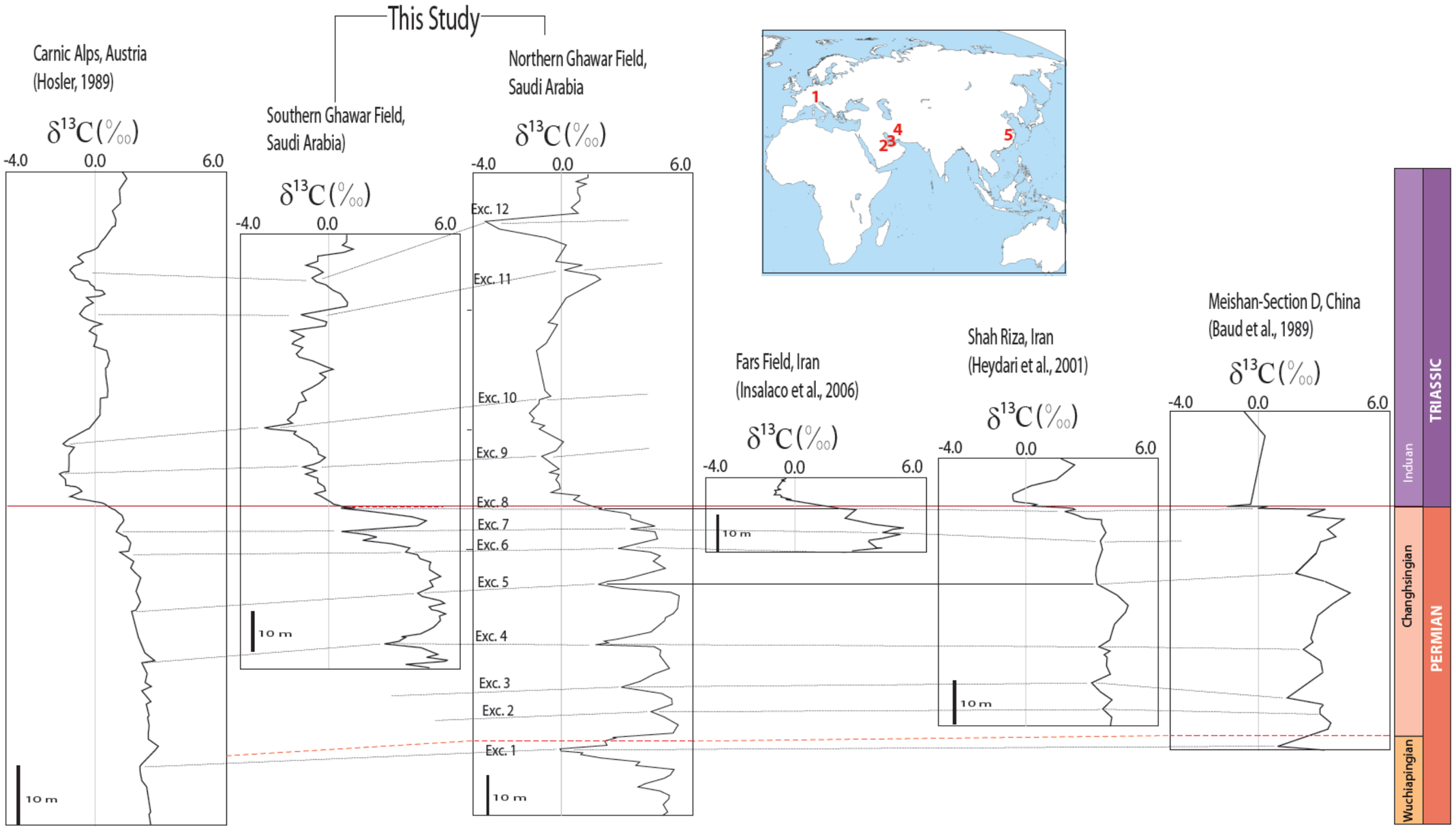

Figure 3.4: $\delta^{13}C$ patterns across the Permo-Triassic boundary successions. Six sections are correlated. Data for Carnic Alps, Austria from Holser et al. (1989); Fars Field, Iran from Insalaco et al. (2006); Shah Riza, Iran from Heydari et al. (2001); for Meishan Section D, China from Baud et al. (1989). Data for Ghawar Field, Saudi Arabia are from this study.

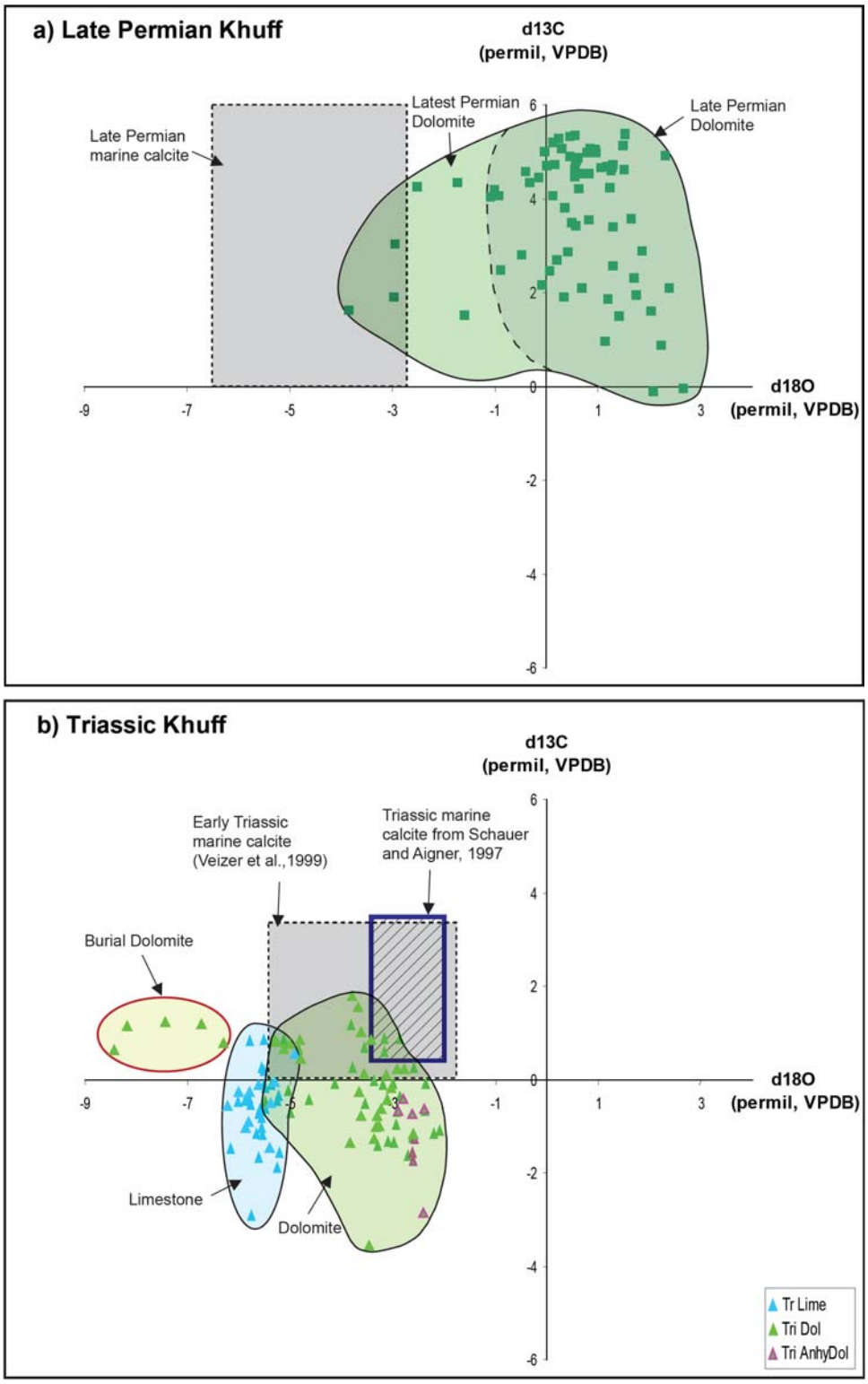

Figure 3.5: Ghawar C-O isotope cross plot for (a) dolomite in the Upper Permian and (b) dolomite vs. calcite in the Early Triassic. Marine calcite isotopic compositions are estimated from Veizer et al. (1999; outlined in grey using ±1 б), and from Schauer and Aigner (1996; outlined in dark blue).

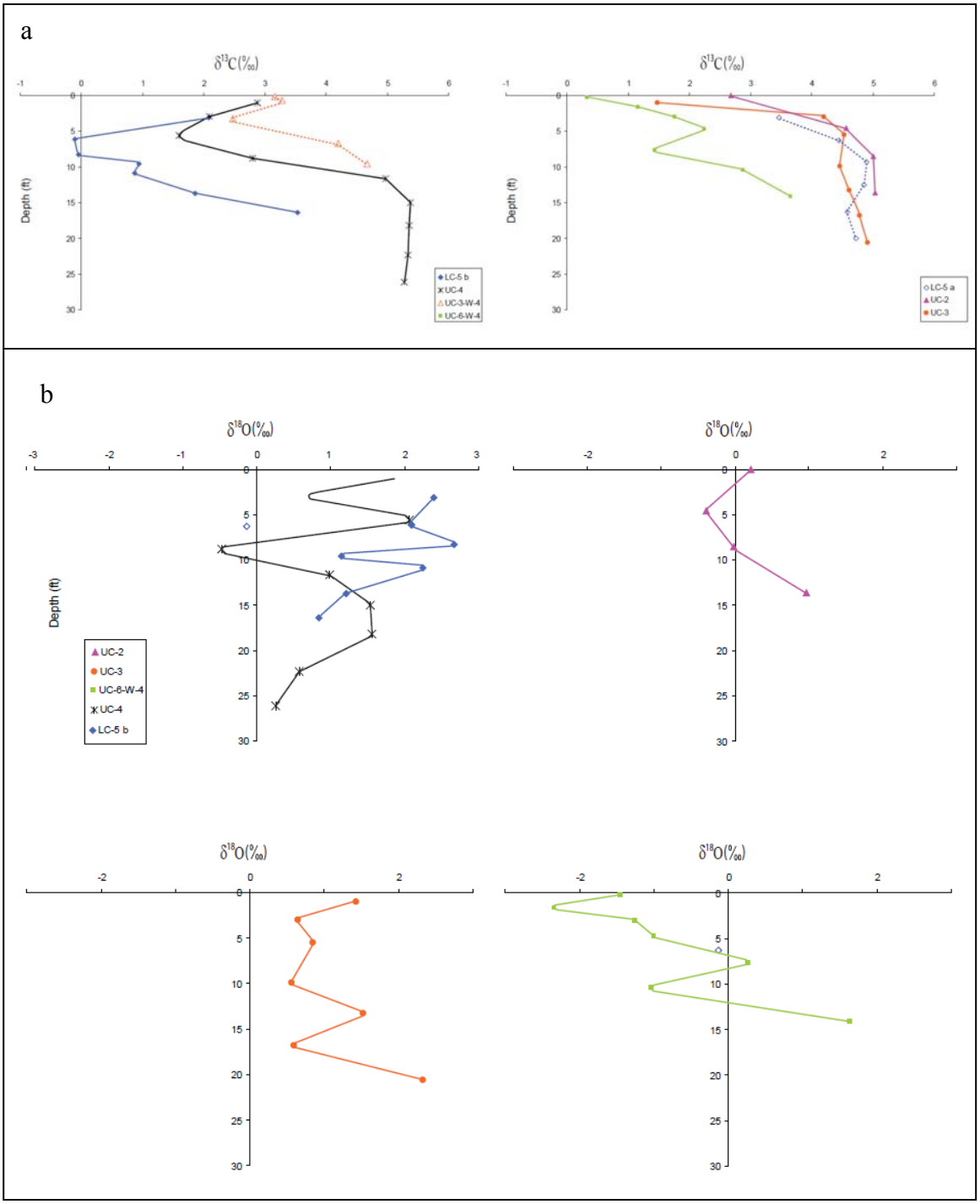

Figure 3.6: Short chemostratigraphic profiles extending down beneath emergence surfaces: (a) C-isotope profiles and (b) O-isotope profiles within Permian dolomite units. Note that the profiles extend down from the exposure surface, through several of the underlying parasequences, rather than through a single parasequence.

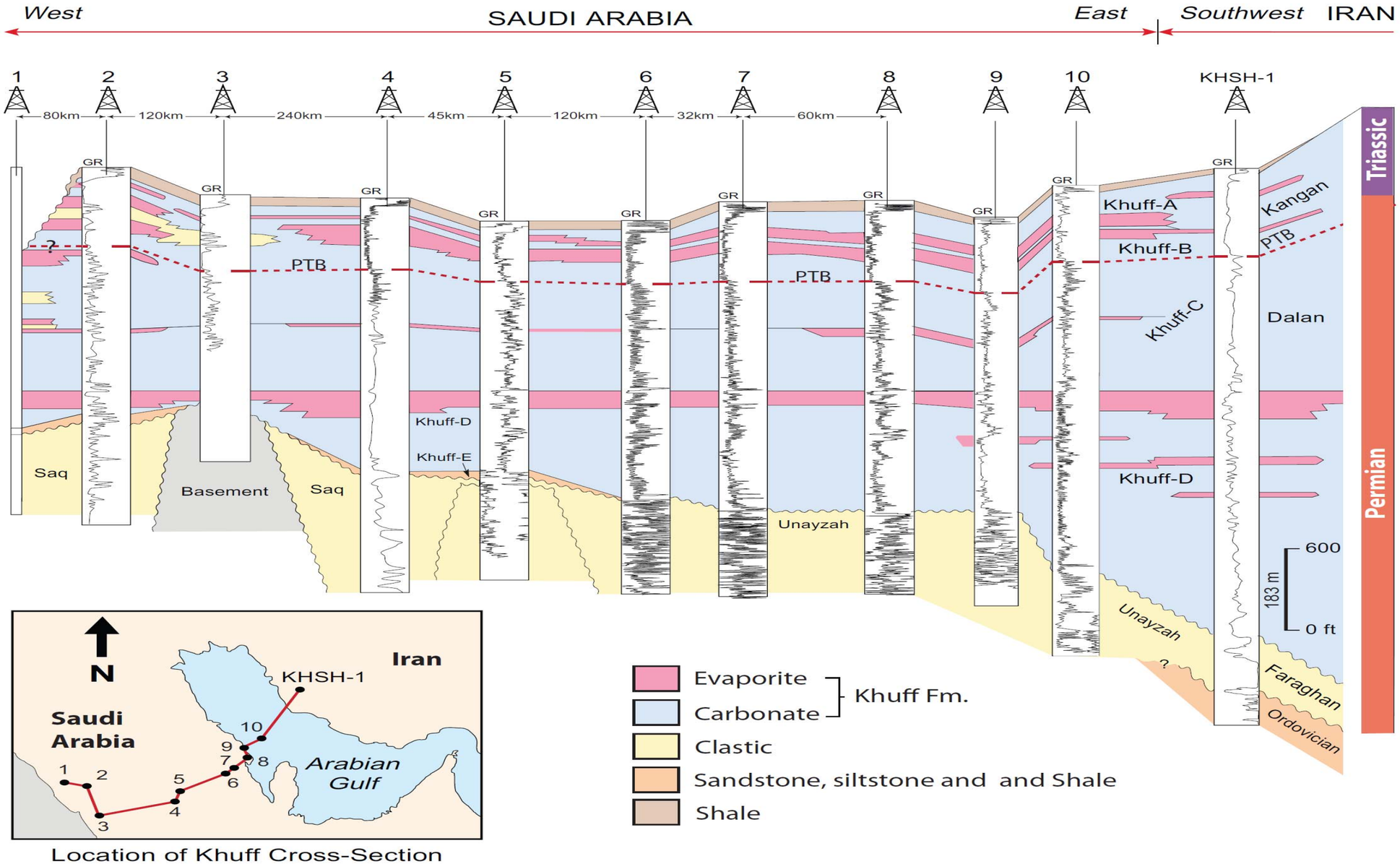

Figure 3.7: Stratigraphic cross section from Saudi Arabia to Iran showing the Khuff members datumed on the top Khuff D anhydrite. The Permo-Triassic Boundary (PTB; red dashed line) is traceable across the region using GR log (modified from Al-Jallal, 1995 and Konert et al., 2001).

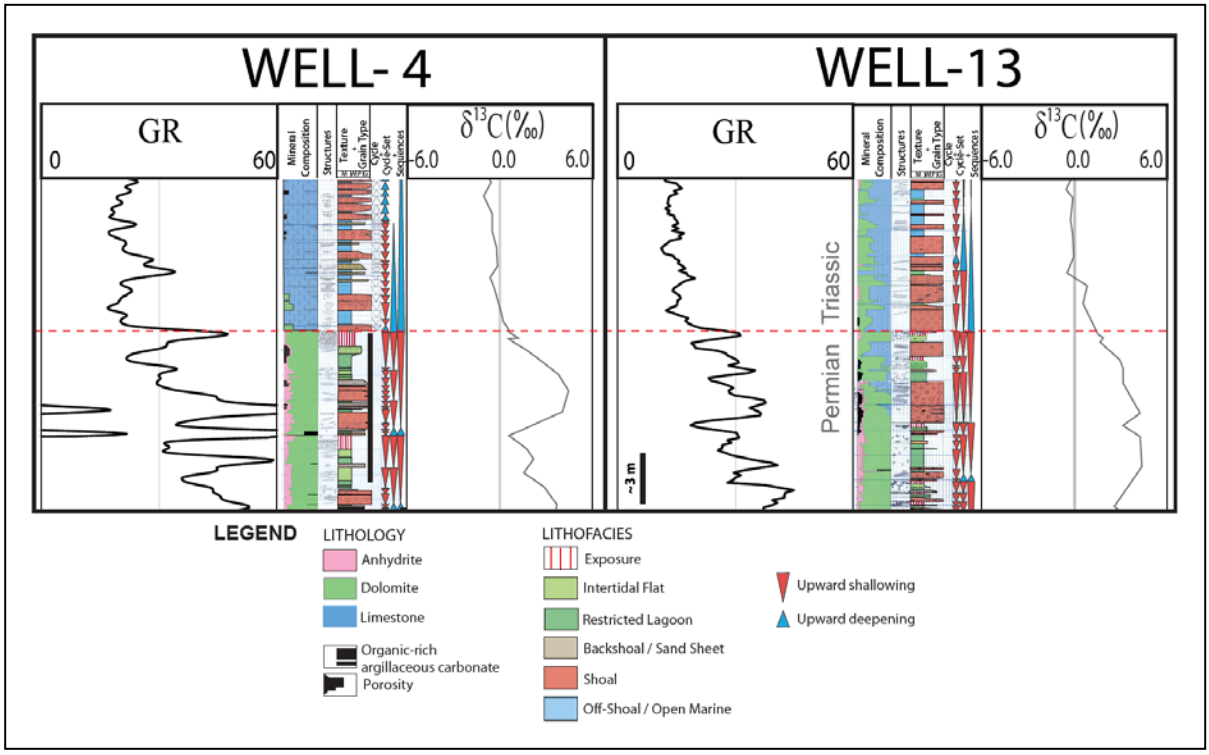

Figure 3.8: A close-up of the Permo-Triassic boundary in Ghawar, along with gamma ray (GR) log and Carbon isotope profile. On core log, left hand column is mineralogy, central column is sedimentary structures, and right hand column is Dunham rock type. See legend for color coded rock types.

TABLES AND TABLE CAPTIONS

Table 3.1. A summary of the C-O isotope values tied to the sequences for the studied wells in Ghawar.

	WELL-4				WELL-13			
Sequence	**$\delta^{13}C$ (‰)**	**Avg.**	**$\delta^{18}O$(‰)**	**Avg.**	**$\delta^{13}C$ (‰)**	**Avg.**	**$\delta^{18}O$(‰)**	**Avg.**
A-4	+0.8 to +0.9	+0.8	-5.8 to -5.1	-5.5	+0.6 to +1.2	+1.1	-8.4 to -6.7	-7.7
A-3	-1.1 to +1.2	-0.1	-5.8 to -3.6	-4.8	-3.6 to +0.8	0.0	-6.3 to -3.5	-4.87
A-2	-0.5 to +0.6	+0.1	-4.1 to -3.2	-3.7	-2.9 to +0.2	-0.9	-3.7 to -2.4	-2.92
A-1	-1.3 to +0.9	+0.1	-3.4 to -2.6	-3.0	+0.1 to +1.8	+1.1	-3.8 to -3.6	-3.66
B-4	-1.7 to -0.1	-1.2	-3.2 to -2.1	-2.6	-0.6 to +0.2	-0.3	-3.2 to -2.8	-2.99
B-3	-1.4 to +0.3	+0.7	-3.3 to -2.4	-2.8	-0.7 to -0.6	-0.7	-2.6 to -2.4	-2.51
B-2	-1.4 to -0.1	-0.7	-3.1 to -2.6	-2.9	-1.17	-1.2	-2.60	-2.60
B-1	-2.9 to +0.2	-0.9	-6.2 to -3.8	-5.4	-1.5 to +0.8	-0.5	-6.2 to -3.1	-4.64
UC-7	+0.5 to +4.4	+2.3	-3.0 to +1.1	-1.4	+1.5 to +4.3	+2.7	-3.9 to -1.6	-3.19
UC-6	+0.3 to +3.7	+1.9	-2.3 to +1.6	-0.7	+3.0 to +4.3	+3.9	-2.9 to -1.7	-2.38
UC-5	+3.5 to +5.1	+4.5	-0.7 to +1.5	+0.1	+2.5 to +4.7	+3.9	-1.1 to +0.7	-0.28
UC-4	+3.3 to +5.3	+4.6	-0.6 to +1.5	+0.3	+1.6 to +5.4	+3.8	-0.9 to +2.1	+0.65
UC-3	+2.5 to +5.4	+4.2	-0.6 to +2.4	+0.4	+1.5 to +4.9	+4.1	+0.6 to +2.3	+1.21
UC-2	-	-	-	-	+2.7 to +5.0	+4.3	-0.4 to +1.0	+0.18
UC-1	-	-	-	-	+1.9 to +5.3	+3.9	+0.1 to +1.8	+1.05
LC-5	-	-	-	-	-0.1 to +5.1	+3.4	-0.1 to +2.7	+1.10

REFERENCES

Al-Aswad, A.A. 1997. Stratigraphy, sedimentary environment and depositional evolution of the Khuff Formation in south-central Saudi Arabia. Journal of Petroleum Geology, v. 20, p. 307.

Al-Dukhayyil, R. K. and A. A. Al-Tawil 2006. Reservoir architecture of the Triassic Khartam carbonate sequence, Khuff outcrop analogue in Al-Qasim, central Saudi Arabia. 7th Middle East Geosciences Conference, Geo 2006 in Bahrain, abstract.

Al-Dukhayyil, R.K., G.A. Al-Eid and A.A. Al-Tawil 2006. Core-and-log signature of high-resolution sequence-and-cycle stratigraphy of Permian Khuff C Reservoir; implications for reservoir characterization and development, Ghawar Field, Saudi Arabia. AAPG Annual Conference in Houston, extended abstract.

Al-Husseini, M.I. 2000. Origin of the Arabian Plate structures: Amar Collision and Najd Rift. GeoArabia, v. 5, no. 4, p. 527-542.

Al-Jallal. I.A. 1989. Depositional environments, diagenesis and reservoir characteristics of the late Permian Khuff Formation in eastern Saudi Arabia: Ph. D. Thesis, University of London, (unpublished).

Al-Jallal, I.A. 1995. The Khuff Formation: Its regional reservoir potential in Saudi Arabia and other Gulf countries; depositional and stratigraphic approach. In M.I. Al-Huseini (Ed.), Middle EastPetroleum Geosciences Conference, GEO'94. Gulf PetroLink, Bahrain, v. 1, p. 103-119.

Alsharhan, A.S. 2006. Sedimentological character and hydrocarbon parameters of the Middle Permian to Early Triassic Khuff Formation, United Arab Emirates. GeoArabia, v. 11, no. 3, p.121-158.

Allan, J. R. and R.K. Matthews 1982. Isotope signatures associated with early meteoric diagenesis." Sedimentology, v.29, p.797-817.

Anderson, T.F. and M.A. Arthur 1983. Stable isotopes of oxygen and carbon and their application to sedimentologic and paleoenvironmental problems. In M. A. Arthur, T. F. Anderson, I. R. Kaplan, J. Veizer and L. S. Land (Eds.), Stable Isotopes in SedimentaryGeology. SEPM Short Course No. 10, p. 1-1 - 1-151.

Angiolini, L., M. Balini, E. Garzanti, A. Nicora, A. Tintori, S. Crasquin-Soleau and G. Muttoni 2003. Permian climatic and palaeogeographic changes in Northern Gondwana: The Khuff Formation of Interior Oman. Palaeogeography, Palaeoclimatology, Palaeoecology, v. 191, nos 3-4, p. 269-300.

Baud, A., W.T. Holser and M. Magaritz 1989. Permian-Triassic of the Tethys: carbon isotope sudies. Geologische Rundschau, v. 78/2, p. 649-677.

Budd, D.A., 1997. Cenozoic dolomites of carbonate islands: their attributes and origin. Earth-Sci. Rev. 42, p. 1–47.

Brookfield, M.E., R.J. Twitchett and C. Gooding 2003. Palaeoenvironments of the Permian-Triassic transition sections in Kashmir, India. Palaeogeography, Palaeoclimatology, Palaeoecology, v. 198, p. 353–371.

Chafetz, H.S., Imerito-Tetzlaff and J. Zhang 1999. Stable-isotope and elemental trends in Pleistocene sabkha dolomites: Descending meteoric waters vs. sulfate reduction. Journal of Sedimentary Research, v. 69, p. 268-278.

Coplen, T.B. 1994. Reporting of stable hydrogen, carbon, and oxygen isotopic abundances. Pure and Applied Chemistry, v. 66, p. 273-276.

Dickson, J. A. D. and A.H. Saller 2006. Carbon isotope excursions and crinoid dissolution at exposure surfaces in carbonates, West Texas, U.S.A. Journal of Sedimentary Research, v. 76, no. 3, p. 404-410.

Ehrenberg, S.N., T.A. Svana and P.K. Swart 2008. Uranium depletion across the Permian – Triassic boundary in Middle East carbonates: Signature of oceanic anoxia. American Association of Petroleum Geologists Bulletin, v. 92, no. 6, p. 691-707.

Erwin, D.H. 1993. The Great Paleozoic Crisis: Life and Death in the Permian. Columbia Univ. Press, New York, 327 p.

Erwin, D.H. 2006. Extinction: How life on Earth nearly ended 250 million years ago. Princetone, Princetone University Press, 296 p.

Fielding, C.R., T.D.Frank, L.P. Birgenheier, M.C. Rygel, A.T. Jones and J. Roberts 2008. Stratigraphic imprint of the Late Palaeozoic Ice Age in eastern Australia: a record of alternating glacial and nonglacial regime. J. Geol. Soc. Lond., vol. 165, p. 129–140.

Frakes, L.A., J.E. Francis and J.I Syktus 1992. Climate modes of the Phanerozoic: the history of the Earth's climate over the Past 600 Million Years. Cambridge University Press, Cambridge, UK, 274 p.

Grasby, S.E., H. Sanei and B. Beauchamp 2011. Catastrophic dispersion of coal fl y-ash into oceans during the latest Permian extinction: Nature Geoscience, v. 4, p. 104–107,

Hallam A and P.B. Wignall 1999. Mass extinctions and sea-level changes. Earth-Science Reviews, v. 48, p. 217-250

Heydari, E., W.J. Wade and J. Hassanzadeh 2001. Diagenetic origin of carbon and oxygen isotope compositions of the Permian-Triassic boundary strata. Sedimentary Geol., v.143, p.191-197.

Heydari, E., J. Hassanzadeh, W.J. Wade and A.M. Ghazi 2003. Permian–Triassic

boundary interval in the Abadeh section of Iran with implications for mass extinction: part 1 – sedimentology. Palaeogeography, Palaeoclimatology, Palaeoecology, v. 193, p. 405–423.

Hughes, G.W. 2005. Saudi Arabia Permo-Triassic biostratigraphy, micropalaentology and palaenvironment. Micrpaleontological Society, Special Publications, p. 91-108.

Hughes, G.W. 2009. Micropaleontology and paleoenvironments of Saudi Arabian Upper Permian carbonates and reservoirs. In Geologic Problem Solving with Microfossils: A volume in Honor of Garry D. Jones. SEPM Special Publication, no. 93, p. 111-126.

Holser, W.T., H.P. Schonlaub, M. Attrep, K. Boeckelmann, P. Klein, M. Magaritz, C.J. Orth, A. Fenninger, C. Jenny, M. Kralik, H. Mauritsch, E. Pak, J.M. Schramm, K. Stattegger and R. Schmoller 1989. A unique geochemical record at the Permian/Triassic boundary. Nature, v. 337, p. 39–44.

Holser, W.T. and M. Magaritz 1987. Events near the Permian–Triassic boundary. Modern Geology, v. 11, p. 155–180

Insalaco, E., A. Virgone, B. Courme, J. Gaillot, M. R. Kamali, A. Moallemi, M. Latfpour and S. Monibi 2006. Upper Dalan Member and Kangan Formation between the Zagros Mountains and offshore Fars, Iran: depositional system, biostratigraphy and stratigraphic architecture. Arabia. GeoArabia, v. 11, no. 2, p. 75-176.

James, N.P. and P.W. Choquette 1990. Limestones - the meteoric diagenetic environment. In: McIlreath, I.A. and D.W. Morrow (Eds.), Diagenesis. Geol. Assoc. Canada, Ontario, pp. 35-74.

Jenkyns, H.C 2010. Geochemistry of oceanic anoxic events. Geochemistry Geophysics Geosystems, v. 11, no. 3, p. 1-30.

Jin, Y.G., Y. Wang, C.M. Henderson, B.R. Wardlaw, S.Z. Shen and C.Q. Cao 2006. The global boundary stratotype section and point (GSSP) for the base of Changhsingian Stage (Upper Permian). Episodes 29, p. 175–182.

Jin, Y.G., Y. Wang, W. Wang, Q.H. Shang, C.Q. Cao and D.H. Erwin 2000. Pattern of marine mass extinction near the Permian–Triassic boundary in South China. Science 289, 432– 436.

Joachimski, M. 1994. Subaerial exposure and deposition of shallowing upward sequences: evidence from stable isotopes of Purbeckian peritidal carbonates (basal Cretaceous), Swiss and French Jura Mountains. Sedimentology, v. 41, p. 805–824.

Knoll, A.H., R.K. Bambach, D.E. Canfield and J.P. Grotzinger 1996. Comparative Earth history and Late Permian mass extinction. Science, v. 273, p. 452–457.

Koehrer, B., M. Zeller, T. Aigner, M. Poeppelreiter, P. Milroy, H. Forke and S. Al-Kindi 2010. Facies and stratigraphic framework of a Khuff outcrop equivalent: Saiq and Mahil formations, Al Jabal al-Akhdar, Sultanate of Oman. GeoArabia, v. 15, no. 2, p. 91-156.

Konert, G., A. Al-Afifi, S. Al-Hajri and H. Dorste 2001. Paleozoic stratigraphy and hydrocarbon habitat of the Arabian Plate. GeoArabia, v. 6, no. 3, p. 407-442.

Korte, C. and H.W. Kozur 2010. Carbon isotope stratigraphy across the Permian-Triassic boundary: a review. Journal of Asian Earth Sciences, v. 39, p. 215–235.

Krull, E.S., and G.J. Retallack 2000. δ13C depth profiles from paleosols across the Permian-Triassic boundary: evidence for methane release. GSA Bulletin, v. 112, p. 1459-1472.

Lehrmann, D.J., J.L. Payne, S.V. Felix, P.M. Dillett, H. Wang, Y.Y. Yu, and J.Y. Wei 2003. Permian-Triassic boundary sections from shallow marine carbonate platforms of the Nanpanjiang Basin, south China: implications for oceanic conditions associated with the end-Permian extinction and its aftermath. Palaios, v. 18, p. 138–152.

Lloyd, R.M. 1966. Oxygen isotope enrichment of sea water by evaporation. Geochimica et Cosmochimica Acta, v. 30, p. 801-814.

Magaritz, M., Krishnamurthy, R. V. & Holser, W. T. 1992. Parallel trends in organic and inorganic carbon isotopes across the Permian/Triassic boundary. American Journal of Science 292: 727–739.

Markello, J.R., 1988. A geologic model for the Khuff Formation, Ghawar Field, Saudi Arabia. Mobil Research and Development Corporation, 168 p. (unpublished).

McKenzie, J.A., K.J. Hsu and J.F. Schneider 1980. Movement of subsurface waters under the sabkha, Abu Dhabi, UAE, and its relation to evaporative dolomite genesis, *in* Zenger, D.H., et al., eds., Concepts and models of dolomitization: Society of Economic Paleontologists and Mineralogists Special Publication, v. 28, p. 11-30.

Ogg, J.G., G. Ogg and F.M Gradstein 2008. The concise geologic time scale. Cambridge, UK, Cambridge University Press, 177 p.

Richoz, S. 2006. Stratigraphie et variations isotopiques du carbone dans le Permien supérieur et le Trias inférieur de quelques localités de la Néo-Téthys (Turquie, Oman et Iran). Mémoire de Géologie de Lausanne, v. 46, 284 p.

Richoz, S.,L. Krystyn, A. Baud, R. Brandner, M. Horacek, P. Mohtat-Aghai 2010. Permian–Triassic boundary interval in the Middle East (Iran and N. Oman): progressive environmental change from detailed carbonate carbon isotope marine curve and sedimentary evolution. J. Asian Earth Sci., v. 39, p. 236–253.

Saller, A. H., D.A. Budd and P.M. Harris 1994. Unconformities and porosity development in carbonate strata: ideas from a Hedberg conference. AAPG Bulletin, v. 78, p. 857–871.

Sarkar, A., H. Yoshioka, M. Ebihara and H. Naraoka 2003. Geochemical and organic carbon isotope studies across the continental Permo–Triassic boundary of Raniganj Basin, eastern India. Palaeogeography, Palaeoclimatology, Palaeoecology 191, p. 1–14.

Sharief, F. A., 1983, Permian and Triassic geological history and tectonics of the Middle East: Journal Petroleum Geology, v.6, p. 95-102.

Sharland, P.R., R. Archer, D.M. Casey, R.B. Davies, S.H. Hall, A.P. Heward, A.D. Horbury and M.D. Simmons 2001. Arabian Plate sequence stratigraphy. GeoArabia Special Publication 2, 371 p.

Sheng, W.Y., J.H. X and F.J. Song 2010. Evidence for sea-level falls in the Permian-Triassic transition in the Ziyun area, South China. Geol. Jour., v. 45, p. 170-185

Strohmenger, C.J., R.H. Alway, R.W. Broomhall, R.F. Hulstrand, A. Al-Mansoori, A.A. Abdalla, A. Al-Aidarous 2002. Sequence stratigraphy of the Khuff Formation comparing subsurface and outcrop data (Arabian Plate, UAE). SPE paper no. 78535, p. 558-568.

Swart, P.K. and G. Mackenzie, 2001a. Geochemical and petrographic observations on the diagenesis of the Khuff Formation, Ghawar Field, Saudi Arabia (Unpublished report).

Swart, P.K. and G. Mackenzie, 2001b. Geochemical and Petrographic Observations on the Diagenesis of the Khuff Formation, Ghawar Field, Saudi Arabia (Unpublished report).

Swart, P.K., D.L. Cantrell, H. Westphal, C.R. Handford, and C.G. Kendall 2005. Origin of dolomite in the Arab-D reservoir from the Ghawar field, Saudi Arabia: Evidence from geochemical and petrographic constraints. Journal of Sedimentary Research, v. 75, p. 476-491.

Tong J.N., H.F. Yin and K.X. Zhang 1999. Permian and Triassic sequence stratigraphy and sea-level changes of eastern Yangtze platform. Journal of China University of Geosciences, v. 10, p. 161–169.

Wignall P B, A. Hallam 1993. Griesbachian (Earliest Triassic) palaeoenvironmental changes in the Salt Range, Pakistan and southeast China and their bearing on the Permo-Triassic mass extinction. Palaeogeography, Palaeoclimatology, Palaeoecology, v. 102, p. 215-237

Vasconcelos, C., J.A. McKenzie, R. Warthmann and S.M. Bernasconi 2005. Calibration of the $\delta^{18}O$ paleothermometer for dolomite precipitated in microbial cultures and natural environments. Geology, v. 33, p. 317–320.

Veizer, J., Ala, D., Azmy, K., Bruckschen, P., Buhl, D., Bruhn, F., Carden, G. A. F., Diener, A., Ebneth, S., Godd´eris, Y., Jasper, T., Korte, C., Pawellek, F., Podlaha, O. G. and H. Strauss 1999. ^{87}Sr /^{86}Sr, $\delta^{13}C$ and $\delta^{18}O$ evolution of Phanerozoic seawater. Chem. Geol., v. 161, p. 5988, 1999.

Weidlich, O. and M. Bernecker 2003. Supersequence and composite sequence carbonate platform growth: Permian and Triassic outcrop data of the Arabian platform and Neo-Tethys. Sedimentary Geology, v. 158, p. 87-116.

Weidlich, O. and M. Bernecker 2011. Biotic carbonate precipitation inhibited during the Early Triassic at the rim of the Arabian Platform (Oman). Palaeogeography, Palaeoclimatology, Paleoecology, v. 308, p.129–150.

Xu, D.Y., Yan, Z., 1993. Carbon isotope and iridium event markers near the Permian=Triassic boundary in the Meishan section section, Zhejiang Province, China. Palaeogeogr., Palaeoclimatol., Palaeoecol, v. 104, p.171–176.

Xu, D.-Y., Yan, Z., Zhang, Q.-W., Sun, Y.-Y., 1986. Three main mass extinctions – significant indicators of major natural divisions of geological history in the Phanerozoic. Mod. Geol., v. 10, p. 365-375.

Yang, Z.Y, S.B. Wu, H.F. Yin, G.R. Xu, K.X. Zhang and X.M. Bi 1993. Permo–Triassic Events of South China. Geological Publishing House, Beijing, 153 p.

Yin, H., Q. Feng, X. Lai, A. Baud and J. Tong 2007. The protracted Permo-Triassic crisis and multi-episode extinction around the Permian-Triassic boundary. Global and Planetary Change, v. 55 (1–3), p. 1–20.

Wender, E. L., J. W. Bryant, M. F. Dickens, A. S. Neville and A. M. Al-Moqbel 1998. Paleozoic hydrocarbon geology of the Ghawar Area, Eastern Saudi Arabia. GeoArabia, v. 2, no. 2, p. 273-302.

Zachos, J.C., M.A. Arthur, T.J. Bralower, and H.J. Spero 2002. Palaeoclimatology – Tropical temperatures in greenhouse episodes. Nature, v. 419, p. 897-898.

Ziegler, M.A., M.L. Hulver and D.B. Rowley 1997. Permian world topography and climate. In: I.P. Martini (ed.), Late glacial and postglacial environment changes-Quaternary, Carboniferous-Permian, and Proterozoic. New York: Oxford University Press, p. 111-146.

Ziegler, M. A., 2001. Late Permian to Holocene paleofacies evolution of the Arabian Plate and its hydrocarbon occurrences. GeoArabia, v. 6, no. 3, p. 445-504.

CHAPTER 4

CONCLUSIONS

Detailed logging of selected cores throughout Ghawar, eastern Saudi Arabia, has allowed a comprehensive depositional model, and high resolution sequence stratigraphic framework to be generated for the Upper Permian and Lower Triassic Khuff Formation, along with a more refined relative sea-level curve for the region. It also allowed time slice maps of the facies distribution within sequences in Ghawar to be developed. Ages were constrained by published biostratigraphy and by new C isotope data. The resultant cross sections and maps should provide a framework for a new generation of 3-D geological reservoir models.

Several scales of depositional sequences are developed, that include the 3rd order sequences of the Permian upper Khuff C, and the Early Triassic Khuff B and the Khuff A sequences, and their correlation with the global curves suggest that they were driven by global eustasy. The 3rd order sequences contain several high frequency sequences, which in the Khuff C are ~400 k.y. duration and probably driven by long term eccentricity, but those in the Khuff B and A, appear to be ~100 to 200 k.y. duration and not easily tied to Milankovitch orbital eccentricity forcing. The high frequency sequences are in turn composed of parasequences, which appear to be 10 to 20 k.y. average durations, suggesting orbital precessional and half precessional forcing. However, many thin locally developed cycles may be autocycles or subprecessional cycles.

The sequence stratigraphic cross sections and facies maps of systems tracts illustrates the subtle interplay between the Ghawar structure and regional paleoslopes. This is evidenced by changes in directions of progradation from one high frequency sequence to the next.

Southward progradation is evident in the Khuff B, while the Khuff A shows initial northward progradation, followed by southward progradation. These trends also could reflect regional changes in areal restriction of platform waters.

Anhydrites are rare in the Permian Upper Khuff C except near the base of the studied interval, and as anhydrite cement within grainstones. Anhydrite units are well developed in the Triassic Khuff B and Khuff A. They mark times of arid climate and restriction over marginal sills. Some anhydrites form transgressive deposits within anhydrite-dominated high frequency sequences, but others are highstand deposits of high frequency sequences although at the parasequence scale, the subaqueous anhydrites appear to be late highstand to lowstand fills of accommodation remaining after carbonate deposition.

This study indicates that the Permian-Triassic boundary on the Arabian Platform was synchronous with a significant relative sea-level drop that exposed at least the inner half of the platform (from the outcrop belt to east of Ghawar). This contrasts with the conformable PT boundary in many other areas, which is characterized by overall transgression. Thin sections of core plugs across the PTB document the mass extinction with a major decrease in biotic groups. Within the Triassic sequences, the extinction was followed by widespread development of subtidal thrombolites, marking decimation of grazing and burrowing faunas, and increased microbial calcification due to decreased bioskeletonization.

The oolite facies are the dominant reservoirs occurring in the uppermost high frequency sequence of the Permian Khuff C, and especially in the Triassic Khuff B and A. Reservoir facies are best developed when non-dolomitized oolitic facies were associated with open lagoon facies and were distant from evaporitic tidal flats. Within dolomitized units, best

reservoirs are associated with oomoldic porosity. Anhydrite plugging destroys reservoir porosity, apparently reflecting proximity to sabkhas or salinas.

Carbon isotope profiles sampled from cored wells of the Khuff Formation, spanning 150 m of section across the Permian-Triassic boundary in Ghawar Field, Saudi Arabia were studied to evaluate their use in local and global correlation, and to evaluate the possible influences of early diagenesis versus global processes. The two major excursions are at the Wuchiapingian-Changhsingian boundary and the Permian-Triassic (PTB). However there are several smaller excursions that also appear to correlate with excursions elsewhere. These smaller excursions, many of which correlate to emergence events in Ghawar, may be due to a combination of early diagenetic and global mechanisms. Their global extent provides a high resolution correlation tool for the Late Permian and Early Triassic succession.

Over 75% of the negative carbon isotope excursions occur beneath emergence surfaces, including the two major excursions at the Wuchiapingian and Changhsingian stage boundaries. The $\delta^{13}C$ profiles beneath the boundaries resemble those associated with early diagenesis associated with isotopically light soil gas. The $\delta^{18}O$ profiles beneath the surfaces are variable, perhaps reflecting variable effects of evaporation on the meteoric input, mixing or overprinting by burial diagenesis.

The presence of the negative C-isotope excursions globally in both $\delta^{13}C_{carbonate}$ and $\delta^{13}C_{organic}$ as well as in deeper water sections lacking emergence surfaces, strongly supports the idea of these excursions being global phenomena related global C cycling, although on the Arabian Platform they appear to have been modified by early diagenesis. U depletion across the boundary is compatible with the postulated origins of the PTB event with bottom waters becoming stagnant and reducing, as a result of warming induced by volcanogenic CO_2

released by Siberian trap volcanism, methane release from thermal metamorphism of coals, and destabilization of clathrates in the deep sea due to ocean warming.